M.Sc. Thesis

On the modelling of installation effects on laterally cyclic loaded monopiles

Author:
T. de Blaeij

Date:
Thursday 17th January, 2013

Supervisors:
Prof. ir. A.F. van Tol
Dr. ir. J. Dijkstra
Ing. H.J. Everts
Ir. H.J. Luger
Ir. W.G. Versteijlen

Personal information:
T. de Blaeij
Piet Heijnstraat 21
3223 SG Hellevoetsluis
Tel. +31 (0)61 523 2267
Student nr. 1353691

Supervisors:
Prof. ir. A.F. van Tol
Civil Engineering and Geosciences
Geo-engineering
TU Delft
Tel. +31 (0)15 278 2092

Dr. ir. J. Dijkstra
Civil Engineering and Geosciences
Geo-engineering
TU Delft
Tel. +31 (0)15 278 3326

Ing. H.J. Everts
Civil Engineering and Geosciences
Geo-engineering
TU Delft
Tel. +31 (0)15 278 5478

Ir. H.J. Luger
Soils and Structures
Deltares
Tel. +31 (0)88 335 7481

Ir. W.G. Versteijlen
Civil Engineering and Geosciences
Offshore Engineering
TU Delft\Siemens Wind Power
Tel. +31 (0)70 333 6920

Acknowledgements

The seven months lasting master thesis is often regarded as an individual process. However, several people - in one way or another - contributed to the establishment of this thesis, for which I am very grateful.

First and foremost, I would like to express my gratitude to my committee members for their important and constructive feedback. To Dr. ir. J. Dijkstra for providing the possibility to work in and with the DUT centrifuge and for his critical, constructive and educative feedback. During the thesis months there were numerous discussion, many geo-engineering related, others not and each discussion was an educational experience on its own. To Prof. ir. A.F. van Tol for providing the possibility to perform this master thesis at Deltares. To Ing. H.J. Everts for the initiation of the project and the cheerful conversations. To Ir. H.J. Luger for his valuable advice on the experimental set-up and interpretation of data due to both his experimental and practical experience. And to Ir. W.G. Versteijlen for his critical and more general thoughts on offshore wind turbines and its monopile foundation.

I am grateful to J.J. de Visser for his practical support and his assistance on the experimental set-up. Furthermore I would like to thank DEMO and especially C. van Beek for construction and instrumentation of the novel actuator.

Finally, I would like to thank many fellow M.Sc. students (club van 3000), researchers and staff of the Geo-Engineering section for the discussions on different subjects, leisure and coffee breaks. To friends and family for their absolute support and interest. And to colleagues at Deltares for their feedback and interest in the topic.

Thursday 17th January, 2013

Abstract

Monopiles are being used more extensively for offshore wind turbine foundation. Current guidelines on the construction of fixed offshore foundations still base the design of laterally loaded piles in sand on empirical data (p-y curves), originating from the oil and gas industry, from field tests executed in 1974 on 0.61 m diameter piles. However, large diameter monopiles can be considered short and rigid, which rotate rather than bend when subjected to lateral loads. As a result, numerous experimental studies have been performed on the response of monopile foundations by means of a geotechnical centrifuge. During these tests there was no consistency in installation conditions (ether at low stress levels ($1 \cdot g$), elevated stress ($N \cdot g$) levels or pre-installed), partly because the effect of the pile installation is still not completely understood.

Research into the behaviour of these large open-ended piles generally does not examine the installation effect on lateral capacity. This research contributes to (i) investigate the effect of pile installation on the lateral response of an open-ended pile in sand and (ii) increasing reliability in the interpretation of existing and future centrifuge research on the investigation of lateral cyclic large strain deformations. The main objective of this thesis is to investigate the effect of monotonically jacked open-ended pile installation, at low and elevated stress conditions, on the large strain lateral soil-pile response during two-way cyclic loading. A series of tests was executed to compare the differences on the lateral pile response from monotonic jacked pile installation at low stress levels ($1 \cdot g$) and at elevated stress levels in the geotechnical centrifuge ($N \cdot g$).

In order to study the effect of monotonic open-ended pile installation on the cyclic lateral capacity a novel actuator, which allows installing the pile in-flight and subsequently loading the pile laterally without interrupting the test, was developed. The load mechanism on the free pile head was designed in a way that no bending moment was transferred to the pile head by means of a hinged connection between pile and actuator. The load mechanism - instrumented with strain gauges - was calibrated for stiffness by means of static loads in the laboratory and for hysteresis at $1 \cdot g$ and $N \cdot g$ in the geotechnical centrifuge. The brass model pile was designed to properly scale the lateral bending stiffness and prevent plugging during installation (large D_i/D_{50}).

In order to investigate influence of the soil state on installation effects a total of two sets of tests have been performed with varying installation conditions and relative densities. The first set ($76 \cdot g$ and $I_d = 60 \pm 3\%$) was executed in duplex to determine the consistency and the accuracy of the preparation method. In the second set ($48 \cdot g$) the relative density was varied ($60 \pm 3\%$ and $80 \pm 3\%$). The second set of tests provided a clear insight into relation between load and displacement during two-way cyclic loading (load – displacement loops).

The results indicate that elevated stress installation of an open-ended pile has a small positive (1 – 5%) effect on the lateral capacity. This effect is mainly visible during primary lateral loading of the soil and decays with the number of load cycles. Hence for open-ended model piles the installation effects are negligible. Moreover, these tests indicate that in all cases the stiffness and lateral capacity increase with the number of load cycles, stress level and/or initial density. These gains in capacity and initial stiffness are much more substantial than the differences found between $1 \cdot g$ and $N \cdot g$ pile installation. The results in this study present an incremental advance in fully modelling the installation effect and subsequent lateral cyclic loading of monopiles.

Synopsis

Offshore windturbines worden steeds vaker gefundeerd op monopalen. Huidige constructieve richtlijnen voor gefixeerde offshore funderingen (i.e. monopalen) baseren hun ontwerpmethodieken voor lateraal belaste palen in zand nog steeds op empirische data die voortschrijden uit de olie- en gasindustrie. Deze data is gebaseerd op veldproeven uit 1974 die zijn uitgevoerd op palen van 0.61 m in diameter. Echter, monopalen met een grote diameter worden beschouwd als relatief kort en rigide, wat betekent dat deze eerder roteren dan buigen wanneer blootgesteld aan laterale belasting. Als gevolg daarvan zijn er talrijke geschaalde experimenten (i.e. geotechnische centrifuge) uitgevoerd om het gedrag van monopaal funderingen te onderzoeken. Gedurende deze proeven was er geen consistentie in de installatiewijze van openbuispalen (laag spanningsniveau ($1 \cdot g$), verhoogd spanningsniveau ($N \cdot g$) of begraven), mede omdat het effect van installatie nog steeds niet begrepen wordt.

Het effect van installatie op lateraal gedrag van grote openbuispalen (monopalen) is in voorgaand wetenschappelijk onderzoek niet in beschouwing genomen. Dit onderzoek draagt bij aan (i) de studie naar het installatie-effect op lateraal gedrag van een openbuispaal in zand en (ii) meer betrouwbare interpretatie van (bestaand) geotechnisch centrifuge onderzoek naar grote laterale deformaties (cyclisch) van monopalen in zand. Het doel van deze thesis is om het effect van monotoon gevijzelde installatie van een openbuispaal op lateraal gedrag tijdens grote verplaatsingen, gedurende cyclische belasting, te onderzoeken. Een serie proeven is uitgevoerd om het verschil in lateraal gedrag tussen monotoon gevijzelde installatie bij een laag ($1 \cdot g$) en verhoogd spanningsniveau ($N \cdot g$) in de geotechnische centrifuge te onderzoeken.

Een nieuw mechanisme is ontworpen om het effect van monotoon geïnstalleerde openbuispalen op lateraal cyclische capaciteit te onderzoeken. Dit mechanisme maakt het mogelijk om een paal gedurende een centrifuge vlucht te installeren om deze vervolgens lateraal te belasten. Het aangrijpingspunt is zo ontworpen dat de paalkop alleen horizontaal belast wordt door middel van een scharnierende connectie. Het belasting mechanisme - geïnstrumenteerd met rekstroken - is gekalibreerd voor de stijfheid door middel van statische belastingen en voor hysterese door middel van cyclische $1 \cdot g$ en $N \cdot g$ proeven in de geotechnische centrifuge. Het messingen buispaaltje is dusdanig ontworpen dat de laterale buigstijfheid correct geschaald is en pluggen van het paaltje voorkomen wordt (grote D_i/D_{50}).

Om de invloed van verschillende "soil states" op het installatie-effect te onderzoeken, zijn twee series proeven uitgevoerd met variërende installatieconditie en relatieve dichtheid. De eerste serie ($76 \cdot g$ en $I_d = 60 \pm 3\%$) is in tweevoud uitgevoerd om de consistentie en nauwkeurigheid van de monster preparatie en meetresultaten te bepalen. Bij de tweede serie ($48 \cdot g$) is er gevarieerd in relatieve dichtheid ($60 \pm 3\%$ en $80 \pm 3\%$). Deze tweede serie gaf een goed inzicht in de relatie tussen belasting en verplaatsing tijdens de verplaatsingscycli.

Resultaten geven aan dat installatie van openbuispalen bij een verhoogd spanningsniveau een klein positief effect ($1 - 5\%$) heeft op de laterale capaciteit. Het kleine positieve effect in laterale capaciteit is hoofdzakelijk zichtbaar tijdens primaire laterale belasting van de grond en het effect verdwijnt naar gelang het aantal cycli toeneemt. Vandaar dat het verschil in installatie methode voor open buispalen verwaarloosbaar is. Dit resultaat is een incrementele vooruitgang in het volledig modelleren van installatie effecten en/op de daaropvolgende laterale cyclische belasting van monopalen.

Contents

List of Figures

List of Tables

Abbreviations and Symbols

Parameter		Significance	Dimensions
D_{10}	=	10 % smallest particle size	$[L]$
D_{50}	=	50 % smallest particle size	$[L]$
D_{60}	=	60 % smallest particle size	$[L]$
a	=	Amplitude	$[L]$
ϕ'_{cv}	=	Angle of internal friction at constant volume	[1]
ω	=	Angular rotational velocity	[1]
f_s	=	Average shear stress from cpt testing	$[F/L^2]$
Q_b	=	Axial base capacity	$[F/L^2]$
Q_{bd}	=	Axial plug bearing capacity	$[F/L^2]$
N_q	=	Bearing capacity factor	[1]
C_u	=	Coefficient of uniformity	[1]
I_R	=	Corrected relative density	[1]
y	=	Deflection	$[L]$
F_D	=	Degradation factor based upon influence of soil density	[1]
F_L	=	Degradation factor based upon loading type	[1]
F_I	=	Degradation factor based upon type of installation	[1]
A^*_{rs}	=	Effective area ratio	[1]
R_e	=	Effective centrifuge radius for the model	$[L]$
γ	=	Effective soil weight	$[F/L^3]$
L_{emb}	=	Embedded length	$[L]$
α	=	Empirical degradation parameter	[1]
A	=	Factor that takes into account the loading type	[1]
FFR	=	Final filling ratio	[1]
EI	=	Flexural stiffness	$[F/L^3]$
f	=	Frequency	$[1/T]$
g	=	Gravitational constant	$[L/T^2]$
N	=	Gravity scale factor	[1]
h_m	=	Height of the model	$[L]$
h_p	=	Height of the prototype	$[L]$
σ'_h	=	Horizontal effective stress	$[F/L^2]$
P	=	Horizontal load	$[F]$
IFR	=	Incremental filling ratio	[1]
p	=	Initial effective surcharge	$[F/L^2]$
$Q_{o,i}$	=	Inner axial shaft capacity	$[F/L^2]$
D_i	=	Inner pile diameter	$[L]$
δ	=	Interface friction angle	[1]

K	=	Lateral earth pressure coefficient	[1]
L	=	Length	$[L]$
L/D	=	Length over diameter ratio (slenderness)	[1]
m	=	Mass	$[M]$
R_z	=	Maximum height of the roughness profile	$[L]$
K_{max}	=	Maximum lateral earth pressure coefficient	[1]
ϕ_{max}	=	Maximum or peak friction angle	[1]
R_a	=	Mean deviation of the roughness profile	$[L]$
σ_m	=	Mean effective stress	$[F/L^2]$
K_{min}	=	Minimum lateral earth pressure coefficient	[1]
k	=	Modulus of subgrade reaction	$[F/L^2]$
I	=	Moment of inertia	$[L^4]$
K_0	=	Neutral lateral earth pressure coefficient (Jaky [1948])	[1]
R_n	=	Normalised roughness	[1]
N	=	Number of cycles	[1]
$Q_{o,s}$	=	Outer axial shaft capacity	$[F/L^2]$
D_o	=	Outer pile diameter	$[L]$
q_{bd}	=	Plug bearing capacity	$[F/L^2]$
n	=	Porosity	[1]
r	=	Radius to any element in the soil model	$[L]$
R_t	=	Radius to the top of the model	$[L]$
D_{ref}	=	Reference diameter of a monopile (0.61 m Reese et al. [1974])	$[L]$
I_d	=	Relative density	[1]
$K_s(1)$	=	Secant stiffness modulus after the 1^{st} load	$[FL]$
$K_s(N)$	=	Secant stiffness modulus after the N^{th} load	$[FL]$
τ_s	=	Shaft friction	$[F/L^2]$
τ	=	Shear stress	$[F/L^2]$
C_1	=	Soil constants	[1]
C_2	=	Soil constants	[1]
C_3	=	Soil constants	[1]
z	=	Soil depth	$[L]$
ρ	=	Specific density of the soil	$[F/L^3]$
Q_{tot}	=	Total axial bearing capacity	$[F/L^2]$
V_{total}	=	Total volume	$[L^3]$
q_b	=	Ultimate end bearing pressure	$[F/L^2]$
p_u	=	Ultimate lateral resistance	$[F/L]$
p_{ud}	=	Ultimate lateral resistance, deep	$[F/L]$
p_{us}	=	Ultimate lateral resistance, shallow	$[F/L]$
σ'_v	=	Vertical effective stress	$[F/L^2]$
$\sigma_m v$	=	Vertical effective stress in model	$[F/L^2]$
e	=	Void ratio	[1]
V_s	=	Volume soil	$[L^3]$
t	=	Wall thickness	$[L]$
W	=	Width	$[L]$
E	=	Young's modulus	$[F/L^3]$
E_s	=	Young's modulus of the soil	$[F/L^3]$

Chapter 1

Introduction

1.1 Offshore wind turbines

Despite slower economic growth and budget crisis, construction of offshore wind farms is in rapid development (GWEC [2011]). Overall the average annual market growth for the next 5 years is expected to be 8%, with a strong dip in 2012 and 2013. For the 2012-2016 period the installation of wind turbines is estimated to yield about 255 GW, and the cumulative market growth averaging just under 16%. This is below the 28% of previous years, but still a substantial growth in difficult times (GWEC [2011]).

Apart from the need for sustainable energy, also the rise in energy prices and the increase of public awareness and safety have caused an increase in demand for wind farms. Wind power, especially offshore, is considered to be one of the most promising sources of 'clean' energy. Offshore wind is attractive because of its minimal environmental impact and higher wind speeds at offshore locations. Due to the large investments necessary for developing these offshore wind farms, quality control and licensing from a third party is essential. Quality control is performed by certifying bodies such as the Germand Lloyds Group (Lloyd & Hamburg [2005]), American Petroleum Institute (API [2007]) and Det Norske Veritas (Veritas [2011]), all recognized by the Dutch accreditation agency. The American Petroleum Institute (API [2007]) is also responsible for the development of technical standards for the offshore industry. It is necessary for the engineering industry to enlarge the knowledge concerning design methodologies that describe the behaviour of offshore wind turbines, and to anticipate on increasing demands from the licensing and certifying parties.

The construction of offshore wind turbines is not profitable without governmental subsidies (Snyder & Kaiser [2009]). Both optimizing wind turbines and fulfilling the environmental, safety and quality regulations make the development of these wind turbines a complex problem. Offshore structures can be subdivided into three different types; rigid structures, flexible structures and floating structures. Constructions that are anchored to the seabed are; suction buckets, tripods and monopiles. Monopiles are the preferred type of foundation for the offshore industry if constructed in shallow to medium water depths because of their low cost. They are widely used as foundation for floating facilities, bottom founded structures and wind turbines. These monopiles are sensitive to both decrease in capacity and permanent deformation due to cyclic external lateral loading such as wind, waves and currents. The geotechnical sensitivity of these monopile foundations has led to considerable research attention.

Cyclic lateral loading was assumed to have a benign effect on the behaviour of the pile such as potential loss of serviceability problems (White [2004]). This assumption is based mainly on experimental data with a low number of load cycles (Cuéllar et al. [2012]). The API [2007], Veritas [2011] and Lloyd & Hamburg [2005] still base their design guidelines for laterally loaded piles in sand on empirical data (p-y curves, Murchison & O'Neill [1983]) originating from the oil and gas sector.

Empirical data came from field tests on 0.61 m diameter piles (Cox et al. [1974])). However, large diameter monopiles are considered to be non-slender (i.e. an embedded length over diameter ratio (L/D) of about 5) and rotate rather than bend when subjected to lateral loads (Byrne et al. [2010], Achmus et al. [2007]). As a result numerous experimental studies have recently been performed on the response of monopile foundations. These studies typically performed the experiments in the field (Little & Briaud [1988], Long & Vanneste [1994] and Lin & Liao [1999]), in the laboratory at $1 \cdot g$ (Byrne et al. [2010], Peng et al. [2011] and Cuéllar et al. [2012]) and at $N \cdot g$ in the geotechnical centrifuge (Barton et al. [1983], Oldham [1985], Dyson & Randolph [2001], Brant & Ling [2007], Rosquoet et al. [2007], Klinkvort & Hededal [2011], Li et al. [2010], Alderlieste [2011] and Bienen et al. [2011]).

1.2 Problem description & objective

Only in a few studies open-ended model piles were installed in centrifuge flight and subsequently subjected to lateral load without interrupting the centrifuge. However, as shown by Craig [1985], White [2004] and Dijkstra [2009] the installation effects of single closed-ended piles are significant and should be incorporated in the tests. Unfortunately, this is complicated due to the scaling conditions, especially in cases where closed-ended piles are used instead of open-ended piles in order to properly scale the lateral stiffness. In previous research there has been no consistency in installation of open-ended or closed-ended piles at low stress condition, elevated stress condition or wished in place (pre-installed). Studies that performed installation at elevated stress level referred to Craig [1985] for necessity of this installation at elevated stress level. However, because of plugging and the high embedded length over outer diameter (L/D) ratio it is uncertain of these recommendations still count for the currently used model piles with a low L/D ratio. The paramount objective of this study is to investigate the installation effect on the lateral large strain soil-pile response during two way cyclic loading. This contributes to the validation of previously performed research that contributed to the investigation of large strain deformations. To this end, physical modelling in a geotechnical centrifuge at Delft University of Technology was used by monotonically jacking an open-ended pile, at low stress conditions ($1 \cdot g$) and at elevated stress conditions ($N \cdot g$), before laterally loading the monopile in a cyclic way, to answer the following research question:

What is the effect of monotonically jacked open-ended pile installation at low and elevated stress conditions on the large strain lateral soil-pile response during two-way cyclic loading.

1.3 Organization of thesis

Chapter 2 provides an overview of the literature concerning offshore wind turbine foundations. The development of wind turbines, various different foundations and the characteristic loads of offshore wind turbines are discussed. Besides, the various theoretical methods for designing laterally loaded piles are discussed and more details on the generally accepted p-y method are presented. After analysing the p-y method, some limitations are discussed and an overview is given of various studies performed to diminish these limitations and/or get more insight in the behaviour in monopile foundations. Finally, the contributions of various mechanisms during open-ended pile installation are discussed, in order to show the complexity of all these interwoven mechanisms. Chapter 3 discusses the necessity and limitations of centrifuge modelling. Moreover, it discusses scale effects regarding the installation of open-ended piles. This chapter describes the Delft University of Technology centrifuge and the novel actuator. Finally this chapter discusses the model properties and the experimental program. Chapter 4 contains the results of the centrifuge tests. Chapter 5 presents conclusions drawn after which Chapter 6 contains recommendations for further research.

Chapter 2

Offshore monopile foundations

This chapter starts with (§2.1) general information concerning offshore wind turbine foundations. Methods used for predicting the lateral soil-pile behaviour are discussed in §2.2. Additionally, this section discusses the initiation of the p-y method, design guidelines, the shortcomings of the p-y method and studies performed until now. §2.3 treats the installation of monopiles and contains an overview of aspects that contribute to the change in soil state such as; pile plugging, cavity expansion, lateral stress change during the installation process and friction fatigue. Finally the chapter ends with a conclusion. Appendix A contains additional information regarding the p-y method, axially loaded piles and the possible plugging of monopiles.

2.1 Offshore wind turbine foundation

2.1.1 Offshore wind turbine development

The average annual market growth for the next 5 years is expected to be 8%, with a strong dip in 2012 and 2013. For the 2012-2016 period the installation of wind turbines is estimated to yield about 255 GW, and the cumulative market growth averaging just under 16%. This is below the 28% in the previous years, but still a substantial growth in difficult times (GWEC [2011]). Environmental public awareness, rise in energy prices and safety cause an immense increase in the interest in sustainable energy. Wind power, and therefore offshore wind turbine farms, offers a possible solution for meeting the demand in renewable energy because of its minimal environmental impact and higher wind speeds at offshore locations.

In general, offshore structures are used for the oil, gas and offshore wind farm industry. Environmental conditions have become harsher due to increasing distance from the shore (Clauss et al. [1988]). Several types of foundations exist for offshore wind turbines. The type of foundation to be used depends on the site and loading conditions. Presently, non-slender (stiff) monopiles piles are used with an outer diameter ranging from 4 to 6 m, driven 20 – 30 m into the seabed. These piles are non-slender because of their low embedded length (L) over diameter (D) ratio of about 5. A wind turbine foundation may account for up to 35% of the installation cost. The cost for each such turbine is estimated at € 1.5 million per megawatt (Byrne & Houlsby [2003]).

Wind turbines are extremely sensitive to rotation of the turbine tower. A small rotation could easily affect the efficiency and the serviceability of the turbine. The design standards require that the serviceability limit for rotation is 0.5° consisting of 0.25° allowable rotation due to installation and 0.25° rotation due to loading (Vattenfall [2008]). These requirements demand a sufficient foundation to transfer loads to the surrounding soil.

Table 2.1 Load characteristics North Sea conditions for a 5 MW turbine (Lesny & Wiemann [2005])

		North Sea Conditions
Vertical Load V	$[MN]$	35
Horizontal Load H	$[MN]$	16
Bending Moment M	$[MNm]$	562
Torsional Moment M_t	$[MNm]$	4

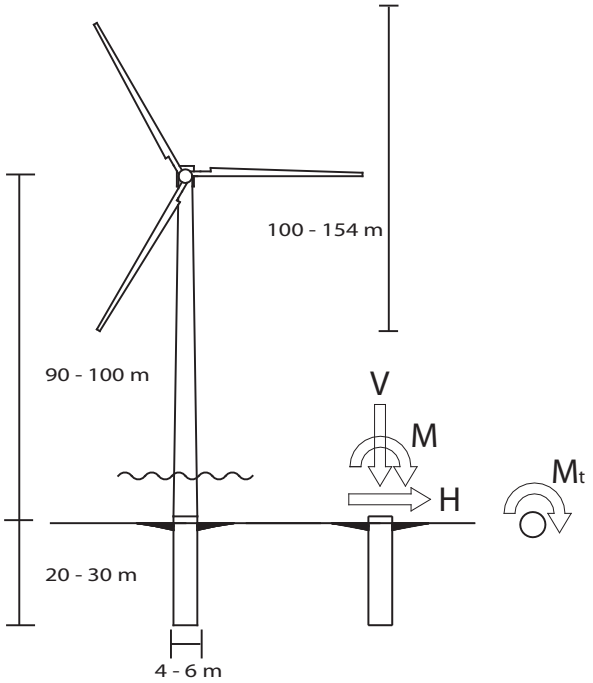

Figure 2.1 Schematization of offshore wind turbine and accompanying characteristic loads

2.1.2 Load characteristics

Lateral cyclic loads on offshore monopiles are produced by waves, wind, currents and boat collision or mooring. These loads are characterized by four loading parameters namely the maximum load, the number of cycles and the load frequency. Huge wind turbines with capacities from 3.5 MW to 6.0 MW are being constructed further offshore. The dead weight of these structures is relatively low in comparison to the overturning moment caused by wind, wave and current loadings. The turbine is generally located at about 90 – 100 m above the mud line and the rotor diameter is in the order of 100 – 154 m (see Figure 2.1). The foundations are subjected to vertical load, horizontal load, bending moment and torsional moments. The maximum vertical load (dead weight) is in the order of 35 MN and the maximum horizontal load is in the order of 16 MN, causing a bending moment of 562 MNm at the mud line. The torsional moment is about 4 MNm. These are values typically for North Sea conditions and are presented in Table 2.1. The frequency of wave loads that produces the maximum energy depends on the location. Wave load frequencies are in the order of 0.07 Hz according to Lesny et al. [2007] and 0.1 Hz according to Alderlieste [2011]. The peak spectral frequency is at 0.14 Hz according to Pierson Jr & Moskowitz [1964]. The wave spectra, in case of North Sea conditions (JONSWAP spectrum, Hasselmann et al. [1973]), could be slightly higher using either the zero-crossing period or the peak period as basis for the wave spectrum (Van der Tempel [2006]). The frequency of the blades is in the range of 0.3 Hz – 1 Hz (Byrne et al. [2010]). These frequencies are location dependent.

Table 2.2 Different types of offshore structures

Rigid structures	Flexible structures	Floating structures
Jackets	Articulated towers	Semi-submersibles
Jack-ups	Guyed towers	Ships
Gravity foundations	Tension leg platform	
Bucket foundations		
Tripods		
Monopiles		

2.1.3 Foundation types

Offshore structures can be subdivided into three different types (Clauss et al. [1988]), namely rigid, flexible and floating structures. Various types of offshore structures are presented in Table 2.2. Constructions that are anchored on or into the seabed are gravity based foundations, suction buckets, tripods, jackets and monopiles (see Figure 2.2). Only the behaviour of the latter three foundation types are significantly influenced by the installation processes such as driving and jacking of piles. The implementation of a certain foundation type depends on several aspects, namely water depth, type of loading, soil conditions, dynamic behaviour, the technical manufacturing conditions and costs.

Both tripods and jackets are legged steel frame structures. The goal of reducing the width of the structure in the upper part is to decrease the wave impact. These structures are fabricated on land and transported to their final location where they are anchored, by means of monopiles or suction buckets, into the seabed (see Figure 2.1). Because of the width of the structure the foundation elements are subjected to tensile, horizontal and compressive loads. These foundation types can be used for sites with water depths ranging between 20 – 25 m.

Monopiles normally consists of a cylindrical steel tube hydraulically driven into the soil. The overlap between monopile and transition peace is grouted (Lesny [2010]). Penetration depth of a monopile can be adjusted in accordance with the environment and soil conditions. This foundation type is well suited for sites with water depths up to 25 m. Advantages of this construction are; the limited impact and footprint of this structure, costs and the ease of construction. Therefore, monopiles have been a popular foundation for offshore wind turbines. However, increasing water depths and higher loads raises interest in other foundation types such as tripods. Environmental considerations contribute to increasing research into other installation methods.

2.2 Laterally loaded monopiles

2.2.1 Methods for designing laterally loaded piles

According to Fan & Long [2005] analysis methods for laterally loaded single piles can be subdivided into Limit State Method (Broms [1964]) e.g. Elasticity Method, Finite Element Method and Subgrade Reaction Method e.g. p-y Method.

The Limit State Method is a relatively simple method for calculating the ultimate lateral capacity of a single pile. The ultimate lateral soil resistance is calculated using simple statics. The Elasticity Method is an extended Limit State Method taking into account the continuity of the soil. However, the response is assumed to be linearly elastic and stiffness increases with stress level. Since soil doesn't behave elastic but elasto-plastic, this method is only useful when calculating small strain displacements (Fan & Long [2005]).

Finite Element Methods (FEM) and Finite Difference Methods (FDM) are capable of modelling soil continuity, soil non linearity, soil-pile interface behaviour and 3-D boundary conditions. This method is more advanced than any other method but primarily used as a research tool. FEM and FDM methods differ in the discretization processes and the way in which variables are approximated.

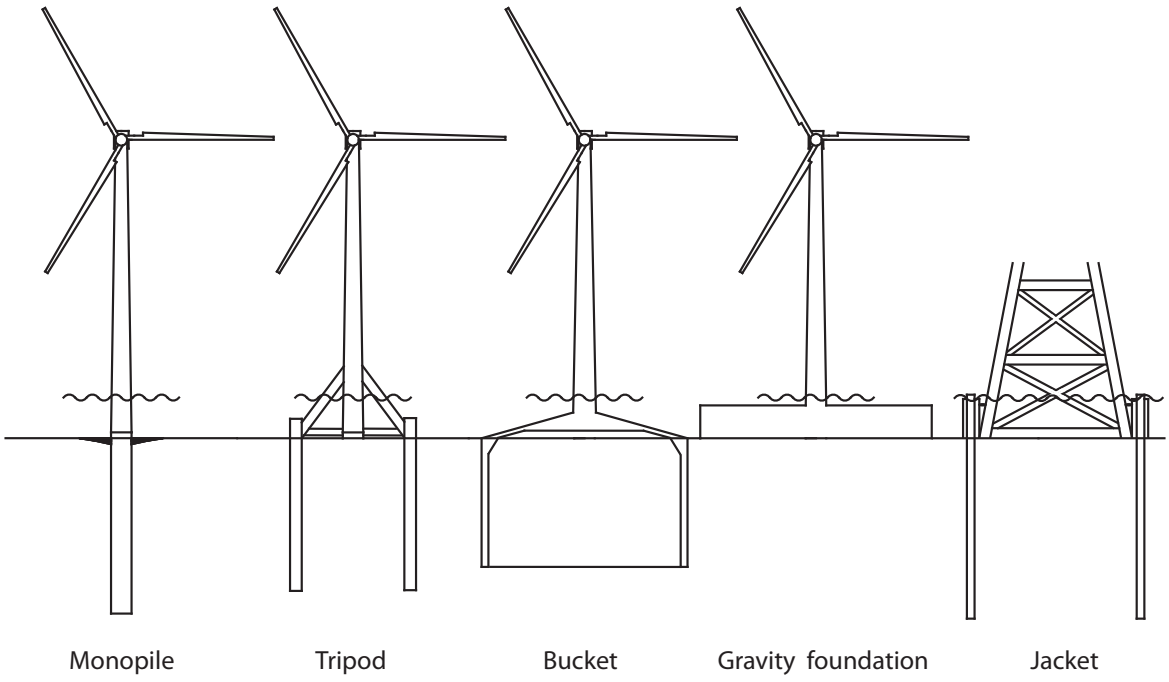

Figure 2.2 Examples of rigid foundation types

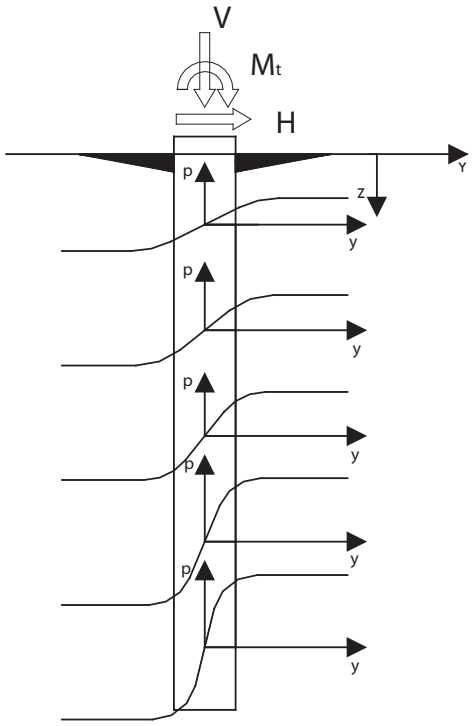

Figure 2.3 Schematization of p-y method for laterally loaded piles

The Subgrade Reaction Model is widely used because of its simplicity and reasonable accuracy. Disadvantages of this model are; the linear relation between lateral soil-pile behaviour, the use of a modulus of subgrade reaction, the assumption that the soil can be modelled as discontinuous springs whereas it normally behaves continuous and indirect consideration of pile geometry. The p-y method is a special Subgrade Reaction Method in which a non linear relation is established between lateral resistance (p) and the lateral displacement (y). The Subgrade Reaction Method and the p-y method are most common analytical tools used to predict the response of laterally loaded piles.

2.2.2 p-y method

The initiation

Terzaghi [1955] discussed the use of horizontal subgrade reaction for laterally loaded piles. In this paper the relation between pressure (p) and displacement (y) is introduced. The idea was that the displacement can be computed on the assumption that the pressure acts on an elastic layer with thickness equal to three times the diameter of the pile. There is no experimental data or an analytical procedure to verify these recommendations. According to Long & Vanneste [1994] the solution of using a linear, elastic soil response was suggested by Reese & Matlock [1956] and Vesic [1977]. The soil reaction modulus (k) was assumed to increase proportionally with depth over the length of the pile.

The actual concept concerning p-y curves was presented in a paper by McClelland & Focht [1958]. These curves were derived from full-scale, instrumented, lateral load tests. It showed that k is a function of pile diameter, deflection and soil properties (Reese & Van Impe [2001]). McClelland & Focht [1958] described a relation between p and y on basis of consolidated undrained triaxial tests, with confining pressure varying over depth and equal to the overburden pressure at that depth. Reese et al. [1974] and Cox et al. [1974] conducted research on driven 0.61 m diameter piles at Mustang Island (L/D of 35). These piles were instrumented with strain gauges and both static and cyclic loads were applied. Installation effects were taken into account in these field tests. However, because of the non-homogeneous soil conditions, only a limited amount of tests were performed and only a single type of installation method was used. There was no extra information available regarding installation effect. The original p-y curves for sand consisting of four sections were replaced with a constant hyperbolic function formulated by Murchison & O'Neill [1983]. This function is described and used by API [2007], Veritas [2011] and Lloyd & Hamburg [2005] (for details see Appendix A). The three guidelines present the same approach for designing laterally loaded piles. There are different views on other subjects such as the installation effect.

Design guidelines

In this section the three most important guidelines are discussed. Other codes of practice such as M.E.L.T [1993] (France) and P.H.R.I. [1980] (Japan) are only relevant guidelines for the local conditions in which they are applicable.

The American Petroleum Institute (API [2007]) is used as a guideline when dealing with lateral soil-pile behaviour. Without presenting a quantified approach, this guideline states that the effect of soil disturbance during pile driving on the lateral soil resistance should be considered. The lateral soil reaction is schematized by elasto-plastic behaviour of the soil in the form of a p-y curve (Murchison & O'Neill [1983]).

All the guidelines refer to API [2007] for applying the p-y method. Another important remark added by Veritas [2011] is that the initial stiffness of the p-y curve is extremely important when dealing with small strain soil-pile responses. The p-y curves are being discretized by calculating the relation between pressure and displacement at key points in the total displacement. To define the initial stiffness, it is necessary to impose a sufficiently fine discretization near the origin of the p-y curves. The Lloyd & Hamburg [2005] guideline specifically mentions that any disturbance of soil, due to scouring or installation of the piles must be considered with great care. This design guideline suggest, in its design criteria for laterally loaded piles, that the pile deflection line matches the zero-toe-kick or vertical tangent condition to minimize the risk of accumulated deformations under cyclic loading. However, the zero-toe-kick condition is inapplicable for the currently used non-slender monopiles.

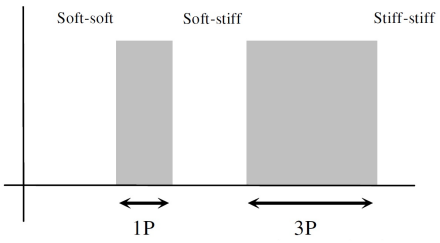

Figure 2.4 Frequency intervals for a variable speed turbine system Van der Tempel [2006]

Shortcomings of the p-y method

The initial stiffness is essential for determining the natural frequency of the necessary support for designing of Serviceability Limit State and Ultimate Limit State loading. The natural frequency of an offshore turbine design should be such that is does not coincide with the 1P and 3P frequency intervals for variable rotors (Van der Tempel [2006]) and wave frequencies. Wave frequencies are generally lower than the rotational frequency of the rotor. 1P and 3P are the frequencies respectively belonging to (*i*) the corresponding peak loads of the rotation frequency of the rotor (1P) and (*ii*) the frequency of all the blades passing (3P). These frequencies divide the frequency range into three intervals (soft-soft, soft-stiff and stiff-stiff) suitable for designing the natural frequency of the wind turbine (see Figure 2.4). The softest stiffness, e.g. lowest natural frequency, is considered to be the best from an investment point of view (Van der Tempel [2006]). The stiffness properties of soil contribute to the overall natural frequency of the turbine. A lower stiffness will result in lower overall natural frequency which may be compensated by increase in monopile diameter (Van der Tempel [2006]). The p-y method originates from calculating the ultimate lateral capacity of the soil pile interaction. Therefore, the API [2007] presents a rough estimation for this initial stiffness still based on research performed on long slender piles with diameters $< 2\ m$ and a length over diameter ratio L/D of 34.4 (Murchison & O'Neill [1983]). Large diameter monopiles are considered to be short and rigid which rotate rather than bend when subjected to lateral loads (Achmus et al. [2007] and Byrne et al. [2010]). The initial stiffness is assumed to be independent of pile properties (L/D), effect of cyclic loading and installation method. The initial stiffness is essential for the design and behaviour of wind turbines and, as a result, numerous studies have been performed on the response of monopile foundations. An elaboration of research performed regarding the shortcomings of the p-y method is presented in §2.2.3.

2.2.3 Studies until now

Various studies have been performed to investigate soil-pile behaviour due to lateral loading. Main and most interesting fields of research are field tests, scaled model tests and numerical modelling. Table 2.3 presents various tests and important characteristics of these reported tests. Hardly any research can be found that investigates the installation effect on the subsequent lateral soil-pile behaviour.

Field studies

Long & Vanneste [1994] recommended a modification of the p-y curve depending on the number of load cycles using the results of 34 cyclic lateral load tests (Little & Briaud [1988]). With this alteration the subgrade reaction and displacements under static loading are corrected. The static loading is equal to the first load cycle. The method is described in Appendix A. Lateral load tests on offshore piers in Tampa Bay (Little & Briaud [1988]) show larger displacements than predicted by the p-y curves, probably because the installation method, load characteristics and numbers of load cycles have not been taken into account. An example of influence of pile installation method

Table 2.3 Summary of the research performed (Pile type: O = Open-ended, C = Closed-ended. Installation method: D = Driven, J = Jacked, W = Wished (pre-installed))

Authors	Pile penetration (L/D_o)	Number of Cycles	Pile type	Installation method	Installation condition
Low stress condition ($1 \cdot g$)					
Cuéllar et al. [2009]	4	5000000	O	W	
Byrne et al. [2010]	5.4	60000	O	D	
Peralta & Achmus [2010]	3.2 – 7.9	10000	O		
Peng et al. [2011]	9.7	10000	O	W	
Cuéllar et al. [2012]	4	5000000	C	J	
Elevated stress condition ($N \cdot g$)					
Barton et al. [1983]	20	20	O	D	
Craig [1985]	21	1	O*	J	$1 \cdot g$ and $52.5 \cdot g$
Dyson & Randolph [2001]	20	1	O, C	W, D, J	$1 \cdot g$ and $160 \cdot g$ **
Brant & Ling [2007]	16	1	O*, C	D	$1 \cdot g$ and $40 \cdot g$
Li et al. [2010]	5	1000	O	J	$1 \cdot g$
Alderlieste [2011]	5	500	O	W	$1 \cdot g$
Klinkvort & Hededal [2011]	6	500	C	J	$1 \cdot g$
Bienen et al. [2011]****	12.5 – 5	1000	O, C	J	$1 \cdot g$, $200 \cdot g$
Klinkvort et al. [2012]	6	500	C	J	$N \cdot g$***
Nummerical modelling					
Achmus et al. [2009]	2.6 – 5.3	10000			
Zania & Hededal [2011]	6	1			
Full scale test					
Cox et al. [1974]	35	25			
Murchison & O'Neill [1983]	34.4	1	O	D	

*Pile plugged during installation.
**Calcareous sands.
***Stopped centrifuge in order to alter load frame.
****Winged pile, $1 \cdot g$ installation for open-ended pile.

on lateral soil-pile response is presented in Figure 2.5. This figure shows that the method does not change the initial stiffness.

$1 \cdot g$ model tests

$1 \cdot g$ modelling is an adequate way for conducting parametric studies on the physical behaviour of phenomena in a relatively cost effective manner, as opposed to centrifuge modelling and fields tests. The response of initial dense sand sample at high mean effective stress level and initial loose sand sample at low mean effective stress level is qualitatively the same (Muir Wood [1991]), indicating the ability to model soil behaviour even at low effective stress ($1 \cdot g$ model tests).

Research has been performed to show the physical phenomena of macro mechanical densification and convective granular flow under quasi static cyclic lateral loading (Cuéllar et al. [2012]). These tests indicated that the number of load cycles significantly influence the densification of the soil. Densification and lateral stress increase contribute to progressive stiffening of the soil around the pile (Byrne et al. [2010], Peng et al. [2011] and Cuéllar et al. [2012]).

Byrne et al. [2010] showed that there is a gradual reduction in the rotation with increasing number of cycles. A slight increase of load over total displacement was discovered for a reduction in frequency (Peng et al. [2011]) indicating the frequency dependency of the lateral behaviour.

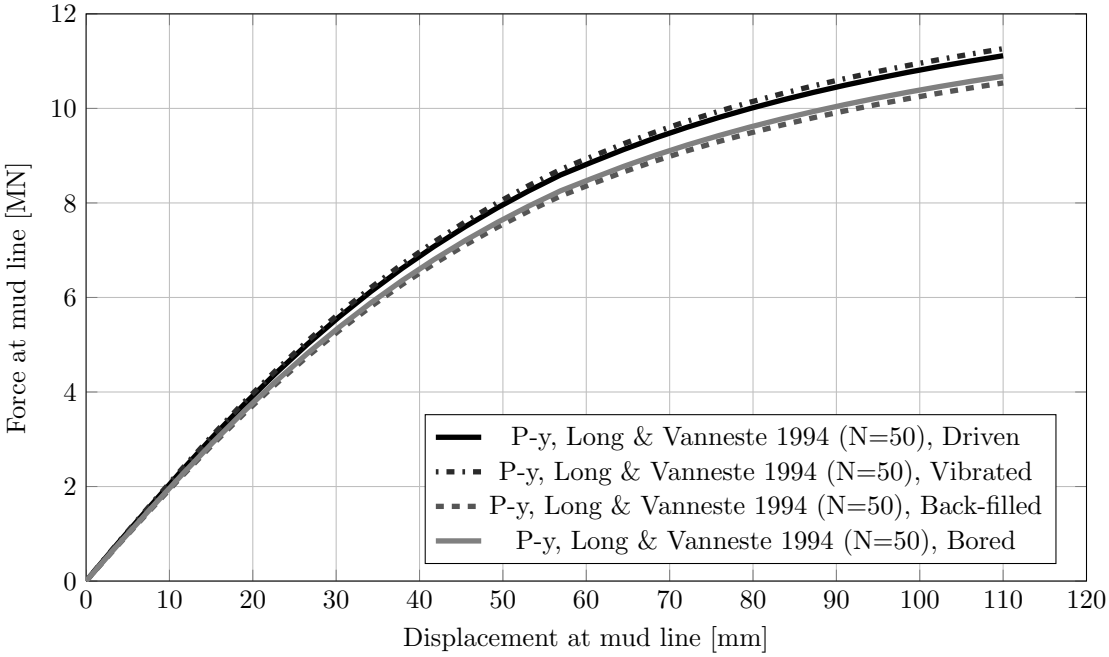

Figure 2.5 Example of installation effect on cyclically loaded pile by Little & Briaud [1988]

Centrifuge modelling

The main advantage of centrifuge modelling over $1 \cdot g$ modelling is that the experiments are carried out at a stress level corresponding to prototype stress condition. Soil behaviour (i.e. soil stiffness) is stress dependent, indicating the necessity of centrifuge modelling. Critical attention has to be paid to the output data since scale effects contribute to discrepancies between model and reality. Centrifuge modelling should therefore be compared with other analytical, numerical or site specific studies (Laue [2002]).

Until 1993 most pile tests were pre-installed (wished in place) in the strongbox before the granular soil sample was prepared (Laue [2002]). Only in few studies the piles were installed in-flight and subjected the pile to lateral load without stopping the centrifuge. However, as shown by Craig [1985], White [2004] and Dijkstra [2009] the installation effects of single closed-ended piles are significant and should be incorporated in the tests. Incorporating installation conditions is complicated by the scaling conditions. Especially in cases where a closed-ended pile is used instead of an open-ended pile, in order to properly scale the lateral stiffness, this could have an over pronounced effect on the resulting lateral capacity.

According to Dyson & Randolph [2001], Brant & Ling [2007], Oldham [1985] and Craig [1985], the lateral soil-pile behaviour is affected by the installation at elevated stress level. Oldham [1985] was the first to use a pneumatic jack in-flight to install the open-ended pile up to 400 mm in length, with an L/D ratio of 20 at $52.5 \cdot g$, prior to static or cyclical lateral loading the pile. It was considered important to drive the piles in-flight to model field conditions, particularly lateral stress distributions following installation, as closely as possible (Oldham [1985]). It seems that overall stiffness of the pile-soil interaction is higher when installation is carried out at high mean stress levels. Dyson & Randolph [2001] performed lateral loading tests on 340 mm long open-ended piles with an embedded L/D ratio of 20. Tests were conducted at $160 \cdot g$ in calcareous soils. Craig [1985] performed tests on open-ended pipe piles with a diameter of 8 mm and a L/D ratio of 47.5 in a relative density of 70% and a gravity scale factor of 52.5. Because of the slenderness of the pile, plugging occurred during installation.

As can be seen in Table 2.3 there has hardly been any consistency in installation condition of

open-ended model piles. Generally, research refers to Craig [1985] for the necessity of installation at elevated stress level. Note that these tests were conducted on plugged open-ended piles, which is unlikely for monopiles with a low L/D and used currently in practice. Hence, the effect of the pile installation on the subsequent lateral pile response is still not completely understood. Klinkvort & Hededal [2011] intentionally install the pile at $1 \cdot g$ to minimize the installation effects.

According to Barton et al. [1983] and Verdure et al. [2003], the lateral response becomes stiffer (secant stiffness) with every cycle until it reaches steady state (6 – 10 cycles). The API method appears to underestimate the initial stiffness (Brant & Ling [2007] and Barton et al. [1983]), but overestimate the lateral resistance for medium dense sands (Ting et al. [1987] and Alderlieste [2011]).

2.3 Installation of monopiles

2.3.1 Pile plugging and cavity expansion

During pile installation, driven or jacked, a column of soil penetrates through the pile. The difference between driving and jacking is that driving is a dynamic event, caused by applying blows on top of the pile, whereas jacking is a static event in which hydraulic rams are used to push the piles into the soil. Penetration of soil through a pile differs from fully plugged, unplugged, to partially plugged mode. The extra resistance created by the soil plug results from arching (Paikowsky [1990]), creating an increase of vertical stresses in the plug that exceeds the gravity effect. This in turn creates higher horizontal stresses and subsequently increases the friction between soil and pile wall. The friction between the wall and a soil element in consideration contributes to an exponential increase of friction between the pile wall and soil element below the considered soil element. Another possibility for plugging is the process of cone formation underneath the open-ended pile (Dijkstra & Broere [2009]). Probably both mechanisms influence pile plugging behaviour. Plugging behaviour of a pile is governed by the state of the soil (i.e. density and stresses, Brucy et al. [1991]).

Coring of a soil plug in an open-ended pile can also be defined as the Final Filling Ratio (FFR). The IFR is a measure of soil displacement near the pile tip and depends on the inner pile diameter, pile wall thickness, plug densification or dilation and installation method (Lehane et al. [2005]). As the IFR approaches zero, the behaviour of the pile is the same as that of a fully plugged pile. If IFR (and FFR) approaches 1 the pile behaves fully cored, which is approximately equivalent to a bored pile (Lehane et al. [2005]). There are hardly any cases that quantify incremental or final filling ratios. A rough estimate is presented in Equation 2.1 (Xu et al. [2005]).

The densification of the soil at the pile tip is related to the horizontal displacement of the soil. The level of displacement can be expressed for both closed-ended and open-ended piles in terms of an "effective area ratio", A^*_{rs} (see Equation 2.2). Schematic streamlines of soil flow and profiles of lateral stress for various plugging mechanisms are presented in Figure 2.6. The strain and stress change due to the passing of the pile tip can be modelled using the cavity expansion theory (Xu et al. [2005]). Cavity expansion theory takes into account the actual penetration process and soil compressibility properties (or densification of the soil). In case of driven piles in medium to dense sand, the soil near the pile shaft tends to loosen (Dijkstra [2009]). It appears that visible horizontal influence of installation of closed-ended piles extends from $3D$ from the pile in loose sand, to $5.5D$ in dense sand (Robinsky & Morrison [1964]).

$$FFR \approx min[1, \frac{D_i}{1.5}^{0.2}] \quad (2.1) \qquad A^*_{rs} = 1 - IFR \cdot \frac{D_i^2}{D_o^2} \quad (2.2)$$

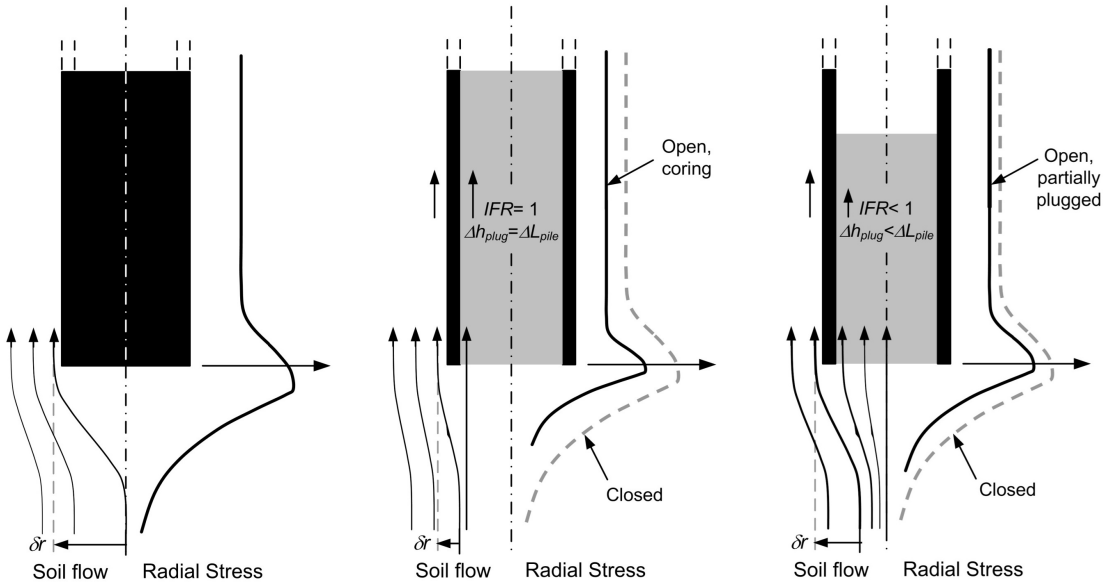

(a) Closed-ended pile, A_{rs}= 1

(b) Cored open-ended pile, IFR= 1, $A_{rs} \sim 0.1$

(c) Partially plugged open-ended pile, $IFR \leq 1$, $0.1 \leq A_{rs} \leq 1$

Figure 2.6 Schematic streamlines of soil flow and profiles of lateral stress (White et al. [2005])

2.3.2 Lateral stress change at the pile tip

A soil element undergoes vertical compression and horizontal extension as the pile tip approaches the soil element in question. Figure 2.8 schematically presents this stress change during stage A – B (White [2005]). As the pile tip descends, the soil moves laterally. Deformation changes to horizontal compression together with vertical extension (rotation of principal stress). As soil passes the pile tip, stresses reduce and the element exerts an upward shear stress on the lower part of the pile shaft (White [2005]). Strain and stress changes due to vertical compression below the pile tip followed by horizontal compression as the soil element flows around the pile shoulders. See Figure 2.6 for a schematic representation of stress increase at pile shoulder (White [2004]). Rotation of principal stresses takes the stress situation (soil state) to point C in Figure 2.8. If penetration occurs in an unplugged manner, τ_{max} may even be lower than f_s due to lower radial displacement (White et al. [2005]). The displacement fields and strain paths during pile installation are found to be relatively independent on the type of granular soil (White & Bolton [2004]).

2.3.3 Friction fatigue

The interface zone adjacent to the shaft of the pile contains broken soil particles, leading to high unrecoverable volume reduction. The interface zone was observed to contract further while shearing along the interface (White [2004]). This phenomenon is also called "Friction fatigue" (Heerema [1978] and Randolph [2003]) which is attributed to gradual densification (contraction) of the interface layer that is confined by the far field soil. According to these tests a reduction of lateral stress and local shaft friction as a function of pile displacement is visible from the measurements. This reduction of lateral stress varies over the length of the pile and depends on the magnitude and cycles imposed by the installation method (White [2005], from point C to E in Figure 2.8). Reduction of lateral stresses is stronger for driven than for jacked piles (one-way installation cycles) (White [2004]). It is demonstrated that the number of loading cycles has a greater influence on the contraction of the interface layer than the net displacement (Kelly [2001] according to White [2005]). White [2004] also shows, by means of Constant Normal Stiffness (CNS) tests, that the reduction is larger for soils with

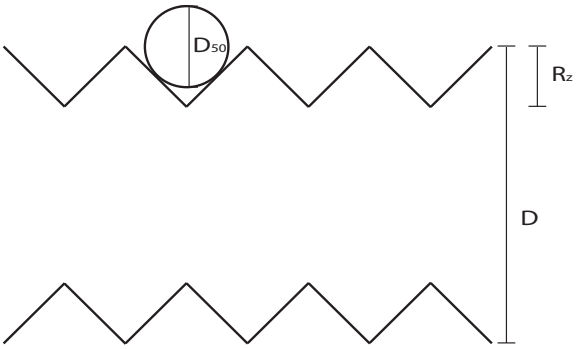

Figure 2.7 Definition of normalized roughness R_n (Garnier & König [1998])

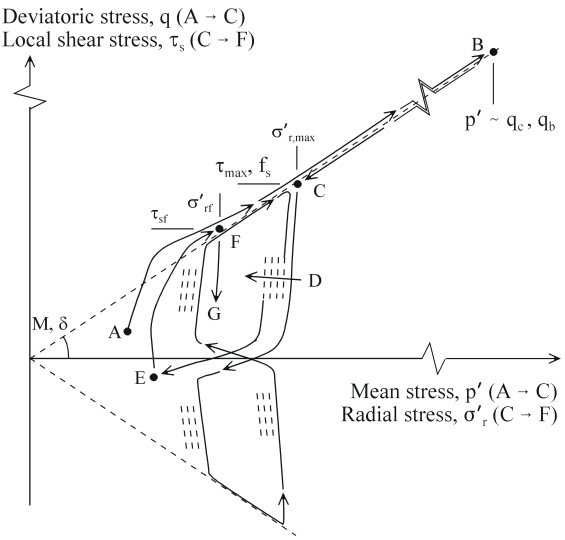

Figure 2.8 Loading history of soil adjacent to a displacement pile (White [2005])

higher stiffness indicating the relevancy of elevated stress installation in a geotechnical centrifuge. Thus, lateral stress change due to pile installation is influenced by the lateral stiffness of the soil and dilative or contractive behaviour of a shear band at the pile interface (Lehane & White [2005]). This factor is governed by the normalized roughness, R_n (Equation 2.3 and Figure 2.7). For low values of $R_n \leq 0.02$, (Paikowsky et al. [1995]) the ratio between maximum shear stress and normal stress is relatively low and no dilatancy occurs (Garnier & König [1998]). In case that $R_n \geq 1$, the surface is rough causing high shear resistance and dilative behaviour of the shear band. According to Lehane et al. [2005] this dilative effect is not significant for offshore piles with large diameter.

$$R_n = R_z / D_{50} \tag{2.3}$$

2.4 Conclusions

Laterally loaded piles are generally calculated using the p-y method. The initial stiffness is assumed to be independent of pile properties, installation method and effect of cyclic loading. This stiffness is essential for the design of dynamically loaded wind turbines because it influences the natural frequency of the structure. Research focused their attention mainly on the ultimate lateral capacity; therefore the knowledge concerning the initial stiffness lags behind. As a result, numerous studies have been performed on the response of monopile foundations (2.3). Only in few studies the piles were installed in-flight and subsequently subjected to lateral load without stopping the centrifuge. However, as shown by Craig [1985], White [2004] and Dijkstra [2009] the installation effects of single closed-ended piles are significant and should be incorporated in the tests. Unfortunately, the latter is complicated due to the scaling conditions. Hence, the effect of the pile installation on the subsequent lateral pile response is still not completely understood. Generally research refers to Craig [1985] for the necessity of installation at elevated stress level. However, these tests were conducted on plugged open-ended piles, which is unlikely for monopiles with a low L/D.

Pile plugging (Paikowsky [1990]) and cavity expansion contribute to densification of the soil (Lehane et al. [2005] and Robinsky & Morrison [1964]). Densification strongly depends on the Internal

Filling Ratio, Final Filling Ratio and the effective area ratio. There are hardly any cases that report incremental or final filling ratios. After the soil passes the pile tip the material dilates temporarily before it contracts during shearing along the pile wall ("Friction Fatigue", Heerema [1978] and Randolph [2003]). The consideration of a specific coefficient of lateral earth pressure, the friction fatigue process, local shear stress distribution and sand dilation offer a possible explanation for changes in lateral stresses (change in soil state). Unfortunately the combined measurement of stress change and density change are scarce (Dijkstra [2009]).

The state in which the soil occurs is defined as the soil state (Muir Wood [1991]). This soil state can be characterized by the relative density of the soil and the stress state in the soil. Behaviour of the soil can be best described by the current soil state and the tendency of the soil to diverge from that state to the critical state. The pile installation process does have an effect on the soil state i.e. densification and lateral stress change due to installation (Xu et al. [2005] and White [2005]), lateral stress change due to rotation of principal stresses (White [2004]) and stiffness dependency of contraction and "Friction fatigue" (White [2004]). Since soil-pile behaviour is governed by the ultimate lateral bearing capacity and initial lateral stiffness - both depending on the soil state - the installation process potentially influences the lateral behaviour. Although lab research is conducted regarding the effect of cyclic loading, hardly any research is performed on the installation effect of open-ended piles on lateral soil-pile behaviour.

Chapter 3

Centrifuge modelling

This chapter contains both the necessity, possibilities and limitations of centrifuge modelling crucial for accomplishing the thesis objectives. §3.1 contains an extensive elaboration on the purpose and motivation for applying centrifuge modelling. Besides it discusses various scaling law limitations. It also contains the different relevant scaling effects and limitations essential for appropriately evaluating the output data. §3.2 presents a summary of the Delft University of Technology centrifuge used for the experiments. §3.3 covers soil, pile and interface properties of the model and the limitations of this model set-up after which §3.4 discusses the experimental program.

3.1 Scaling laws and effects

3.1.1 Scaling laws

Physical modelling is carried out in order to study specific aspects of the behaviour of prototypes. A prototype model is considered to be the representation of the full-scale model. Physical models are generally scaled, as opposed to un-scaled, because it is desired to gain information about physical behaviour more rapidly and with more control over specific details. In physical modelling the goal is to replicate an event in a reduced scaled version, to what exists in a prototype. A special feature of geotechnical modelling is the reproduction of soil behaviour (or realistic failure mechanism) governed by both strength and stiffness (i.e. strain). These soil characteristics are both stress and density (soil state) dependent. Centrifuge modelling allows for a free unstressed upper surface, and within the soil body a reproduction of the linear effective stress increasing profile over depth related to the soil density and acceleration field. If in both the model as well as in the prototype situation similar soil is used, and the centrifuge is subjected to a specific acceleration field (N) times the gravitational constant, then the vertical stresses in the model correspond to prototype (Taylor [1995]). Accurately modelling the stresses according prototype stresses is crucial when modelling the mechanical behaviour of; pile shaft response during installation, distribution of internal stresses during installation and lateral soil response during loading.

If material behaviour would be entirely linear and homogeneous, for loads that are applied in the model and expected in the prototype, then it may be a simple matter to scale up the model observations (Muir Wood [2004]). But since material behaviour is nonlinear and the material used is not homogeneous the development of an underlying theoretical model will become more difficult. Therefore scaling laws, to consider model as a prototype observations, need to be understood. Table 3.1 presents relevant general scaling laws used to reproduce a prototype in a centrifuge model (Kutter [1995], Taylor [1995], Muir Wood [2004] and Garnier et al. [2007]).

As Muir Wood [2004] mentions there are two stiffness elements that can be considered; the small strain stiffness which controls dynamic response, and the nonlinear stiffness due to large strain

deformation. The small strain stiffness can be considered to be first order dependent on the effective stress level. Application of critical state soil mechanics theory is advised to ensure similarity between model and prototype for medium strain deformation and argue for similar values of state variable between both prototype and model situations (Muir Wood [2004]).

The scale factor for stiffness (Table 3.1) controls the scale factor for strain in the physical model. Especially when the geotechnical system in question is dominated by relative movements between interfaces such as separate blocks of soil, or between the soil and a structural element such as pile or section reinforcement. Then the behaviour between interfaces is controlled by relative displacement across the interface and a small physical model may have difficulty in correctly reproducing the system response (Muir Wood [2004]). In case of prototype pile installation the displacement of material (for which the shear stress varies nonlinearly with displacement) under the pile tip (failure surface) will be large enough to ensure that only a limited part of the failure surface preserves stress above the residual value. Only soil at the emerging end of the failure surface attains the peak of the shear stress. In a small-scale model a much higher proportion of the failure surface, because of lower stiffness and thus strains, will attain stresses above the residual value. There is even a possibility that no part of the failure surface will fully lose strength, indicating a more intact soil state in comparison to the actual prototype installation for which the largest part of the failure surface already is in critical state (Muir Wood [2004]). In case of soil adjacent to the pile shaft, the increase in lateral stress is shown to be related to the radial stiffness of the soil mass constraining dilation of the shear band (Lehane & White [2005]).

3.1.2 Varying gravity scale factor

As discussed above, it is essential to ensure similarity in stress levels between model and corresponding prototype. Equation 3.1a shows that the vertical stress in the model depends on the height of the soil column above the considered soil element, the gravity scale factor times the gravitational constant (acceleration) and the soil density. Equation 3.1b indicates that the acceleration depends on the angular velocity and the radius to the considered soil element. Since acceleration increases linearly over model depth (combination of Equation 3.1b and Equation 3.1c) there is a slight variation in

Table 3.1 Scaling laws

Parameter	Scaling factor (model/prototype)
Acceleration	N
Linear dimension	$1/N$
Stress	1
Strain	1
Soil stiffness	1*
Density	1
Mass or Volume	$1/N^2$
Unit weight	N
Force	$1/N^2$
Bending Moment	$1/N^2$
Flexural Stiffness	$1/N^4$
Frequency	N
Velocity	1
Time (dynamic/inertia)	$1/N$ (Kutter [1995])
Time (diffusion/seepage)	$1/N^2$ or $1/N$** (Kutter [1995] and Muir Wood [2004])
Time (creep)	1 (Muir Wood [2004])

*for medium strain deformation response, the optimum approach to ensure some resemblance is to invoke critical state soil mechanics (Muir Wood [2004]).

**scaling of pore fluid to equalize scale factor for diffusion and dynamic time (Muir Wood [2004]).

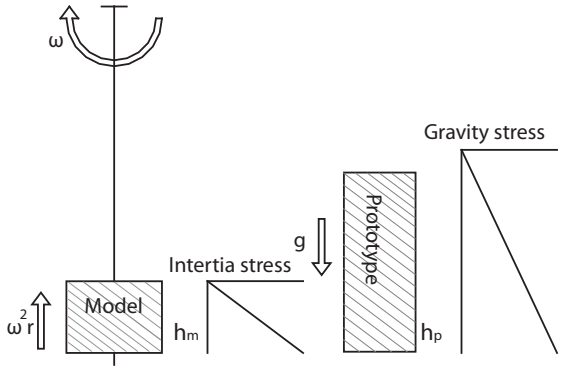

Figure 3.1 Inertia stresses in a centrifuge model and corresponding gravitational stresses in prototype, modified from Taylor [1995]

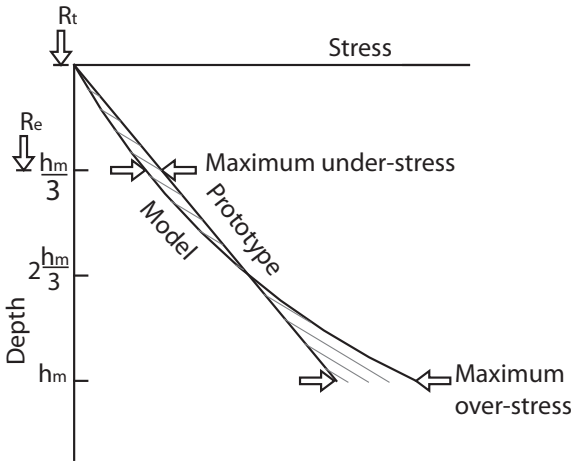

Figure 3.2 Comparison of stress variation with depth in a centrifuge model and its corresponding prototype, modified from Taylor [1995] and Schofield [2005]

acceleration throughout the model (depicted in Figure 3.2). An optimization in correspondence between model and prototype is obtained by determining the required acceleration at one-third of the height of the model (Schofield [1980] and Taylor [1995]).

$$\sigma_{vm} = \rho \cdot N \cdot g \cdot h_m \quad (3.1a) \qquad N \cdot g = \omega^2 \cdot r \quad (3.1b) \qquad \omega = \frac{v}{r} \quad (3.1c)$$

3.1.3 Saturated soils

During dynamic lateral loading of a pile; consolidation, seepage and other dynamic inertia events such as turbulent flow take place. Consolidation is a coupled process of deformation and pore fluid flow. Pore fluid flow is influenced by generation, diffusion and dissipation of excess pore pressure and depends on the coefficient of consolidation, time and drainage path to the power two. If the same soil is used for the model as in the prototype the scale factor for time equals $1/N^2$ (Kutter [1995]). The decrease of consolidation time is a result of reduced geometrical scale of the model (Taylor [1995]). When dealing with dynamic inertia events, the scale factor for time equals $1/N$ (Muir Wood [2004]). For laminar flow problems in porous media, where inertia forces are unimportant, this can be ignored (Kutter [1995]).

In order to properly capture pore pressure generation by unifying the time scaling factor for dynamic and consolidation events, the viscosity of the pore fluid needs to be increased, e.g. with a chemical substance (Taylor [1995]) such as melotose and glycerol. However, there is a possibility that contact behaviour between particles and damping behaviour are affected or incorrectly scaled. Ellis et al. [1998] determined that there is an increase in damping at small strain, due to the presence of pore fluid with high viscosity. This could be due to viscous energy dissipation in the pore fluid, acting in addition to the soil damping. The soil stiffness properties are not affected by applying another type of pore fluid.

3.1.4 Particle size effect

Generally similar soil is used in the model and in the prototype, to ensure similar mechanical properties of the soil (Bolton & Lau [1988]). rain sizes are un-scaled because of the similarity in soil causing a discrepancy between used and desired particle size. During pile installation, deformation of the shear band takes place at the interface between the soil and structure (§2.3). The thickness of this shear band depends on the average grain size (particle) and pile roughness. The shear band thickness typically is about 10 – 15 times the average grain size (Garnier & König [1998] and Muir Wood [2002]). Since soil particles are not scaled down to a model sized particle, the shear band - depending on the pile roughness - could become unrealistically wide (Lehane et al. [2005]). Boulon [1986] and Foray et al. [1998] demonstrated that a scale effect in shaft friction measured on model piles can be expected due to localization of deformations and the influence of interface dilative properties, which is higher in the model than in the prototype. In fact, displacement and interface behaviour can better be controlled by the particle diameter. Some of the problems associated with reduced model displacement could be overcome by reducing particle size whilst maintaining constitutive response. Possibilities are limited because particle shape is difficult to scale and abrasion of asperities occur to large particles rather than to small particles. And if particles become too small, inter particle forces become significant in relation to mechanical forces and the character of the particle interaction will change (Muir Wood [2004]).

Limiting scale effect in shaft friction due to the excessive formation of a shearband is shown by different authors (Equation 3.3). According to Foray et al. [1998] and Bałachowski [2006] the D_i/D_{50} should be 200 for dilative or contractive soils. The scale effect is determined by direct shear interface tests with constant normal stiffness (Boulon [1986]). Balachowski [1995] and Garnier & König [1998] (as cited in Dijkstra [2009]) note that a D_o/D_{50} larger than 100 is necessary for reducing the scale effect. This was established by performing lateral tension loads and torsional loads on model piles. These tests are performed on rectangular closed-ended piles and could only be relevant for fully plugged open-ended piles.

$$\left(\frac{\text{mean soil particle size}}{\text{Inner pile diameter}}\right)_m = \left(\frac{\text{mean soil particle size}}{\text{Inner pile diameter}}\right)_p \tag{3.2}$$

Correct modelling of interaction between pile and soil requires a specific ratio of particle size over pile wall thickness (Equation 3.3). Nguyen et al. [2011] mentions that ratio of pile wall thickness over average grain size should be larger than 10 to minimize scale effects. Randolph [2012] cannot confirm that there has ever been a definitive test for assessing a sufficient t/D_{50} ratio of 10. According to various authors the ratio of key structural dimension to average particle size should not be less than 15 – 30 (described by Ovesen [1979] according to De Nicola & Randolph [1997], Dyson & Randolph [2001] and Verdure et al. [2003]).

$$\left(\frac{\text{mean soil particle size}}{\text{Pile wall thickness}}\right)_m = \left(\frac{\text{mean soil particle size}}{\text{Pile wall thickness}}\right)_p \tag{3.3}$$

Regarding grain effects on soil-pile interaction for laterally loaded piles no significant effect was detected in modelling of model tests with D_o/D_{50} larger than 44 (Nunez et al. [1988]) or D_o/D_{50} larger than 60 (Remaud et al. [1998]).

3.1.5 Soil plugging behaviour

When the pile is installed (driven or jacked), a column of soil enters the pile. When the height of the soil column entering the pile is lower than the penetration depth of the pile, this is considered to be partially or fully plugged (also discussed in §2.3.1). Fully or partially plugged installation could be identified by the incremental filling ratio. This plugging behaviour positively influences the axial bearing capacity of the soil because of increasing shaft friction inside the pile. Large diameter piles in granular material tend to rely on pile tip resistance. As inner diameters increase the possibility of plugging of the pile decreases (becomes unrealistic) because it is harder to create a shear resistance large enough to activate a plug. It was found that plug length increased with increasing relative density of the soil during driving, and decreased with increasing relative density during jacking (De Nicola & Randolph [1997]). This is in contrast to sleeved-ended driven piles for which it was found that during jacking the height of the soil column for open-ended piles was higher than for sleeve-ended piles, contrary to the purpose of the internal sleeve. These findings show that, in absence of dynamic effects, high normal stresses are locked into the soil plug, increasing the possibility of plugging (De Nicola & Randolph [1997]). As presented in Equation 2.1, it is highly unexpected in prototype, and therefore unwanted for the model pile, to plug during centrifuge testing.

3.1.6 Boundary conditions of strongbox

Boundary conditions are important; (*i*) when simulating repeated dynamic and seismic loading (boundary wave reflection) in complex models (Taylor [1995]) and (*ii*) during the formation of shear planes and convection of soil volume due to cyclic lateral loading. According to Barton et al. [1983] the soil should extend radially to a distance of 35 pile diameters and to a depth of 30 pile diameters during lateral loading in order to reduce the boundary effect on the formation of shear planes. Prakasha et al. [2005] mentions that the depth from tip to base of the container should preferably be twice the diameter. According to De Nicola [1996] the spacing between pile and boundary should be at least 6 pile diameters in case of open-ended pile installation. Schnaid & Houlsby [1991] presents a more conservative consideration; the distance from closed-ended piles to the nearest boundary should be larger than $20D_o$ for very dense sands and $15D_o$ for loose sands.

Although rectangular containers are often used, circular containers are useful due to their lateral stiffness and light mass (Taylor [1995]). Circular containers have the advantage that with the least amount of material, a maximum soil area can be created. In order to minimize boundary effects a container known as 'stacked-ring', with its impedance similar to that of the medium, can be used.

3.1.7 Conclusion

Centrifuge modelling presents the possibility to simulate a prototype full-scale model/event in a small-scale model in order to investigate the system behaviour. It allows the reproduction of linear increasing effective stress profile over depth. Important scaling effects are mentioned and will be further applied in the model set-up for investigating cyclic lateral loading event as described in §3.2. The effect of a varying gravity scale factor will be reduced by applying the acceleration at one-third of the height. The tests will be performed in dry material because of practical limitations and limiting knowledge in scaling of pore fluid. Regarding grain size effect on pile installation; the structural dimensions compared to the average grain size will be evaluated using recommendations from De Nicola & Randolph [1997]. According to which; t/D_{50} ought to be larger than 10 and D_i/D_{50} larger than 200. Boundary considerations are controlled with a criteria of 6 pile diameter between pile and boundary of the strongbox as mentioned by De Nicola [1996]. The grain size effects on soil-pile interaction for laterally loaded pile should suffice a D_o/D_{50} of 44 (Nunez et al. [1988]) or 60 (Remaud et al. [1998]).

Figure 3.3 Delft University of Technology centrifuge

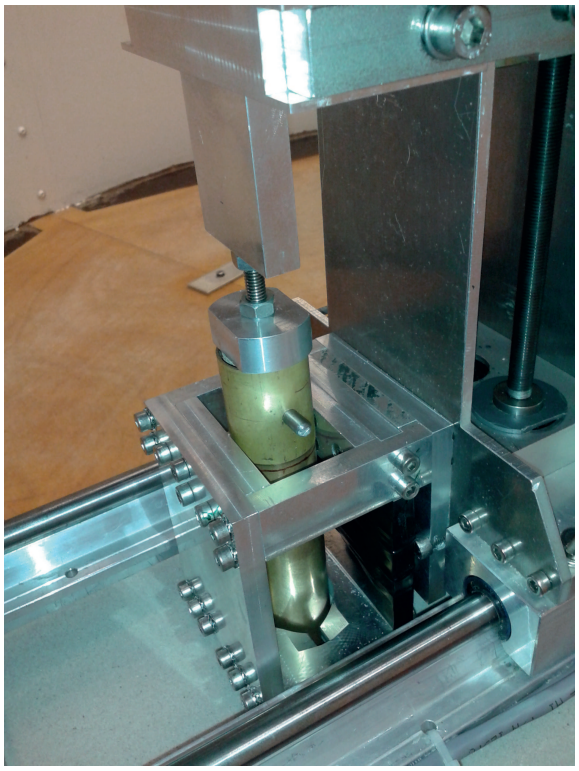

Figure 3.4 Load mechanism installed on load frame, scaled monopile and actuator

3.2 Experimental apparatus

3.2.1 The Delft University of Technology centrifuge

The centrifuge at the Delft University of Technology was built in 1990 by Allersma and co-workers and is located in the Geo-Engineering lab at the Faculty of Civil Engineering and Geosciences. After disassembling of the centrifuge the system was reassembled (2009) by Dijkstra and co-workers. Figure 3.3 presents a photo of the current centrifuge. The geotechnical centrifuge at Delft University of Technology is a small beam centrifuge with a radius of 1.22 m and is equipped with all the necessary data acquisition and camera facilities for contemporary centrifuge testing.

3.2.2 New loading mechanism

The aim of the newly designed actuator is to allow for the simulation of the installation stage, whilst at the same time offering a possibility to apply a lateral load on the pile head after installation is finished. The load application of the mechanism on the free pile head is designed such that no bending moment is transferred to the pile head. To accomplish this, a transversal rod through the top of the model pile (which fits in the template of the actuator) acts as a hinge at the pile head. This is illustrated in Fig. 3.4. This new actuator allows a 106 mm vertical penetration of the model pile and 55 mm lateral displacement, which is about two times the outer pile diameter (D_o is 27.36 mm). The displacement of the pile head is measured by registering the absolute position of the actuator. To maximize the penetration length, at present no load cell is applied in between the actuator and the pile head. The idea behind this loading frame is more extensively elaborated in Appendix D.

The loading mechanism is designed such that the maximum lateral load is measured whilst preserving resolution at small loads. This is done by modelling it as clamped on both the upper and lower side of the mechanism. After construction of the frame it is calibrated for static loads, $1 \cdot g$ and

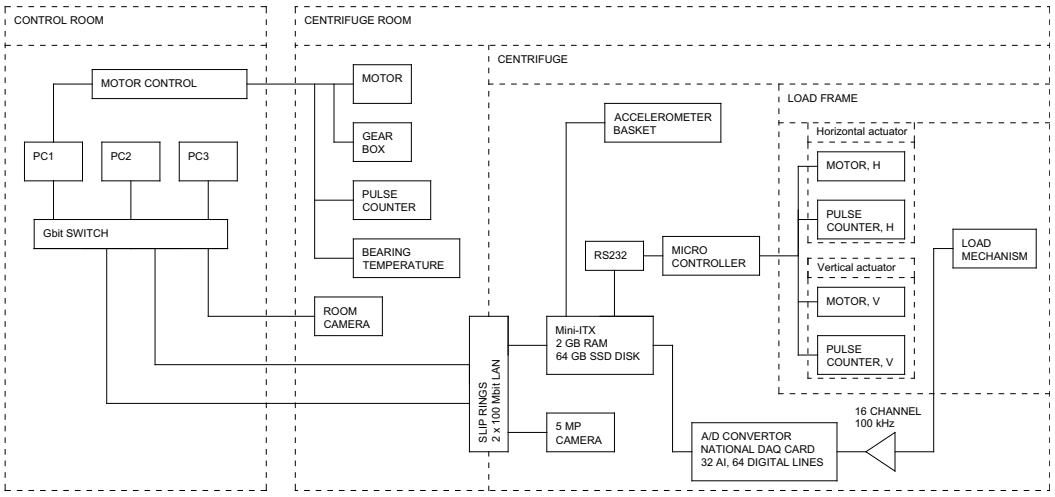

Figure 3.5 Schematic representation of centrifuge set-up, modified from Alderlieste [2011]

$N \cdot g$ conditions. This ensures proper calibration for internal varying stresses and strains, stiffness of the load mechanism and hysteresis of the loading frame during $N \cdot g$ loading of the pile. Temperature, aging and noise in the measurements also have an influence on the measured load. However, this is assumed to be negligible compared to the load components. $1 \cdot g$ calibration is done with a load higher than the load applied during testing to reduce the effect of yielding material. Eventually a 0.1% accuracy of the strain gauges is expected (Van Beek [2012]). Figure 3.5 presents a schematic representation of the centrifuge set-up and its equipment for all the necessary data acquisition.

3.2.3 Pile installation methods

The installation method in the centrifuge can be subdivided into three types: Monotonic installation where the pile is continuously pushed into the sand at a certain rate (De Nicola & Randolph [1999] at 0.5 mm/s, Lehane et al. [2005] at 0.2 mm/s and Lundberg et al. [2012] at 1.0 mm/s), jacked installation where the pile is installed in a series of jacking strokes and pseudo-dynamic installation where the pile is installed in a series of jacking increments and extraction. Monotonic installation present the largest increase in lateral stress in comparison to jacked or pseudo dynamic installation (Lehane et al. [2005]). In reality it is almost impossible to monotonically install a pile in a single stroke Dijkstra [2009]. Pile installation at the TUD centrifuge can either be performed by monotonically jacking or staged jacking. Because of practical limitations the pile is monotonically jacked in one single stroke at a rate of 0.5 mm/s.

3.3 Model properties

3.3.1 Soil properties

The model pile tests are performed in a homogeneous single layer of dry sand with a varying relative density of 60 ± 3% and 80 ± 3%. The error of 3% is calculated by assuming a possible difference in soil sample height of two average grains sizes and a surface settlement of 0.3 mm (Alderlieste [2011]) during centrifuge testing. The sand consist of uniformly graded quartz grains, with a D_{50} of about 230 μm, which is representative for North Sea soil conditions. In order to find the maximum friction angle, plane strain direct shear tests are performed to examine dilation of the material for various soil states (density and stress). All samples were prepared by pouring dry soil into a direct shear membrane using a funnel. The initial goal was to use Bolton [1986] (Equation 3.4) to define the peak friction angle (ϕ_{max}). But since dilation measurements differed significantly from the calculated

Table 3.2 Soil properties

Property	Symbol		Unit
Particle density	γ_s	2645.7	$[kg/m^3]$
Average grain size	D_{50}	230	$[\mu m]$
Maximum void ratio	e_{max}	0.82	$[-]$
Minimum void ratio	e_{min}	0.54	$[-]$
Constant volume friction angle	ϕ'_{cv}	30.1 ± 1.0	$[^\circ]$
Peak friction angle (I_d= 60 ± 2%)	ϕ'_{max}	31.5 ± 0.6	$[^\circ]$
Peak friction angle (I_d= 80 ± 2%)	ϕ'_{max}	36.5 ± 0.6	$[^\circ]$

Table 3.3 Interface characteristics

Property	Symbol		Unit
Constant volume interface friction angle	ϕ'_{cv}	13.2 ± 1.2	$[^\circ]$
Peak interface friction angle (I_d= 60 ± 2%)	δ'_{max}	13.3 ± 1.0	$[^\circ]$
Peak interface friction angle (I_d= 80 ± 2%)	δ'_{max}	17.6 ± 2.2	$[^\circ]$

values, the decision was made to perform another series of tests to define the ϕ_{max} for a larger relative density. The significant difference could be due to overestimation of the plane strain angle of friction of highly dilatant soils (Jewell [1989]) and the mathematical simplicity of the Bolton's rule. Besides that the measured values are influenced by both vertical and top boundary conditions of the direct shear box. The angle of internal friction at constant volume angle (ϕ'_{cv}) of the soil is 30.1° ± 1.0°. The peak friction angle (ϕ'_{max}) for both densities are 31.5° ± 0.6° and 36.5° ± 0.6° (averages) for 60 ± 2% and 80 ± 2% respectively. The soil properties are summarized in Table 3.2 and further elaborated in Appendix B.

$$\phi'_{max} = \phi'_{cv} + 0.8 \cdot \psi'_{max} \tag{3.4}$$

3.3.2 Pile and interface properties

The model pile, depicted in Figure 3.6, is designed to properly scale the lateral bending stiffness of a prototype pile Alderlieste [2011] and to prevent plugging during installation (large D_o/D_{50}). The acceleration during centrifuge flight is $76 \cdot g$ and $48 \cdot g$ at two third of the model (as discussed in §3.1.2 and depicted in Figure 3.2), resulting in different prototype piles (Table 3.4).

The pile roughness plays an important role during installation because of dilative properties of soil and pile interface as discussed in §3.1.4 and §2.3. The maximum height of the roughness profile (R_z) of the pile is 1.54 μm and the mean deviation of the roughness profile (R_a) is 0.37 μm. The low normalized roughness (R_n) of 0.007 implies a smooth interface and the dilative behaviour of the shear band is expected to be low (Paikowsky et al. [1995] and Garnier & König [1998]).

The maximum interface friction angles (δ_{max}) are 13.3° ± 1.5° and 17.4° ± 3.0° for I_d= 60 ± 2% and I_d= 80 ± 2% respectively. The average constant volume interface friction angle (δ_{cv}) for this type of soil is 13.0° ± 2.0° (Appendix B).

3.3.3 Scalling limitations

Contrary to the general limitations of scaling as discussed in §3.1, this section discusses the mitigation for correct scaling of the interaction between pile and soil. As mentioned in §3.1 there is a varying gravity scale factor over depth and width of the strongbox. Figure 3.7 depicts these varying gravitational fields over the strongbox for the two acceleration levels at which the tests are conducted.

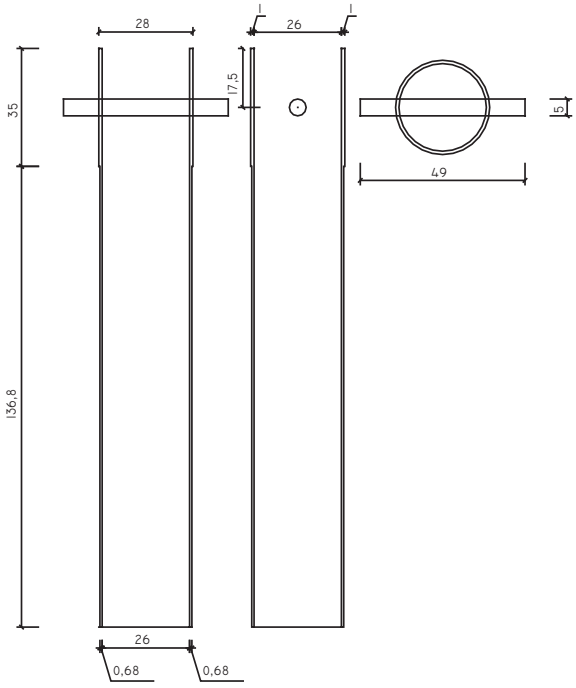

Figure 3.6 Model pile

Table 3.4 Characteristics prototype and model pile

	Prototype pile $76 \cdot g$	**Prototype pile** $48 \cdot g$	**Model pile**	**Unit**
D_o	2.1	1.31	0.02736	$[m]$
t	0.052	0.032	0.00068	$[m]$
L_{emb}	10.3	6.45	0.135	$[m]$
L/D	5.00	5.00	5.00	$[-]$
A	0.089	0.035	1.52E-05	$[m^2]$
E	110.00	110.00	110.00	$[GPa]$
I	0.17	0.026	5.07E-09	$[m^4]$
EI	1.93E+10	2.91E+09	5.58E+02	$[Nm^2]$

Because of the significant arm length of the TUD centrifuge, the variation of the gravitational field is limited.

Since generally the same material is used as in the prototype situation, it is almost unpractical and impossible to correctly scale the pile wall thickness in a way that it satisfies Equation 3.3. In order to satisfy continuum conditions, the average particle size of the soil should be one-tenth of the pile wall thickness (Equation 3.5, De Nicola [1996]). In these centrifuge tests, the ratio t/D_{50} is about 3. According to De Nicola [1996] the ratio D_i/D_{50} should be at least 200, whereas in these centrifuge tests, the ratio D_i/D_{50} is about 113. Regarding the grain size effects on soil-pile interaction for laterally loaded piles the ratio suffices the values described in §3.1.4. Installation of an incorrectly scaled pile could have a negative effect on the legitimacy of the model, i.e formation of shear band and distortion of soil resulting in erroneously scaled installation effects, could influence lateral pile-soil behaviour.

$$\frac{D_{50}}{t} \leq \frac{1}{10} \tag{3.5}$$

Due to the lack of experience in scaling of consolidation and dynamic events with viscous fluids, dry sand is used. Therefore modelling of time for consolidation and dynamic events, both during pile installation as well as during lateral loading of the pile are not taking into account, the tests performed only apply for fully drained conditions. Note that dry soil causes an increase in effective stress in comparison to offshore conditions and will have a positive effect on lateral soil capacity.

There are other restrictions that need to be dealt with regarding the geometrical considerations. The strongbox has been specifically designed for the centrifuge of the Technical University of Delft. This strongbox consists of a steel basis and an aluminium extension. The internal dimensions are 170 mm, 238 mm and 222 mm (H, L and W). This means a spacing of $3.85D_o$ between the wall and the pile, and $1.3D_o$ between the bottom of the pile and the bottom of the strongbox (B_1 and B_2 in Figure 3.9). As mentioned in §3.1.4 the distance to the closest boundary should be larger than $6D_o$ (De Nicola [1996]) during installation, due to practical limitations this value is not achieved. The boundary conditions are irrelevant for small lateral displacements (Alderlieste [2011]).

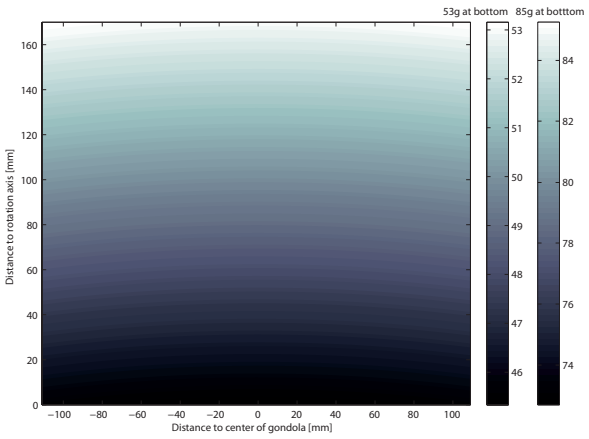

Figure 3.7 Gravity scale factor over depth and width strongbox

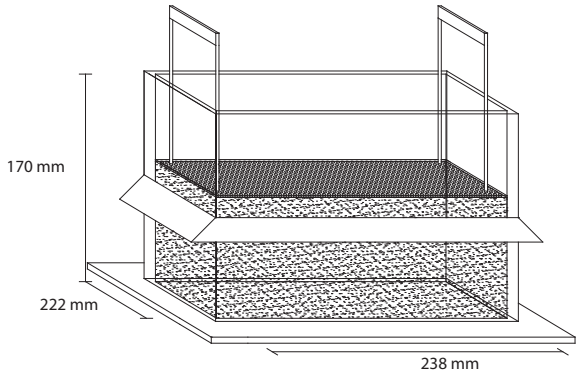

Figure 3.8 Strongbox and sample preparation

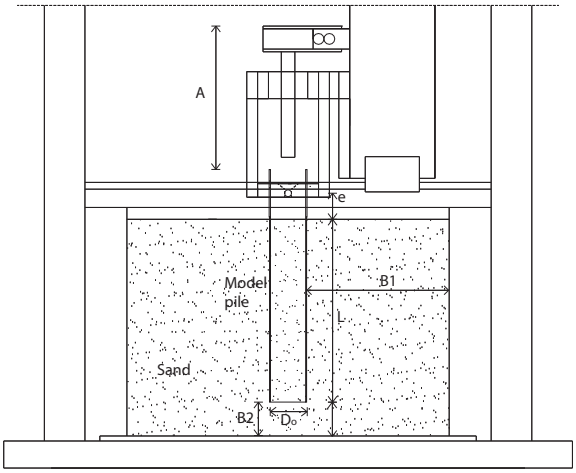

Figure 3.9 Installation amplitude, embedded length and eccentricity

3.4 Experimental program

3.4.1 Sample preparation and density

Loose samples with a relative density of 60 ± 3% are prepared by incrementally filling the strongbox using a funnel. Material is dispersed over a sieve (see Figure 3.8) wich is subsequently retracted after each incremental filling step, creating a very loose sample. After the necessary amount of soil is dispersed in the strongbox, vibrations are applied to achieve the desired average density of the soil. Because of the uniformity of the sand, there is no graded layering of material. This method does not necessarily produce a homogeneous layer of soil. However, the reproducibility and consistency of this method suffices to meet objectives. Denser samples with a relative density of 80 ± 3% are prepared by the same incremental filling sequences but the material was densified up to the required volume in the strongbox by applying longer vibration and a surcharge load on top of the sample.

3.4.2 Test procedure and details

After preparation of the sample, installation of the strongbox and placing of the pile, different procedures are followed for the installation of the piles. In order to systematically investigate the installation effect only the initial density (60 ± 3% to 80 ± 3%) and installation condition ($1 \cdot g$, $48 \cdot g$ and $67 \cdot g$) (i.e. installation sequences as shown in Table 3.6) are varied. Table 3.6 presents these sequence for both low stress level installation ($1 \cdot g$) as installation at elevated stress level ($48 \cdot g$). As presented

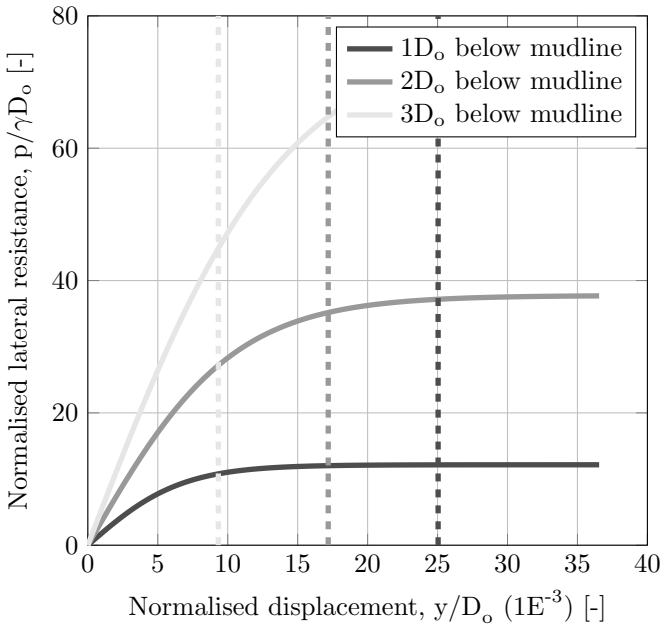

Figure 3.10 p-y curves and accompanying lateral displacement during testing

Table 3.5 Soil parameters for I_d is 60% and model dimensions for N is 53

Parameter		Unit
I_d	60	[%]
ϕ'_{max}	31.8	[°]
ϕ'_{cv}	31.1	[°]
γ'	16	$[kN/m^3]$
C_1	2.1	[−]
C_2	2.8	[−]
C_3	30	[−]
k	13600	$[kN/m^3]$
N	53	[−]
D_o	1.31	$[m]$
L_{emb}	6.45	$[m]$

in this table both sequences end with a similar lateral loading scheme - amplitude, frequency and amount of cycles - before stopping the centrifuge. Since plugging of the pile is undesirable, initial tests are performed at higher stress level. These tests indicate, via visual observation, that plugging did not occur.

The loading set-up is depicted in Figure 3.9. Dimensions such as eccentricity (e, $0.71D_o$), distance to vertical boundary (B1, $3.85D_o$), distance between bottom and pile tip (B2, $1.3D_o$), embedded pile length (L, $5D_o$) and installed pile length (A1, $3.9D_o$) are kept constant during the experiment. Despite of geometrical optimization (i.e. not using a load cell) the installation length of the pile ($3.9D_o$) was not equal to the entire pile length ($5D_o$), in total $1.1D_o$ was pre-installed at $1 \cdot g$.

Multi-directional loads that occur in prototype conditions are modelled as two-way cyclic loading. This is a simplified representation of loading without inertia or damping. The loading applied in the model is an idealized loading necessary for systematically approaching the test objective (Byrne et al. [2010]). Displacement of the loading frame is measured by registering the absolute position of the actuator.

The displacement of 1 mm ($0.037D_o$) is considered to be large strain. Figure 3.10 demonstrates this by depicting several p-y curves and the accompanying lateral displacements (both p-y displacements as maximum displacements of the pile during loading) at various points below the mudline. It is clear that the displacement of the pile is in the plastic zone of the p-y curve (not in the small strain elastic zone). Parameters used for the calculation of the p-y curves are presented in Table 3.5 and the origin of these parameters is more extensively elaborated in Appendices A, B, C.

Table 3.6 Test execution details

$1 \cdot g$ **installation**	$N \cdot g$ **installation**
Monotonically jack the pile 106 mm at 0.5 mm/s	Slowly spin up of the centrifuge to $N \cdot g$
Slightly retract the actuator	Monotonically jack the pile 106 mm at 0.5 mm/s
Slowly pin up of the centrifuge to $N \cdot g$	Slightly retract the actuator
Cyclically displace the load frame with a predefined amplitude of 1 mm, a velocity of 0.23 mm/s and 200 cycles	
Stop the centrifuge	

3.5 Conclusion

The Delft University of Technology centrifuge is used to simulate prototype conditions in a scaled model. A new actuator is designed, allowing for the simulation of the installation stage, whilst at the same time offering the possibility to apply a lateral load on the pile head after installation has finished. Piles are monotonically jacked into the soil at $1 \cdot g$ and $N \cdot g$ to investigate the effect of stress conditions. Soil properties and pile interface properties are discussed. The relatively smooth pile is properly designed to scale the lateral bending stiffness (Alderlieste [2011]). The possible scaling limitations that could provoke erroneous installation effects and modelling of lateral loading are pile wall thickness over grain size, inner diameter over grain size and the distance between pile and vertical strongbox boundary considering lateral loading. This latter effect is reduced by only applying small displacements.

Table 3.7 Test details

	Test	**Test code**	**Installation condition**	**Relative density**	**Number of cycles**
			$1 \cdot g$ or $N \cdot g$ $[m/s^2]$	I_d [%]	N [−]
Set 1	1	T01-60-$N \cdot g$	$76 \cdot g$	60 ± 3	200
	2	T02-60-1 $\cdot g$	$1 \cdot g$	60 ± 3	200
	3	T03-60-1 $\cdot g$	$1 \cdot g$	60 ± 3	200
	4	T04-60-$N \cdot g$	$76 \cdot g$	60 ± 3	90
Set 2	5	T11-60-1 $\cdot g$	$1 \cdot g$	60 ± 3	200
	6	T12-60-$N \cdot g$	$48 \cdot g$	60 ± 3	200
	7	T13-80-$N \cdot g$	$48 \cdot g$	80 ± 3	200
	8	T14-80-1 $\cdot g$	$1 \cdot g$	80 ± 3	200

The acceleration level was reduced from $76 \cdot g$ in the first set of of tests (set 1) to $48 \cdot g$ in the second set of tests (set 2) because of limitations of the installation actuator

Chapter 4

Experimental results

This chapter presents the results of the centrifuge tests. §4.1 covers general observations that occurred during testing. §4.2 discusses the propagation of lateral cyclic displacement. §4.3 treats the lateral capacity of the cyclic loading tests conducted at $48 \cdot g$ and $76 \cdot g$. §4.4 presents the load-displacement loops from centrifuge tests in which lateral loading was conducted at $48 \cdot g$. §4.5 describes the change in energy necessary for carrying out a load–displacement cycles.

4.1 Introduction

Visual observations during the tests indicate that no plugging occurred during installation. Moreover, it is visible that at the end of each cyclical lateral load test the soil surface has changed near the back and front of the pile (elliptical shape in plan view). The largest disturbance is found in line with the loading direction (see Figure 4.1).

The reported pile head displacements are corrected for both the stiffness of the actuator and the hysteresis of the frame (Appendix D). For ease of comparison the initial offset of the loops are zeroed. The effect of these corrections of the loops is shown in Appendix E. Two sets of tests where stress level ($48 \cdot g$ & $76 \cdot g$) and initial soil density ($60 \pm 3\%$ & $80 \pm 3\%$) have been varied are performed.

4.2 Lateral pile head displacements

The peak lateral displacements per cycle are presented in Figures 4.2 and 4.3, for the $1 \cdot g$, $48 \cdot g$ and $76 \cdot g$ installation in soil with a relative density of $60 \pm 3\%$ and $80 \pm 3\%$. The applied pile head displacement is about $0.03D_o$ which makes the amplitude about $0.06D_o$.

The peak displacements (maximum and minimum) in Figures 4.2 and 4.3 show two phenomena, namely: (i) the top of the pile is drifting away from the initial location and (ii) the absolute displacement amplitude reduces with increasing number of cycles. The first observed phenomenon seems large when comparing the final location with the initial location ($0.007D_o$ after 200 cycles) however, per cycle displacement error is limited to a maximum of 1‰ of the amplitude or $0.0002D_o$.

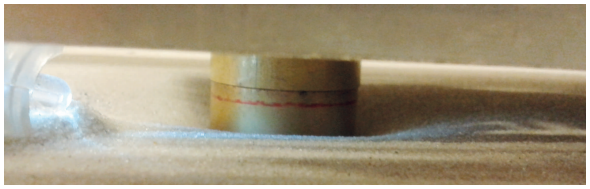

Figure 4.1 Soil surface deformation around the model pile

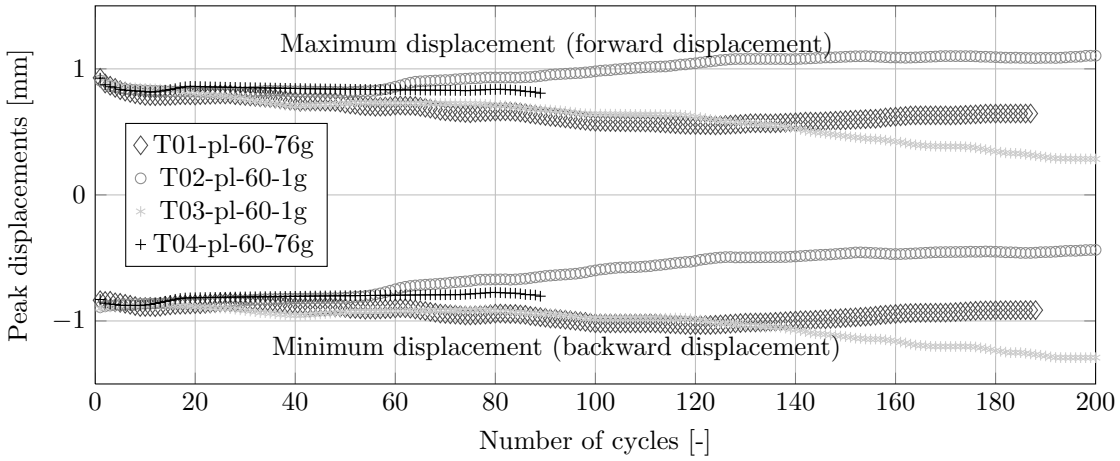

Figure 4.2 Peak displacements of the first set of tests

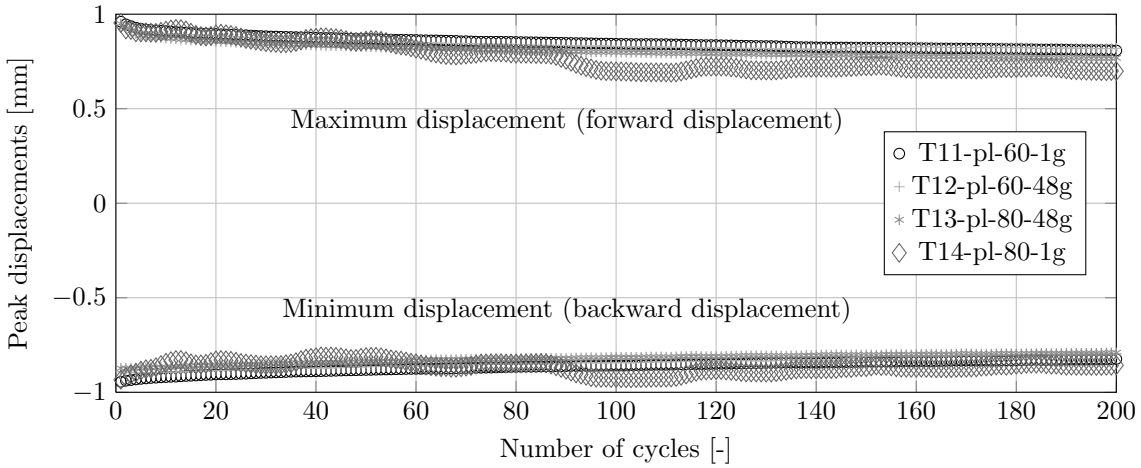

Figure 4.3 Peak displacements of the second set of tests

The second phenomenon occurs due to stiffness correction of the displacement readings, since the absolute displacement amplitude decreases with an increase in peak loads.

4.3 Lateral peak pile head loads

Figures 4.4 – 4.11 present the lateral peak loads per cycle in for the same tests as presented above. The difference in peak loads for $48 \cdot g$ and $1 \cdot g$ installation in $I_d = 60 \pm 3\%$ (Figures 4.10 and 4.11) can be attributed to subtle differences in initial relative density. The peak loads increase for every cycle, especially for the first 20 cycles (Figures 4.9 and 4.15). This stiffening phenomena (secant stiffness, shown in Figures 4.6 – 4.13) of the lateral response results from a combination of stress increase and densification of the soil.

The peak loads and secant stiffness show a similar trend when comparing the response of the forward (initial) loading direction for $1 \cdot g$, $48 \cdot g$ and $76 \cdot g$ installation. In the backward direction some differences are noticed. In contrast to the forward displacement, a progressive stiffening in the beginning is not observed (Figure 4.4). It appears that during (inclined) installation the pile already pre-loaded the actuator, which skews the loading response of the initial cycle. The peak loads are not affected by the drift in the applied displacements (e.g. Figure 4.5).

These results show that the different pile installation regimes do not significantly alter the cyclic

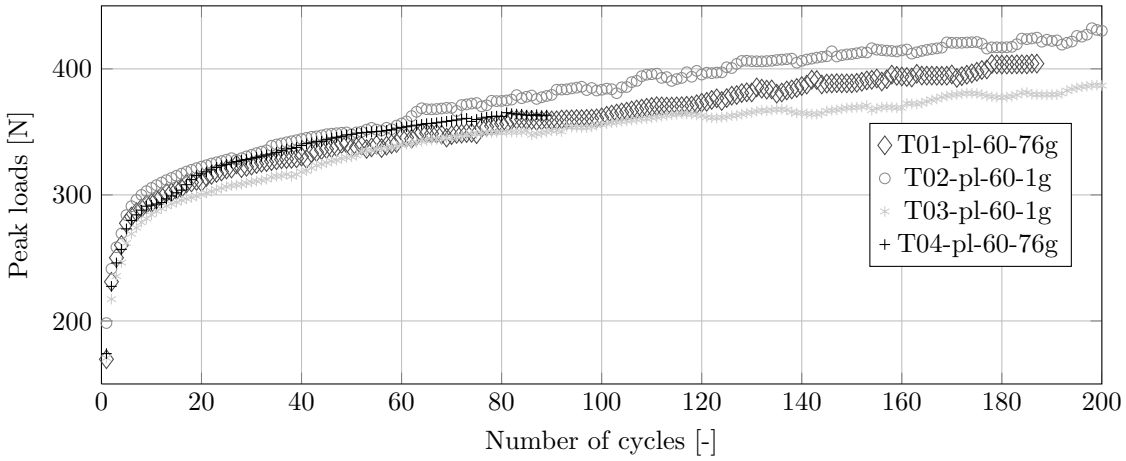

Figure 4.4 Peak loads, forward displacement (maximum), of the first set of tests

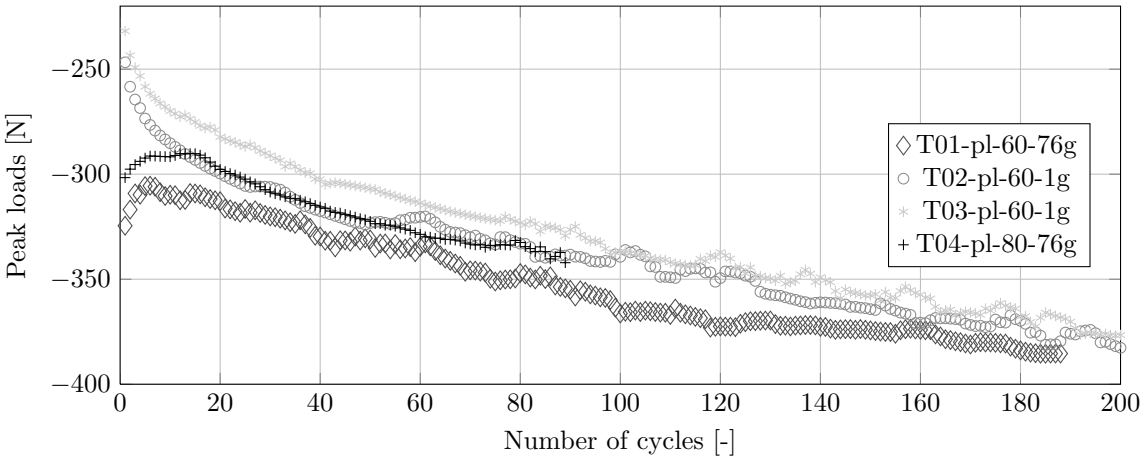

Figure 4.5 Peak loads, backward displacement (minimum), of the first set of tests

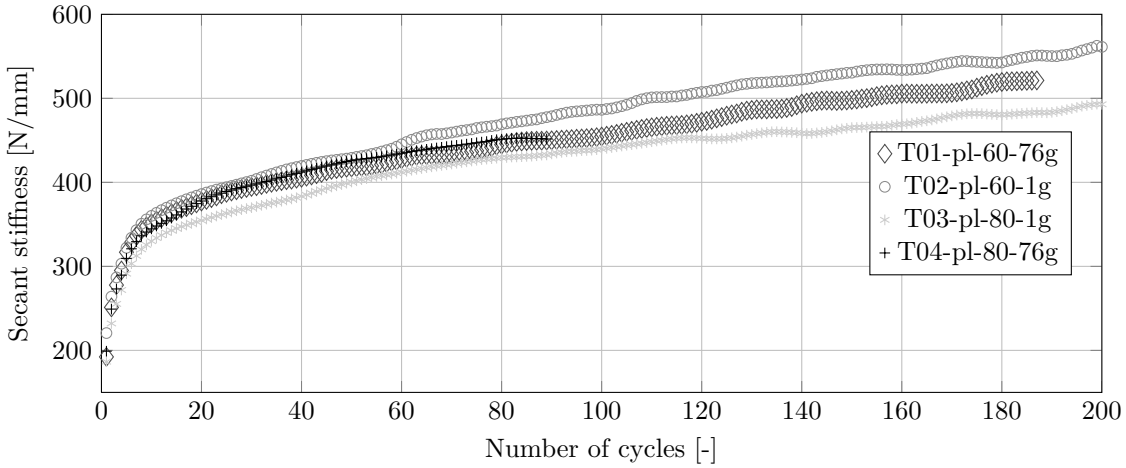

Figure 4.6 Secant stiffness, forward displacement, of the first set of tests

lateral pile response. Especially, after a larger number of cycles the differences become negligible.

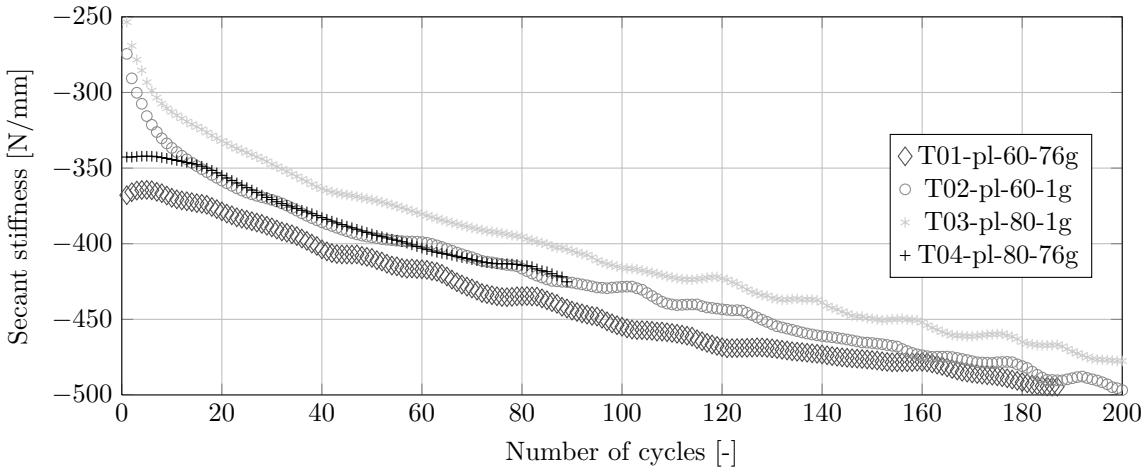

Figure 4.7 Secant stiffness, backward displacement, of the first set of tests

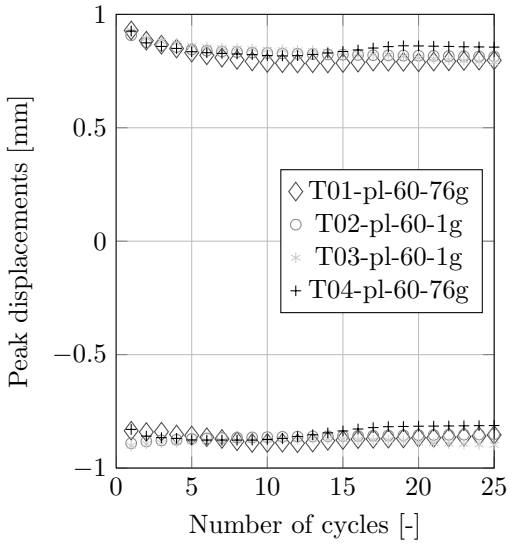

Figure 4.8 First 25 peak displacements of the first set of tests

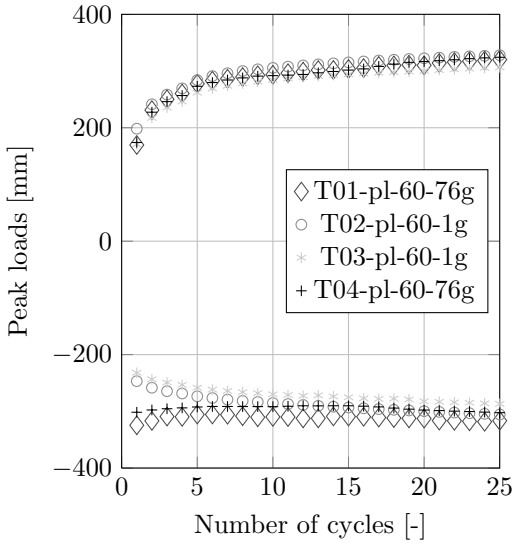

Figure 4.9 First 25 peak loads of the first set of tests

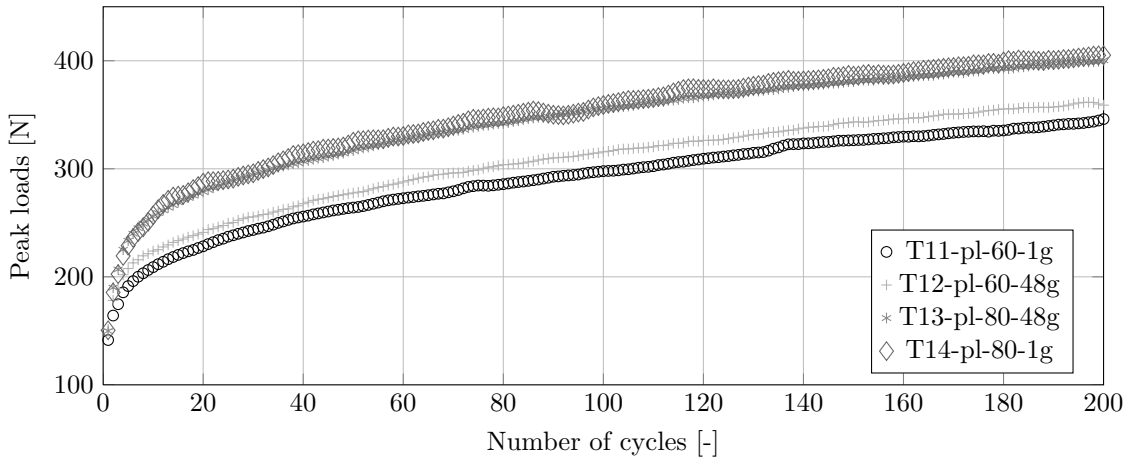

Figure 4.10 Peak loads, forward displacement (maximum), of the second set of tests

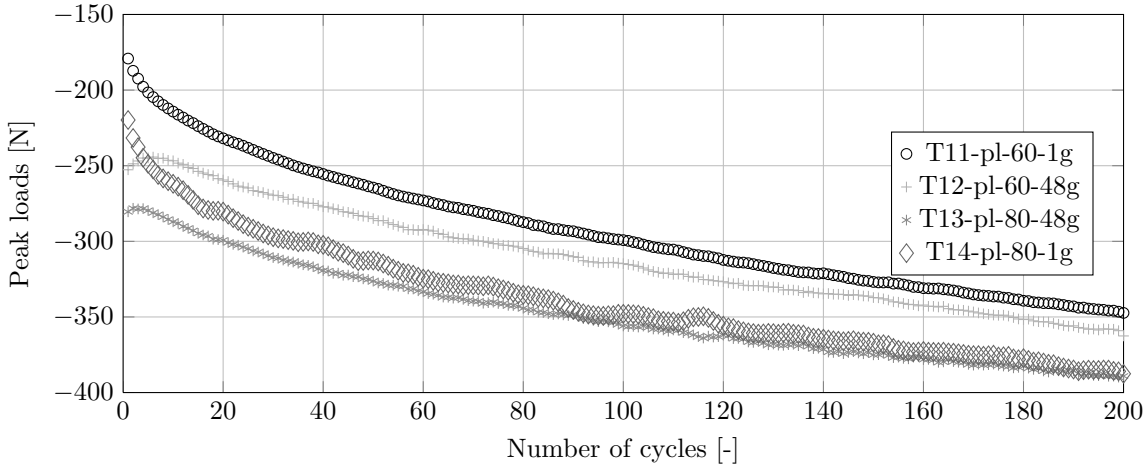

Figure 4.11 Peak loads, backward displacement (minimum), of the second set of tests

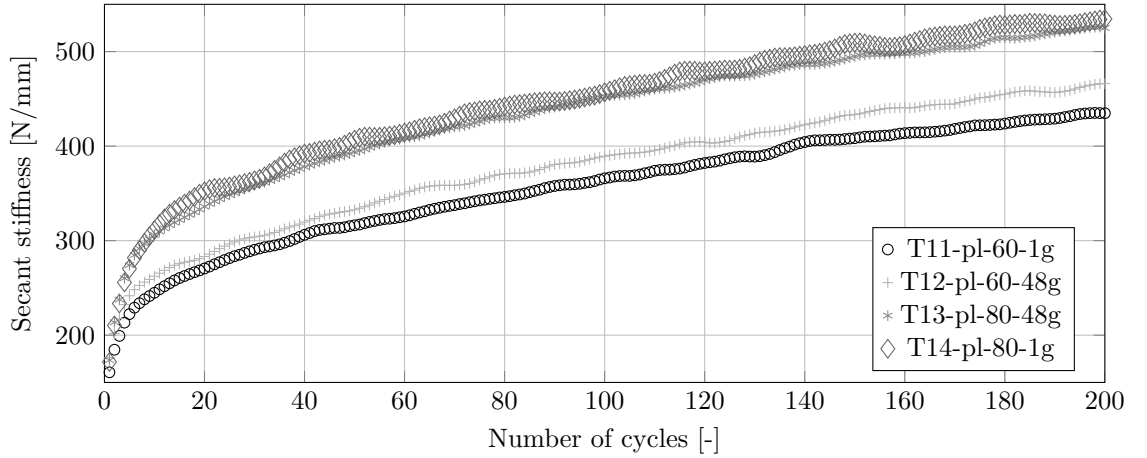

Figure 4.12 Secant stiffness, forward displacement, of the second set of tests

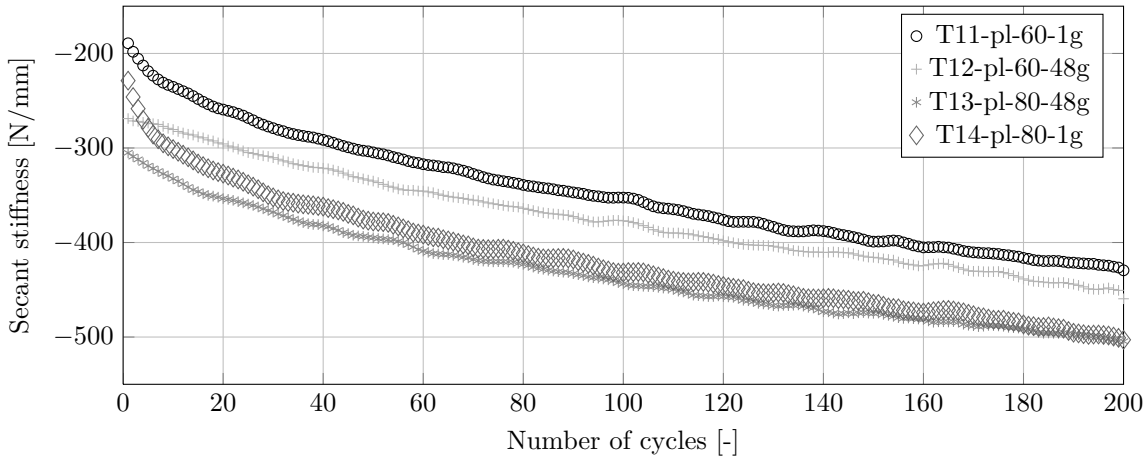

Figure 4.13 Secant stiffness, backward displacement, of the second set of tests

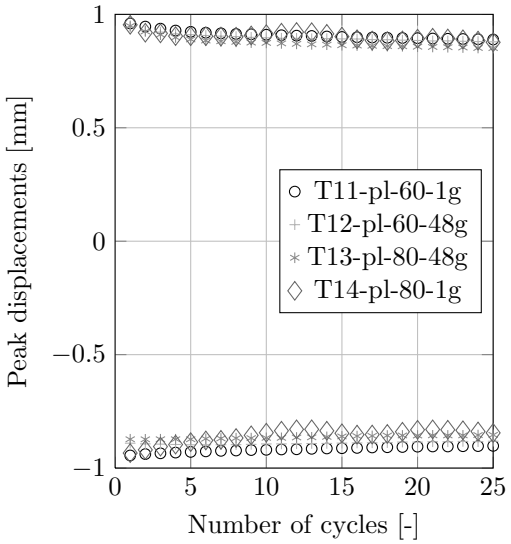

Figure 4.14 First 25 peak displacements of the second set of tests

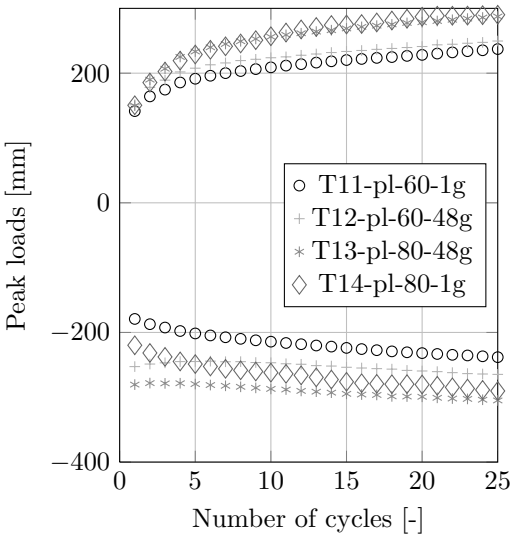

Figure 4.15 First 25 peak loads of the second set of tests

4.4 Load – displacement cycles

If the load – displacement response for the first, second, 50^{th} and 150^{th} cycle are compared (Figures 4.16 – 4.19) it becomes apparent that with increasing cycle number the differences in lateral response from $1 \cdot g$ and $N \cdot g$ installed piles vanish. The soil state of the soil near the pile after pile installation is changed due to the lateral sweeping of the pile. Although the installation effects vanish, a higher initial density still results in larger peak load and peak secant stiffness.

If the pile would be used for statically lateral loads, i.e. forward loading in the first load cycle, the differences from installation range between 1 – 5%. However, an artificial initial negative pile head load and initial response, resulting from the $N \cdot g$ pile installation, is observed in the results (Figure 4.16). The latter is highlighted by the rather large differences in load in backward loading. These differences are also swept out due to repeated loading.

All load – displacement loops show a similar response. Depending on the pile displacement the pile is gradually mobilizing passive resistance on the front and active pressures on the backside of the pile, while always mobilizing shear planes on the sides. It seems that the passive earth pressure is mobilized gradually whereas the active earth pressure decreases more rapidly after reversal of the displacement (loading direction).

The small strain stiffness of the soil in (re-)loading cannot be obtained from this test data because: (i) the rigidity and the tolerances of the spindle in the frame are too low to ensure a properly displacement controlled small strain loading/unloading cycle, hence the small strain response is not solely that of the soil (ii) the resolution of the measurement system is inadequate for measuring sub-micron displacements which is required for measuring small strains($< 100‰$ according to Jardine et al. [1986], $< 1‰$ according to Davich et al. [2004]).

4.5 Energy dissipation

The necessary energy for one cycle is the enclosed surface of the loop. The surface has been quantified by numerical integration, using the Quadrature method, of 4^{th} order polynomial fit. Figure 4.20 presents the energy dissipation of tests performed at $48 \cdot g$ (second set). Figure 4.21 shows the energy dissipation relative to cycle 2, of the second set of tests. Figure 4.20 indicates that the average energy necessary for one cycle is eventually $\approx 270\ Nmm \pm 4\%$. T12 shows an increase of about 7% from 140 cycles onwards. This could be due to a measurement inaccuracy resulting from the displacement readings. The lateral resistance for T11 is much lower than other tests (as depicted in Figure 4.17) causing a significant reduction in integrated area encompassed by the cycle (energy).

This information is inconclusive for quantifying dissipation of energy during in situ lateral loading due the relatively large applied displacements and displacement controlled loading rather than load controlled loading.

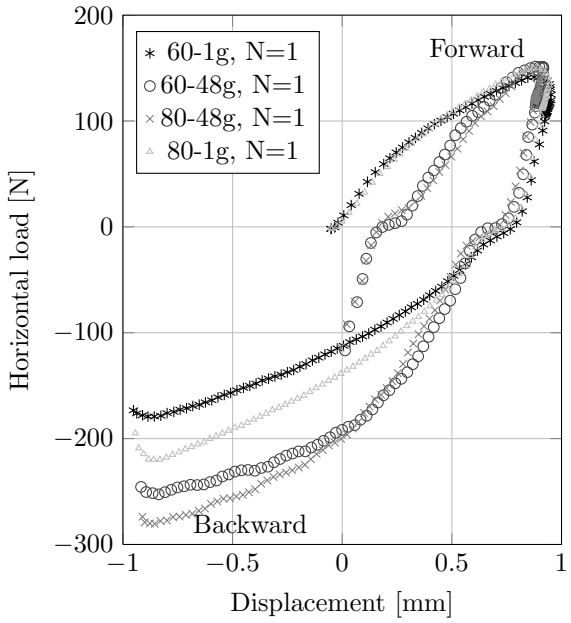

Figure 4.16 Cycle 1 of the second set of tests

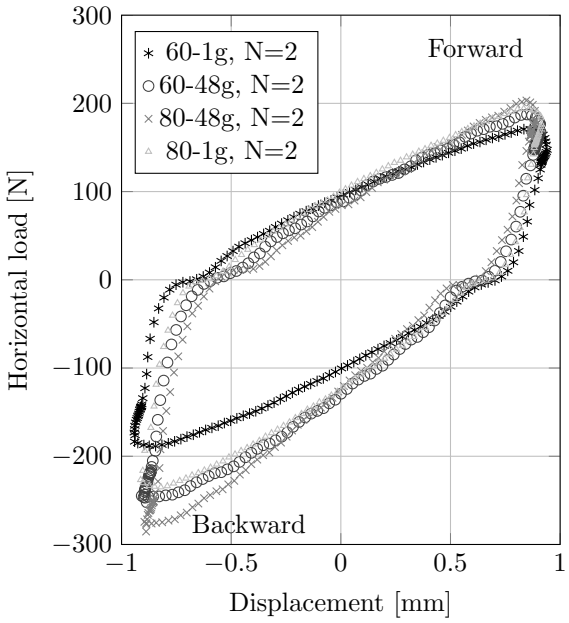

Figure 4.17 Cycle 2 of the second set of tests

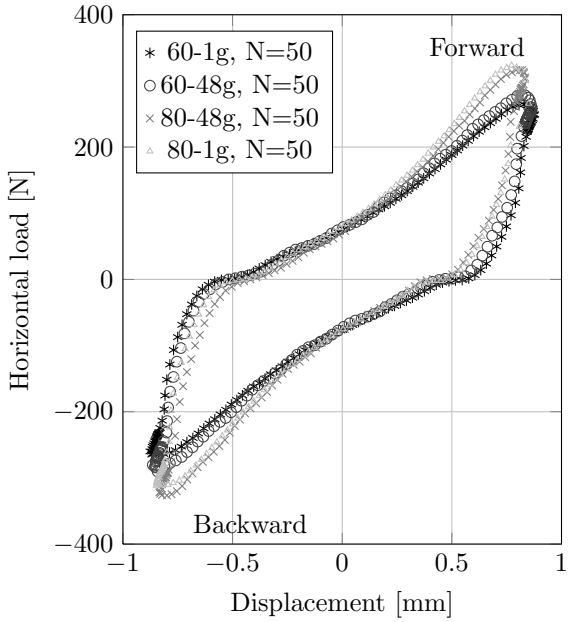

Figure 4.18 Cycle 50 of the second set of tests

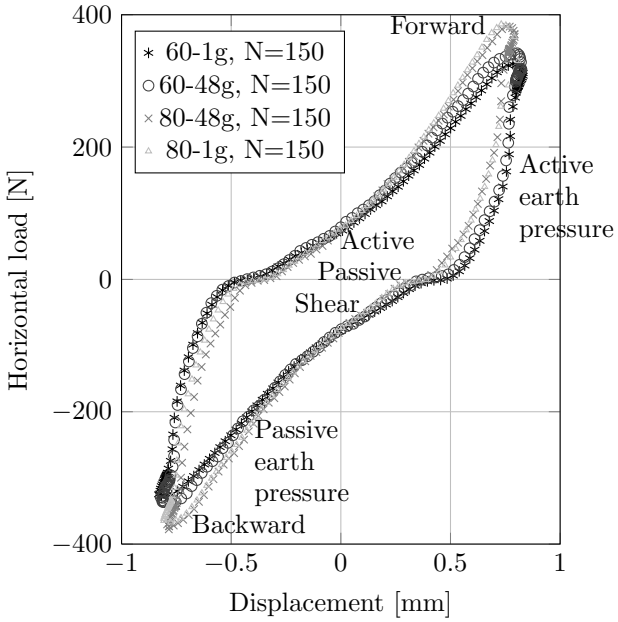

Figure 4.19 Cycle 150 of the second set of tests

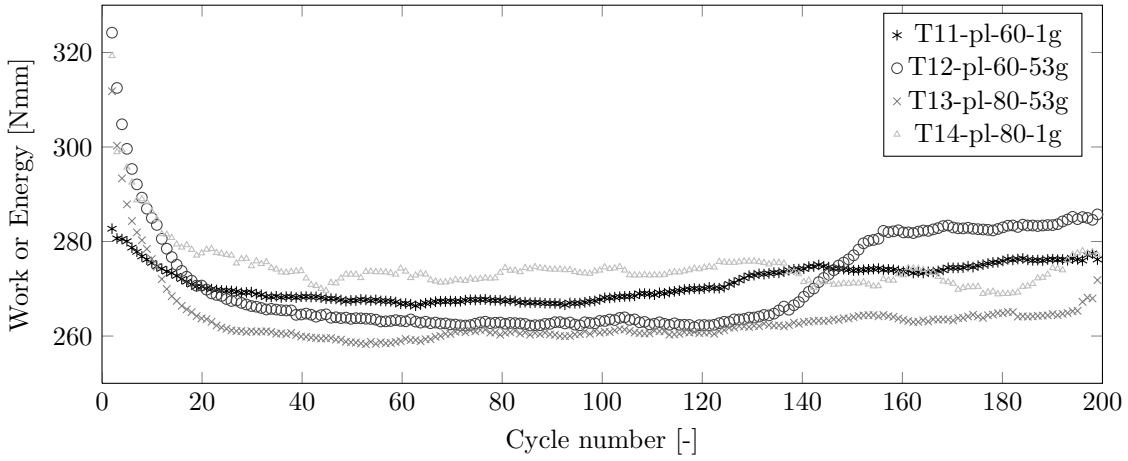

Figure 4.20 Energy dissipation of the second set of tests

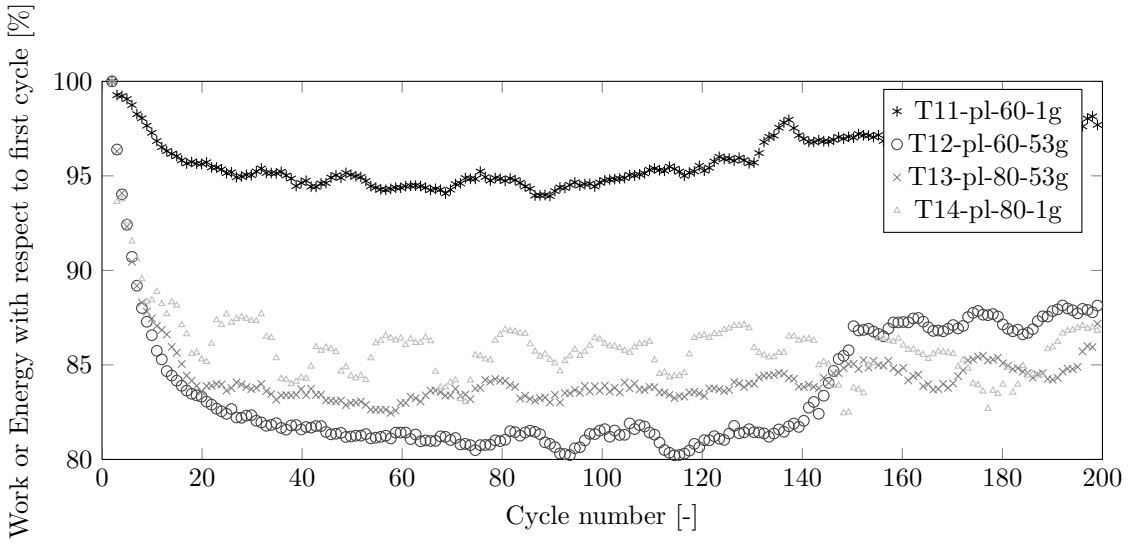

Figure 4.21 Energy dissipation relative cycle 2, of the second set of tests

Chapter 5

Conclusions

In previous research on the physical modelling of cyclic lateral capacity of piles there has been no consistency in accounting for the installation of the model pile. Before testing in the geotechnical centrifuge the piles are either installed at low stress levels ($1 \cdot g$), at elevated stress ($N \cdot g$) levels or not installed at all (pre-installed). Correct installation of an open-ended model pile is complicated by the scaling conditions. In order to improve the reliability of the interpretation of these existing tests, and future tests this study seeks to clarify the effect of the installation conditions on the subsequent tests.

The aim of this study is to investigate the effect of pile installation on the lateral response of an open-ended pile in sand. A series of tests was executed to compare the differences on the lateral pile response from monotonic jacked pile installation at low stress levels ($1 \cdot g$) and at elevated stress levels in the geotechnical centrifuge ($N \cdot g$).

A new actuator was developed to install and subsequently laterally load the monopile without interrupting the test. The novel re-design of the actuator captures the pile at the end of installation in a template. Together with the pile this template forms a hinge that only transfers lateral loads. In turn these loads are locally measured using a set of strain gauges. The model pile, $L/D = 5$, was designed in such a way that the bending stiffness is correctly scaled and no plugging will occur during installation.

The effect of initial density of the sand and the stress level on the differences between $1 \cdot g$ and $N \cdot g$ pile installation are studied in 8 centrifuge tests. The initial relative density and the acceleration level of the base line test (in duplex) are respectively $I_d = 60 \pm 3\%$ and $48 \cdot g$. The effect of a higher initial density ($I_d = 80 \pm 3\%$) or a higher acceleration level $76 \cdot g$ on the difference between $1 \cdot g$ and $N \cdot g$ pile installation has been studied in an additional set of tests. After the $1 \cdot g$ or $N \cdot g$ installation stage the pile was subjected to 200 two-way lateral load cycles at large strain amplitude ($0.03D_o$). In all these tests the lateral loading stage was performed at an elevated stress level.

The results indicate that only small differences between $1 \cdot g$ and $N \cdot g$ pile installation can be measured for all tests. In all tests the $N \cdot g$ installation initially yielded a 1 – 5% increase in lateral capacity, however after 150 load cycles this difference is diminished. A similar result is observed for the lateral stiffness response of the pile, i.e. a small initial difference evens out with increasing number of load cycles.

The individual tests results indicate that in all cases the stiffness and lateral capacity increase with the number of load cycles. Also, an increase in stress level and/or initial density results in an increase in capacity and stiffness. These gains in capacity and initial stiffness are much more substantial than the differences found between $1 \cdot g$ and $N \cdot g$ pile installation.

Chapter 6

Recommendations

In order to guide further investigations on the effect of model pile installation in sand and investigations on the subsequent (lateral) pile response in the geotechnical centrifuge, the following is recommended:

1. In the current study deviant grain size over wall thickness ratio ($t/D_{50} = 3$) and pile roughness ($R_n = 0.007$) have been chosen. This has an effect on the size of the failure mechanism underneath and adjacent to the pile. Especially, the thickness of the shear band, which typically remains constant at a width of around $10 - 15$ grains is improperly scaled. Therefore, in future tests that investigate the pile installation behaviour in detail, and rather than just observing difference, an increase of this ratio is recommended.

2. An optimization of the installation actuator is proposed in order to install piles at higher stress levels, without inclination. Rather than improving the current actuator a new design with an improvement for the vertical axis is suggested. This should reduce the bending moment on the spindle, hence improving the penetration efficiency.

3. The experiments are performed in dry sand, i.e. in fully drained conditions. Given that most monopiles are installed offshore, future research should incorporate pore water. The latter will have a significant effect on the installation effects and subsequent loading cycles. In order to properly scale the pore water response in the geotechnical centrifuge the pore fluid could be replaced by a viscous fluid such as melotose, glycerol or alternatively, the loading rate could be scaled accordingly.

4. Lateral displacement in this model set-up is constrained by both the vertical and horizontal boundaries of the strongbox ($3.85D_o$). Larger ratios of about $6D_o$, as mentioned in the report, between pile diameter and distance to the strong box boundaries are highly recommended.

5. The idealised displacement controlled loading, in the centrifuge model test, is a simplification of the by wind, wave and currents (or a combination) controlled loading spectrum occurring in reality. Therefore, load control with a more realistically scaled loading spectrum is desired instead of displacement controlled loading. Also, it is desired to expand the model set-up capabilities such that the model pile can be loaded from various directions. A good starting point for the implementation of load control is the implementation of a local PID (Proportional Integral Derivative) control loop on the load.

6. The soil behaviour of the (model) sand should be studied in more detail on element level, e.g. (cyclic) triaxial test, hollow cylinder tests, in order to feed and/or formulate more advanced constitutive models. Preferably such a model should capture nonlinear drained and undrained soil response, hysteric energy dissipation and accumulation of irreversible strain during cyclic deviatoric loading (e.g. bounding surface plasticity models).

7. The lateral stress dependent soil behaviour could be more accurately investigated in the geotechnical centrifuge by measuring local displacement and instrumentation of the model pile with strain gauges. This additional instrumentation contributes to the study in the development of stresses, bending moments and displacements at specific points along the model pile.

8. For the operation of wind turbines the natural frequency and the damping properties of the soil are of great interest. To better describe these phenomena a proper characterization of the initial stiffness and damping at small strain are required. Therefore, the set-up needs to be optimized for measurement of small strain soil-structure response. Apart from the instrumentation of the model pile with strain gauges to give more insight in the stress and bending moment of the pile during installation and loading, the acceleration and inclination of the model pile should also be measured. As a result the small strain stiffness and damping response of the pile-soil response are captured from the natural frequency after impulse loading.

Bibliography

Achmus, M., Abdel-Rahman, K., & Kuo, Y. (2007). Numerical modelling of large diameter steel piles under monotonic and cyclic horizontal loading. In *Tenth International Symposium on Numerical Models in Geomechanics*, pp. 453–459. Taylor & Francis London.

Achmus, M., Kuo, Y.-S., & Abdel-Rahman, K. (2009). Behavior of monopile foundations under cyclic lateral load. *Computers and Geotechnics 36*(5), 725–735.

Alderlieste, E. (2011). Experimental modelling of lateral loads on large diameter mono-pile foundations in sand. Msc thesis, Delft University of Technology.

API (2007). *Recommended Practice for Planning, Design and Constructing Fixed Offshore Platforms - Working Stress Design*. American Petroleum Institute. ERRATA AND SUPPLEMENT 3, AUGUST 2007.

Balachowski, L. (1995). *Différents aspects de la modélisation physique du comportement des pieux: Chambre d'Etalonnage et Centrifugeuse*. Ph. D. thesis.

Bałachowski, L. (2006). Scale effect in shaft friction from the direct shear interface tests. *Archives of Civil and Mechanical Engineering 6*(3).

Baldi, G., Bellotti, R., Ghionna, V., Jamiolkowski, M., & Pasqualini, E. (1986). Interpretation of cpt's and cptu's; 2nd part: drained penetration of sands. In *Proceedings of the Fourth International Geotechnical Seminar, Singapore*, pp. 143–156.

Bardet, J. (1997). *Experimental soil mechanics*. Prentice Hall.

Barton, Y., Fin, W., Pary, R., & Ikuo, T. (1983). Lateral pile response and p-y curves from centrifuge tests. *Offshore Technology Conference Paper number OTC 4502*.

Bekken, L. (2009). Lateral behavior of large diameter offshore monopile foundations for wind turbines. Master's thesis, Delft University of Technology.

Bienen, B., Dührkop, J., Grabe, J., Randolph, M., & White, D. (2011). Response of piles with wings to monotonic and cyclic lateral loading in sand. *Journal of Geotechnical and Geoenvironmental Engineering 138*(3), 364–375.

Bijnagte, J. & Luger, H. (2010). *D-pile Group, 3D modelling of single piles and pile groups*. Deltares.

Bolton, M. (1986). The strength and dilatancy of sands. *Géotechnique 36*(1), 65–78.

Bolton, M. & Lau, C. (1988). Scale effects arising from particle size. In *Proceedings of the International Conference on Geotechnical Centrifuge Modeling, Paris*.

Boulon, M. & Foray, P. (1986). Physical and numerical simulation of lateral shaft friction along offshore piles in sand. *3rd International Conference in Numerical Methods in Offshore Piling Nantes, France*, 127–147.

Brant, L. & Ling, H. (2007). Centrifuge modeling of piles subjected to lateral loads. *Soil Stress-Strain Behavior: Measurement, Modeling and Analysis*, 895–907.

Broms, B. (1964). Lateral resistance of piles in cohesionless soils. *Journal of Soil Mechanics and Foundation Division 90*(SM3), 123–156.

Brucy, F., Meunier, J., & Nauroy, J. (1991). Behavior of pile plug in sandy soils during and after driving. In *Offshore Technology Conference*.

Byrne, B. & Houlsby, G. (2003). Foundations for offshore wind turbines. *Philosophical Transactions of the Royal Society of London. Series A:Mathematical, Physical and Engineering Sciences 361*(1813), 2909–2930.

Byrne, B., Leblanc, C., & Houlsby, G. (2010). Response of stiff piles in sand to long-term cyclic lateral loading. *Geotechnique 60*(2), 79–90.

Campanella, R. (1988). Current status of the piezocone test. In *Proc. 1st International Symposium on Penetration Testing*, Volume 1, pp. 93–116. ISOPT.

Clauss, G., Lehmann, E., & Östergaard, C. (1988). *Meerestechnische Konstruktionen*. Springer.

Cox, W., Reese, L., & Grubbs, B. (1974). Field testing of laterally loaded piles in sand. *Offshore Technology Conference OTC 2079*, 459–472.

Craig, W. (1985). Installation studies for model piles. *Publication of: Balkema (AA)*.

Cuéllar, P., Baeßler, M., & Rücker, W. (2009). Ratcheting convective cells of sand grains around offshore piles under cyclic lateral loads. *Granular Matter 11*(6), 379–390.

Cuéllar, P., Georgi, S., Baeßler, M., & Rücker, W. (2012). On the quasi-static granular convective flow and sand densification around pile foundations under cyclic lateral loading. *Granular Matter*, 11–25.

Davich, P., Labuz, J., Guzina, B., & Drescher, A. (2004). Small strain and resilient modulus testing of granular soils. Technical report.

De Nicola, A. (1996). *The performance of pipe piles in sand*. Ph. D. thesis, The University of Western Australia.

De Nicola, A. & Randolph, M. (1997). The plugging behaviour of driven and jacked piles in sand. *Géotechnique 47*(4), 841–856.

De Nicola, A. & Randolph, M. (1999). Centrifuge modelling of pipe piles in sand under axial loads. *Geotechnique 49*(3), 295–318.

Dijkstra, J. (2009). *On the Modelling of Pile Installation*. Ph. D. thesis, Technische Universiteit Delft. ISBN: 9789085704324.

Dijkstra, J. & Broere, W. (2009). Experimental investigation into plugging of open ended piles. In *Proceedings of the ASME 28th International Conference on Ocean, Offshore and Arctic Engineering*.

Dyson, G. & Randolph, M. (2001). Monotonic lateral loading of piles in calcareous sand. *Journal of Geotechnical and Geo-environmental Engineering 127*, 346–352.

Ellis, E., Soga, K., Brandsby, M., & Sato, M. (1998). Effect of pore fluid viscosity on the cyclic behaviour of sands. In *Centrifuge 98*.

Fan, C. & Long, J. (2005). Assessment of existing methods for predicting soil response of laterally loaded piles in sand. *Computers and Geotechnics 32*(4), 274–289.

Foray, P., Balachowski, L., & Rault, G. (1998). Scale effect in shaft friction due to the localisation of deformations. In *Centrifuge 98*.

Garnier, J., Gaudin, C., Springman, S., Culligan, P., Goodings, D., Konig, D., Kutter, B., Phillips, R., Randolph, M., & Thorel, L. (2007). Catalogue of scaling laws and similitude questions in geotechnical centrifuge modelling. *International Journal of Physical Modelling in Geotechnics 7*(3), 1–23.

Garnier, J. & König, D. (1998). Scale effects in piles and nails loading tests in sand. In *Centrifuge 98*.

GWEC (2011). Global wind report. Technical report, Global Wind Energy Council.

Hasselmann, K., Barnett, T., Bouws, E., Carlson, H., Cartwright, D., Enke, K., Ewing, J., Gienapp, H., Hasselmann, D., Kruseman, P., et al. (1973). Measurements of wind-wave growth and swell decay during the joint north sea wave project (jonswap).

Heerema, E. (1978). Predicting pile driveability: Heather as an illustration of the "friction fatigue" theory. In *SPE European Petroleum Conference*.

Jaky, J. (1948). Pressure in silos. In *Proceedings of the 2nd International Conference on Soil Mechanics and Foundation Engineering*, Volume 1, pp. 103–107.

Jamiolkowski, M. (1985). New developments in field and laboratory testing of soil. *Proc. of XI ICSMFE 1*, 57–153.

Jardine, R., Potts, D., Fourie, A., & Burland, J. (1986). Studies of the influence of non-linear stressstrain characteristics in soilstructure interaction. *Géotechnique 36*(3), 377 – 396.

Jewell, R. (1989). Direct shear tests on sand. *Geotechnique 39*(2).

Kelly, R. (2001). Development of a large diameter ring shear apparatus and its use.

Klinkvort, R. & Hededal, O. (2011, October). Centrifuge modelling of offshore monopile foundation. In *Frontiers in Offshore Geotechnics II*, pp. 581–586–. CRC Press.

Klinkvort, R., Leth, C., & Hededal, O. (2012). Centrifuge modelling of monopiles in dense sand at the technical university of denmark.

Kutter, B. (1995). 3rd international conference on recent advances in geotechnical earthquake engineering and soil dynamics. *State-of-the-Art Paper 2*, 927–942.

Laue, J. (2002). Centrifuge technology. In *Workshop on Constitutive and Centrifuge Geotechnical Modelling: Two Extremes. Springman, SM, Editor. Monte Verità, Ascona, Switzerland: Swets & Zeitlinger Publishers*, pp. 75–105.

Lehane, B., Schneider, J., & Xu, X. (2005). The uwa-05 method for prediction of axial capacity of driven piles in sand. In *Proc., Int. Symp. Frontiers Offshore Geomech. ISFOG, Perth*, pp. 683–689.

Lehane, B. & White, D. (2005). Lateral stress changes and shaft friction for model displacement piles in sand. *Canadian geotechnical journal 42*(4), 1039–1052.

Lesny, K. (2010). *Foundations for Offshore Wind Turbines: Tools for Planning and Desing*. VGE-Verlag.

Lesny, K., Paikowsky, S. G., & Gurbuz, A. (2007). Scale effects in lateral load response of large diameter monopiles. In *Contemporary Issues In Deep Foundations*.

Lesny, K. & Wiemann, J. (2005). Design aspects of monopiles in german offshore wind farms. In *Proceedings of the International Symposium on Frontiers in Offshore Geotechnics*, pp. 383–389. AA Balkema Publishing.

Li, Z., Haigh, S. K., & Bolton, M. D. (2010). Centrifuge modelling of mono-pile under cyclic lateral loads. *7th International Conference on Physical Modelling in Geotechnics 2*, 965–970.

Lin, S. & Liao, J. (1999). Permanent strains of piles in sand due to cyclic lateral loads. *Journal of geotechnical and geoenvironmental engineering 125*(9), 798–802.

Little, R. & Briaud, J. (1988). Full scale cyclic lateral load tests on six single piles in sand. Technical report, DTIC Document.

Lloyd, G. & Hamburg, G. (2005). Guideline for the certification of offshore wind turbines.

Long, J. H. & Vanneste, G. (1994). Effects of cyclic lateral loads on piles in sand. *Journal of Geotechnical Engineering 120*, 225–244.

Lundberg, A., Dijkstra, J., & van Tol, A. (2012). On the modelling of piles in sand in the small geotechnical centrifuge.

MATLAB (2011). *version 7.13.0.564 (R2011b)*. Natick, Massachusetts: The MathWorks Inc.

McClelland, B. & Focht, J. J. (1958). Soil modulus for laterally loaded piles. *ASCE 123*(8), 1049–1026.

M.E.L.T (1993). *Technical Rules of Design and Calculation of the Foundations of the Works of Civil Engineering*. Ministere de l'equipement, du logement et des Transports.

Muir Wood, D. (1991). *Soil behaviour and critical state soil mechanics*. Cambridge university press.

Muir Wood, D. (2002). Some observations of volumetric instabilities in soils. *International journal of solids and structures 39*(13), 3429–3449.

Muir Wood, D. (2004). *Geotechnical modelling*, Volume 1. Taylor & Francis.

Murchison, J. & O'Neill, M. (1983). *An Evaluation of p-y Relationships in Sands*. Report (American Petroleum Institute). University of Houston-University Park.

Nguyen, C., van Lottum, H., Holscher, P., & van Tol, A. (2011). Centrifuge modelling of rapid load tests with piles in silt and sand. In *Frontiers in Offshore Geotechnics II*, pp. 537–524. CRC Press.

Nunez, I., Philips, R., Randolph, M., & Wesselink, B. (1988). Modeling laterally loaded piles in calcareous sand. In *Centrifuge 88*.

Oldham, D. (1985). Experiments with lateral loading of single piles in sand. *Publication of: Balkema (AA)*.

Ovesen, N. (1979). The scaling law relationship. In *Proc. of the Seventh European Conference on Soil Mechanics and Foundation Engineering, Brighton*, Volume 4, pp. 319–323.

Paik, K. & Lee, S. (1993). Behavior of soil plugs in open-ended model piles driven into sands. *Marine Georesources & Geotechnology 11*(4), 353–373.

Paikowsky, S. (1990). The mechanism of pile plugging in sand. In *Offshore Technology Conference*.

Paikowsky, S., Player, C., & Connors, P. (1995). A dual interface apparatus for testing unrestricted friction of soil along solid surfaces. *ASTM geotechnical testing journal 18*(2), 168–193.

Peng, J., Clarke, B., & Rouainia, M. (2011). Increasing the resistance of piles subject to cyclic lateral loading. *Journal of Geotechnical and Geoenvironmental Engineering 137*(10), 977–982.

Peralta, P. & Achmus, M. (2010). An experimental investigation of piles in sand subjected to lateral cyclic loads. In *Physical Modelling in Geotechnics, Two Volume Set*, pp. 985–990. CRC Press.

P.H.R.I. (1980). *Technical Standards for Port and Harbour Facilities in Japan*. Port an Harbour Research Institute.

Pierson Jr, W. & Moskowitz, L. (1964). A proposed spectral form for fully developed wind seas based on the similarity theory of sa kitaigorodskii. *Journal of geophysical research 69*(24), 5181–5190.

Poulos, H. & Hull, T. (1989). The role of analytical geomechanics in foundation engineering. In *Foundation Engineering@ sCurrent Principles and Practices (GSP 22)*, pp. 1578–1606. ASCE.

Prakasha, K., Joer, H., & Randolph, M. (2005). Establishing a model testing capability for deep water foundation systems. In *Proceedings of the 15th International Offshore and Polar Engineering Conference and Exhibition. Korea Seoul:[sn]*, pp. 309–315.

Randolph, M. (2003). Science and empiricism in pile foundation design. *Géotechnique 53*(10), 847–876.

Randolph, M. (2012, August). Scaling effect. personal communication.

Randolph, M., Leong, E., & Houlsby, G. (1991). One-dimensional analysis of soil plugs in pipe piles. *Géotechnique 41*(4), 587–598.

Reese, L., Cox, W., & Koop, F. (1974). Analysis of laterally loaded piles in sand. *Offshore Technology Conference OTC 2080*, 473–486.

Reese, L. & Matlock, H. (1956). Non-dimensional solutions for laterally loaded piles with soil modulus assumed proportional to depth. In *8th Texas conference on soil mechanics and foundation engineering*.

Reese, L. & Van Impe, W. (2001). *Single Piles and Pile Groups Under Lateral Loading*. Taylor & Francis.

Remaud, D., Garnier, J., & Frank, R. (1998). Pieux sous charges latérales: étude de l'effet de groupe. *Comptes rendus des Ves Journées nationales Génie côtier-Génie civil, Toulon*, 13–15.

Robinsky, E. I. & Morrison, C. F. (1964). Sand displacement and compaction around model friction piles. *Canadian Geotechnical Journal 1*(2), 81–93.

Rosquoet, F., Thorel, L., Garnier, J., & Canepa, Y. (2007). Lateral cyclic loading of sand-installed piles. *Soils and foundations 47*(5), 821–832.

Schnaid, F. & Houlsby, G. (1991). Assessment of chamber size effects in the calibration of in situ tests in sand. *Géotechnique 41*(3), 437–445.

Schofield, A. (1980). Cambridge geotechnical centrifuge operations. *Géotechnique 30*(3), 227–268.

Schofield, A. (2005). *Disturbed soil properties and geotechnical design*. Thomas Telford Services Ltd.

Snyder, B. & Kaiser, M. (2009). Ecological and economic cost-benefit analysis of offshore wind energy. *Renewable Energy 34*(6), 1567 – 1578.

Taylor, R. (1995). *Centrifuge modelling: principles and scale effects*, pp. 19–33. Blackie Academic & Professional.

Terzaghi, K. (1955). *Evaluation of coefficients of subgrade reaction.* Harvard soil mechanics series. Harvard Univ., Div. of Engineering and Applied Physics.

Ting, J., Kauffman, C., & Lovicsek, M. (1987). Centrifuge static and dynamic lateral pile behaviour. *Canadian Geotechnical Journal 24*(2), 198–207.

Van Beek, C. (2012, August). Designing the novel actuator. personal communication.

Van der Tempel, J. (2006). *Design of support structures for offshore wind turbines.* Ph. D. thesis, Technische Universiteit Delft. ISBN: 9076468117.

Vattenfall (2008). Kriegers flak offshore wind farm-design basis foundations. Technical report, Vattenfall Vindkracft AB.

Verdure, L., Garnier, J., & Levacher, D. (2003). Lateral cyclic loading of single piles in sand. *International journal of physical modelling in geotechnics 3*(3), 17–28.

Veritas, D. (2011). Dnv-os-j101 offshore standard - design of offshore wind turbine structures.

Vesic, A. (1977). Design of pile foundations. *NCHRP Synthesis of Highway Practice* (42).

White, D.J. & Lehane, B. (2004). Friction fatigue on displacement piles in sand. *Géotechnique 54*, 645–658.

White, D. (2005). A general framework for shaft resistance on displacement piles in sand. In *Proceedings of the 1st International Symposium on Frontiers in Offshore Geotechnics, ISFOG 2005*, pp. 697–704. Taylor and Francis.

White, D. & Bolton, M. (2004). Displacement and strain paths during plane-strain model pile installation in sand. *Géotechnique 54*(6), 375–397.

White, D., Schneider, J., & Lehane, B. (2005). The influence of effective area ratio on shaft friction of displacement piles in sand. In *Proceedings of the 1st International Symposium on Frontiers in Offshore Geotechnics, ISFOG 2005*, pp. 741–748. Taylor and Francis.

Wiemann, J. (2006). *Bemessungsverfahren für horizontal belastete Pfähle- Untersuchungen zur Anwendbarkeit der p-y-Methode.* Mitteilungen aus dem Fachgebiet Grundbau und Bodenmechanik der Universität Duisburg-Essen. VGE-Verlag.

Wiemann J., Lesny K., R. W. (2007). Evaluation of the pile diameter effects in soil-pile stiffness. In *Proceedings of the 7th German Wind Energy Conference (DEWEK).*

Xu, X., Schneider, J., & Lehane, B. (2005). Evaluation of end-bearing capacity of open-ended piles driven in sand from cpt data. In *Proceedings of the 1st International Symposium on Frontiers in Offshore Geotechnics, Perth, Australia*, pp. 19–21.

Zania, V. & Hededal, O. (2011). Friction effects on lateral loading behavior of rigid piles. In *GeoCongress 2012@ sState of the Art and Practice in Geotechnical Engineering*, pp. 366–375. ASCE.

Appendices

Appendix A

Extra literature

A.1 p-y method

A.1.1 Literature concerning initiation p-y curves

Originally the p-y curves are composed out of three parts (by Reese et al. [1974]) as schematically represented in Figure A.1. The first part of the p-y curve consists of local subgrade reaction increasing linearly with the depth (Equation A.1a). The second part of the p-y curve is presented in Equation A.1b in which C is obtained from a theoretical maximum subgrade reaction. n depends on the ratio between the subgrade reaction and displacement at point m multiplied with the slope of the curve at point m. The third part between point m and w is a straight line (Equation A.1c). At displacement y_u the maximum subgrade reaction is reached (Equation A.1d). The three different parts of the original p-y curve is schematically presented in Figure A.1.

$$p(y,z) = k \cdot x \cdot y \qquad \text{(A.1a)} \qquad p(y,z) = C \cdot y^{1/n} \qquad \text{(A.1b)}$$

$$p(y,z) = m \cdot y(z) \qquad \text{(A.1c)} \qquad p(y,z) = p_u(z) \qquad \text{(A.1d)}$$

The maximum of the subgrade reaction (lateral resistance, $p_u(z)$) is based on two failure modes (Reese et al. [1974]). Near the surface a three dimensional earth pressure failure mode as shown in Figure A.1a is considered. The passive earth pressure is calculated according to Coulomb and the active earth pressure according to Rankine. At greater depth a two dimensional failure mode was implemented since the assumption was that at greater depth the failure behaviour would not be governed by shear plains but rather by the deformation of a confined layer, see Figure A.1b.

A.1.2 Application according to API [2007]

The initial p-y curves, as presented in previous section (§A.1.1), were altered into continuous equations by Murchison & O'Neill [1983]. Calculation of the ultimate lateral soil resistance is subdivided into two components, either applicable for shallow or larger depths, Equation A.2a and Equation A.2b respectively. C_1, C_2, C_3 are soil constants determined from Figure A.2a.

The soil resistance-deflection for sand is also nonlinear and approximated for specific depths by

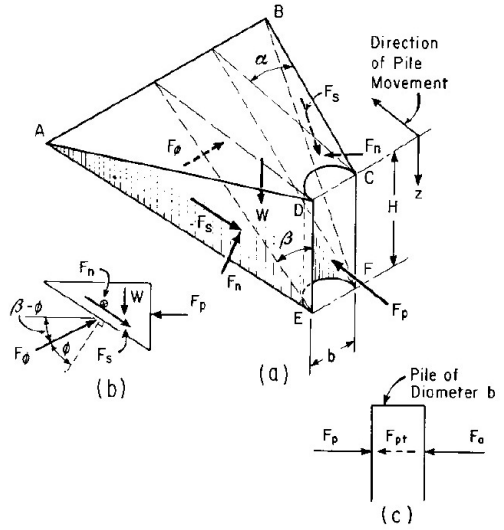

(a) Assumed passive wedge (a) general shape of wedge, (b) Force on wedge, (c) Force on pile

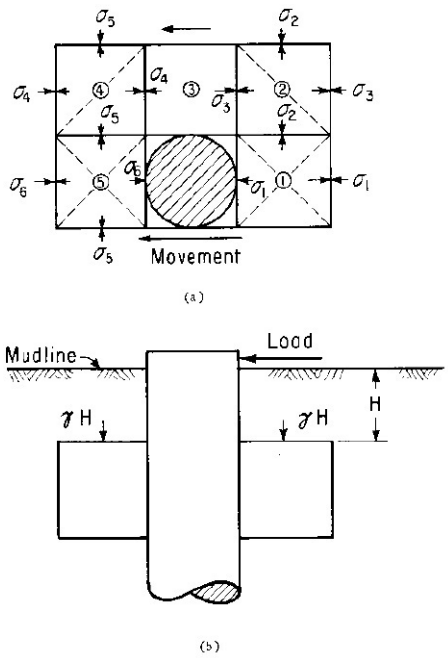

(b) Assumed mode of soil failure by lateral flow around pile. (a) section through the pile, (b) evaluation of the pile

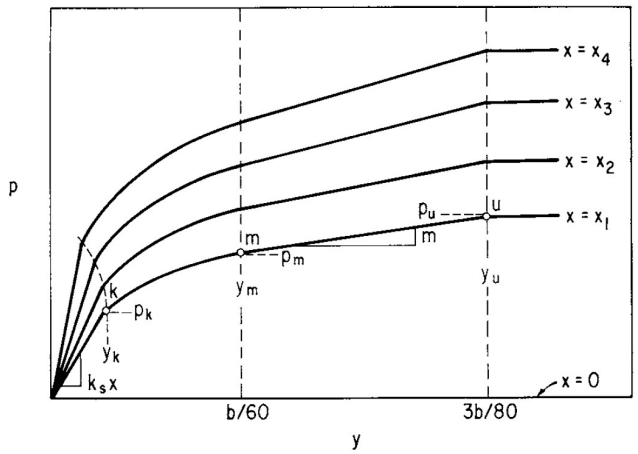

(c) Typical family of p-y curves

Figure A.1 Shallow and deep failure modes and typical p-y curves(Reese et al. [1974])

means of a linearly increasing subgrade reaction (*tanh* and z respectively in Equation (A.3)) in which A is the factor that takes into account cyclic ($A = 0.9$) or static loading ($A = (3.0 - 0.8 \cdot \frac{H}{D}) \geq 0.9$). The modulus of subgrade reaction (k) can be obtained from Figure A.2b using either the relative density or the peak friction angle.

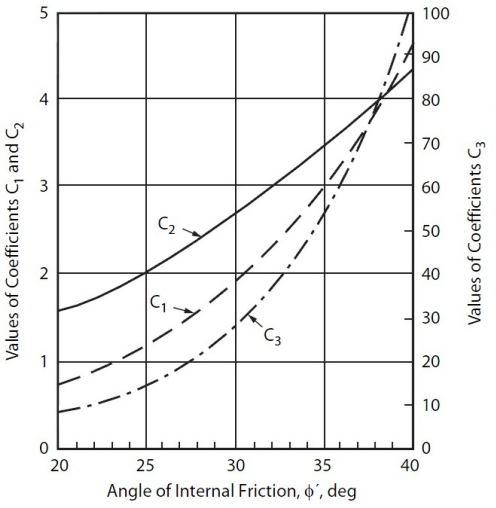

(a) Coefficients as function of ϕ' (Murchison & O'Neill [1983])

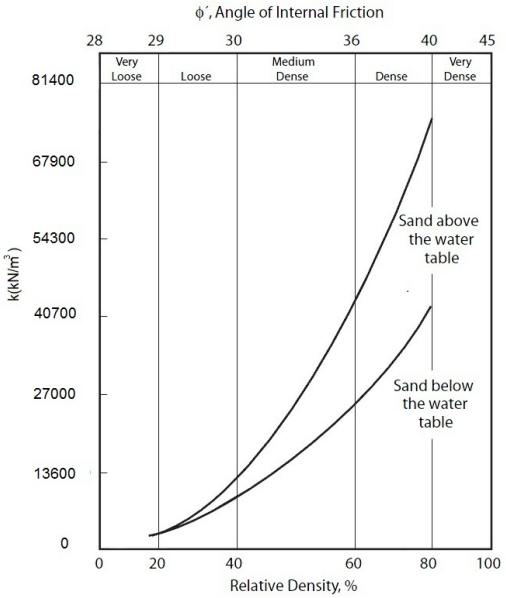

(b) Modulus of subgrade reaction as a function of ϕ' or I_d (Murchison & O'Neill [1983])

$$p_{us} = (C_1 \cdot z + C_2 \cdot D_o) \cdot \gamma \cdot z \qquad \text{(A.2a)}$$

$$p_{ud} = C_3 \cdot D_o \cdot \gamma \cdot z \qquad \text{(A.2b)}$$

$$p_u = min[p_{us}, p_{ud}] \qquad \text{(A.2c)}$$

$$p = A \cdot p_u \cdot tanh(\frac{k \cdot z}{A \cdot p_u} \cdot y) \qquad \text{(A.3)}$$

A.2 Additional developments

A.2.1 Development p-y method based on FE modelling

Deformations due to extreme static loads are underestimated by the p-y design method (Achmus et al. [2009]). Overall reason is a probable overestimation of the initial soil stiffness (oedometer modulus) in large depth by the API [2007] (Wiemann J. [2007]). The suitability of the zero-toe-kick or vertical tangent criterion, required by Lloyd & Hamburg [2005] and other design criteria for horizontally loaded offshore piles seems to be inappropriate for large diameter monopiles (Wiemann [2006] and Bekken [2009]). There is a limit to which pile length has any influence on the lateral head displacement under static loading (Wiemann [2006]). In contrast to the linearly increasing stiffness a parabolic distribution of the oedometer modulus is more realistic (Equation A.4a, Wiemann J. [2007]). The decreasing L/D ratio led to suggesting a modification for the dimension of the pile diameter (Equation A.4b, Wiemann [2006]). Empirical values for the exponents a are 0.6 for medium dense sands and 0.5 for dense sands. The dimension of the reference pile are equal to the pile for which the p-y method was originally deduced ($D_{ref} = 0.61$ (Reese et al. [1974])).

Table A.1 Factors for determining the degradation parameter a (Long & Vanneste [1994], Lesny [2010])

Influence of the load ratio	F_L [-]
H_{min}/H_{max} = -1.0	0.2
H_{min}/H_{max} = -0.25	0.4
H_{min}/H_{max} = 0 and 0.5	1.0
H_{min}/H_{max} = 1.0 (static loading)	0.0
Influence of the type of installation	F_I [-]
Driven or back-filled and compacted	1.0
Vibrated	0.9
Back-filled	1.4
Bored	1.3
Cyclically preloaded (irrespective of type of installation)	1.0
Influence of density	F_D [-]
Loose	1.1
Medium dense	1.0
Dense	0.8
Cyclically preloaded (irrespective of type of installation)	1.0

$$k^*(z) = k \cdot \frac{z_{ref}}{z}^{a} \quad \text{(A.4a)} \qquad k^*(D) = k \cdot \frac{D_{ref}}{D}^{\frac{4(1-a)}{4+a}} \quad \text{(A.4b)}$$

A.2.2 Developments p-y method based on field tests

Long & Vanneste [1994] recommended a modification of the p-y curve depending on the number of load cycles. With this alteration the subgrade reaction and displacements under static loading are corrected. The static loading is equal to the first load cycle. Equations A.5a and A.5b are used for determining the decrease in subgrade reaction or displacement. The parameter β normally results from a differential equation of the deflection line of the beam and varies between 0 and 1, indicating whether the displacement or the subgrade reaction is decomposed. The modification can also be described as a decomposition of the reaction modulus by the number of cycles (Equation A.6a). a is an empirical degradation parameter and depends on multiple factors namely; load ratio, type of installation and density. The factors for determining the degradation parameter a (Equation A.6b) are presented in Table A.1. Suggested values for F_L, F_I, and F_D are based on results of 34 field tests. The amount of tests performed to define the influence is limited to 500 cycles. Degradation of soil resistance as a function of number of load cycles, method of pile installation, soil density, and character of cyclic load is presented in Figure A.2.

$$p(N) = p(1) \cdot N^{(\beta-1)\cdot a} \quad \text{(A.5a)} \qquad y(N) = y(1) \cdot N^{\beta \cdot a} \quad \text{(A.5b)}$$

$$\frac{K_s(N)}{K_s(1)} = N^{-a} \quad \text{(A.6a)} \qquad a = 0.17 \cdot F_L \cdot F_I \cdot F_D \quad \text{(A.6b)}$$

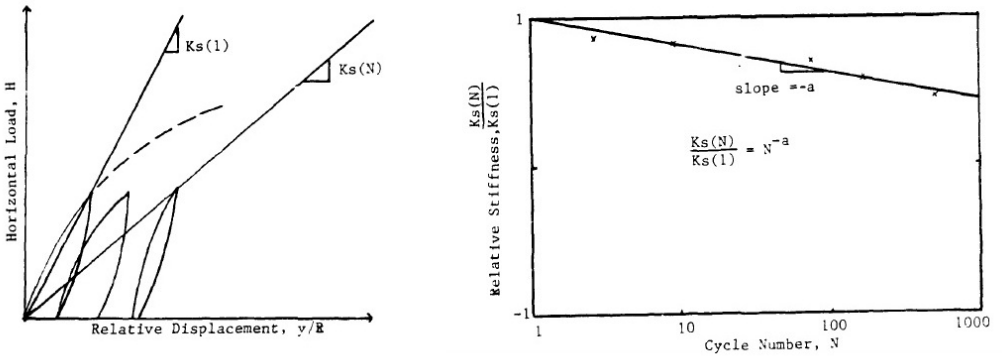

Figure A.2 Dependence of the degradation index $N^{-a} = K_s(N)/K_s(1)$ on the number of cycles (N) for the subgrade reaction modulus (Little & Briaud [1988])

A.3 Axially loaded piles

A.3.1 Design method

An axially loaded pile transfers the load to the soil by means of shear stresses acting along the shaft and normal stress on the pile tip, i.e. base capacity and shaft capacity as presented in Equation A.7a. Two methods are used for the design of axial capacity in sand namely the indirect method (β-method), used by API [2007], and a direct method. Equation A.8a presents the ultimate bearing pressure as a function of the bearing capacity factor and vertical effective stress. This bearing capacity varies a lot for different densities, also literature has not reached consensus. The formulation for calculating the shaft friction is presented in Equation A.10a. The bearing capacity is either calculated for a closed-ended (Equation A.7a), coring (Equation A.7b) or partially plugged pile (Equation A.7c).

$$Q_{tot} = Q_b + Q_{o,s} = \frac{\pi \cdot D_o^2}{4} \cdot q_b + \pi \cdot D_o \cdot L \cdot \tau_s \tag{A.7a}$$

$$Q_{tot} = Q_b + Q_{o,s} + Q_{i,s} = \frac{\pi \cdot (D_o - D_i)^2}{4} \cdot q_b + \pi \cdot D_o \cdot L \cdot \tau_s + \pi \cdot D_i \cdot L \cdot \tau_s \tag{A.7b}$$

$$Q_{tot} = Q_b + Q_{o,s} + Q_{bd} = \frac{\pi \cdot (D_o - D_i)^2}{4} \cdot q_b + \pi \cdot D_o \cdot L \cdot \tau_s + \frac{\pi \cdot D_i^2}{4} \cdot q_{bd} \tag{A.7c}$$

$$q_b = N_q \cdot \sigma'_v \tag{A.8a}$$

$$q_b = q_c \tag{A.8b}$$

The direct method correlates measured cone resistance (q_c) directly to base resistance while taking into account pile type and shape of the pile base (Equation A.8b). The cone resistance can be correlated to the relative density according to Equations A.9a and A.9b (Jamiolkowski [1985]). There is a wide variety, depending on the type of soil, of different soil constants C_1, C_2 and C_3.

$$q_c = C_1 \cdot (\sigma'_m)^{C_2} \cdot e^{C_3 \cdot I_d} \quad \text{(A.9a)} \qquad \sigma'_m = \frac{\sigma'_v(1 + 2 \cdot K_0)}{3} \quad \text{(A.9b)}$$

A.3.2 Plugging behavior

The soil plug bearing capacity can be calculated by integration of the internal shear stress between soil and pile wall. The shear stress of a certain element is calculated by both the pressure of the soil column exerting on that element plus the vertical stress caused by caused by the soil elements situated above the element considered. Therefore shear stresses increase exponentially. In undrained condition the soil plug can be treated as a series of horizontal discs, see Figure A.4. If no excess pore pressure develops then the change of vertical stress over depth may be written as Equation A.10b in which the friction can be calculated according to Equation A.10a. The total bearing capacity of the pile exists of the soil plug bearing capacity, the outer shear friction and the pile tip resistance (Equation A.7c). Randolph et al. [1991] presented an integrated solution for calculating the end-bearing capacity of the soil plug (Equations A.11a and A.11b).

$$\tau_s = K \cdot \sigma'_v \cdot tan(\delta) \quad \text{(A.10a)} \qquad \frac{d\sigma'_v}{dz} = \gamma' + \frac{4}{D_i} \cdot \tau_s \quad \text{(A.10b)}$$

$$q_{bd} = (e^{\chi} - 1)(p + \frac{\gamma' \cdot z}{\chi}) - \gamma' \cdot z \quad \text{(A.11a)} \qquad \chi = \frac{4 \cdot K \cdot tan(\beta) \cdot z}{D_i} \quad \text{(A.11b)}$$

Besides the original constant earth pressure coefficient (K_0) by Jaky [1948] presented in Equation A.12, the earth pressure coefficient can be considered variable along the length of the pile. As demonstrated by Paik & Lee [1993] the value of K is expected to reduce from a maximum (K_{max}) value to a minimum value (K_{min}) at mud line, shown in Figure A.5. This maximum value depends on the dilative characteristics of the soil (Figure A.3). The minimum value is considered to be equal to the relative density ($\frac{I_d}{100}$).

$$K_0 = 1 - sin(\phi) \quad \text{(A.12)}$$

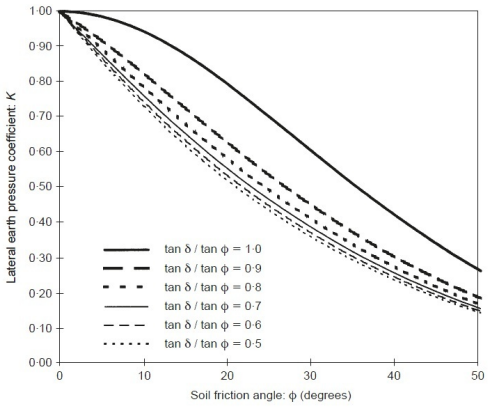

Figure A.3 Variation of minimum lateral earth pressure coefficient with friction angles ϕ and δ De Nicola & Randolph [1997]

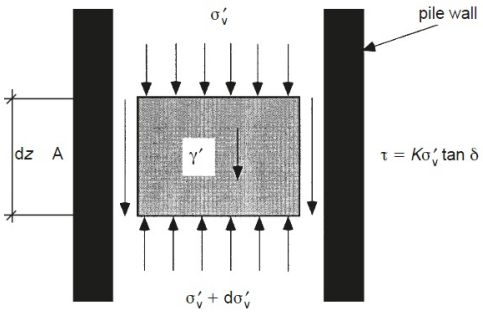

Figure A.4 Equilibrium of horizontal slice of soil Randolph et al. [1991]

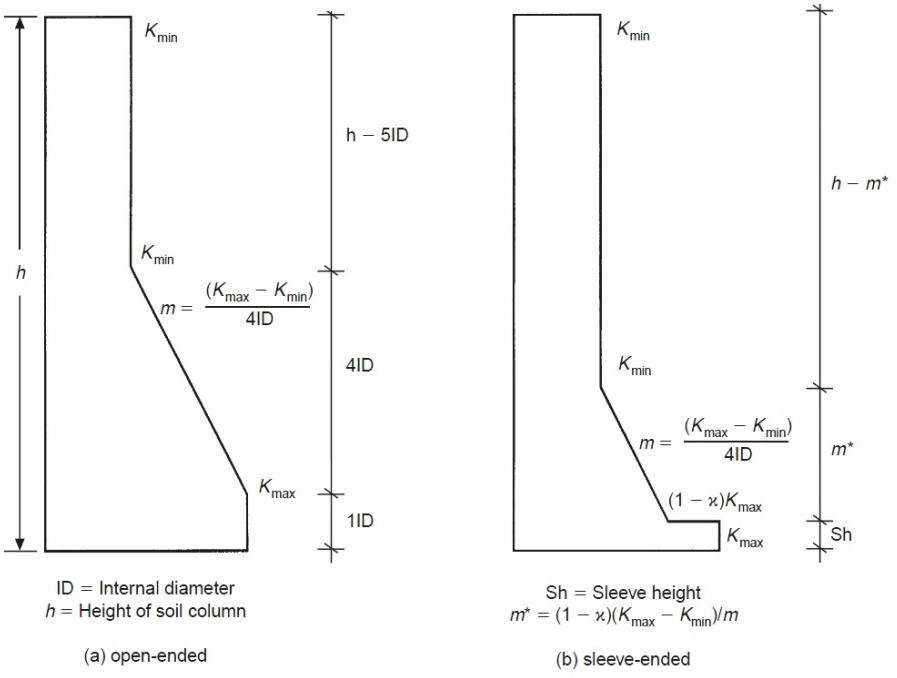

(a) open-ended **(b)** sleeve-ended

Figure A.5 Lateral earth pressure coefficient design profiles (Paik & Lee [1993])

Appendix B

Soil and soil-structure characteristics

This chapter treats the soil and model properties more specifically. §B.1 elaborates the soil properties and in more detail the; physical soil properties and mechanical soil properties. §B.2 elaborates on the interface friction characteristics.

B.1 Soil properties

B.1.1 Physical soil properties

Dry sieving is used to determine the particle size distribution and coefficient of uniformity. Two sieve tests are performed that match perfectly. The outcome of the sieving test is presented in Table B.1 and Figure B.1. Equation (B.1) is used to calculate the coefficient of uniformity, indicating indicates quite a uniform soil.

$$C_u = \frac{D_{60}}{D_{10}} \tag{B.1}$$

B.1.2 Mechanical soil properties

Defining friction angle

The peak friction angle, or maximum friction angle (ϕ'_{max}) consists of two parts namely the constant volume friction or critical state friction angle and dilation. The constant volume friction angle (ϕ'_{cv}) is independent of the relative density but whereas the maximum dilation (ψ'_{max}) is. According to Alderlieste [2011] ϕ'_{cv} of the material used is 31° (Figure B.2). For plane strain situation a relation between ϕ'_{cv} and ϕ'_{max} can be found (Equation B.2 by Bolton [1986]). Work performed by Bolton [1986] also showed that the peak friction angle could be related to the relative density of the sand

Table B.1 Particle size and coefficient of uniformity

Soil property		Unit
D_{10}	160	μm
D_{50}	230	μm
D_{60}	260	μm
C_u	1.6	[-]

Table B.2 Calculating maximum and minimum void ratios (Alderlieste [2011])

		Highest density			**Lowest density**	
Volume	V_{total}	0.113E-3	m^3	V_{total}	0.113E-3	m^3
Average mass	m_{avg}	0.19	kg	m_{avg}	0.16	kg
Average specific density	ρ_{avg}	17.2E5	kg/m^3	ρ_{avg}	14.5E5	kg/m^3
Volume soil	V_s	7.4E-05	m^3	V_s	6.2E-05	m^3
Porosity	n_{min}	0.35	-	n_{max}	0.45	-
Void ratio	e_{min}	0.54	-	e_{max}	0.82	-

corrected for the mean effective stress. This correlation is presented in Equation B.3. The maximum friction angle can then be calculated according to Equation B.4.

$$\phi'_{max} = \phi'_{cv} + 0.8 \cdot \psi'_{max} \tag{B.2}$$

$$I_R = I_d(10 - ln(p')) - 1 \tag{B.3}$$

$$\phi'_{max} = \phi'_{cv} + 3 \cdot I_R(degrees) \tag{B.4}$$

Soil-soil direct shear tests

There are various advantages and disadvantages for measuring the shear strength of soil with direct shear tests. The direct shear test is inexpensive and reliable for simulating the long term drained failure of fine-grained soils on predetermined failure surfaces Bardet [1997]. The mechanical soil properties derived from these direct shear tests are presented in Table B.3 and Table B.4. Steps taken to derive these properties are explained in Bardet [1997]. This includes correcting the shear stress for a varying surface area during shearing. Figure B.3b and Figure B.4b present the shear stress normalized over the normal stress. In the beginning the plot shows a relatively constant shear stress. These tresses are either caused by boundary effects of the proctor mold or internal strength of the soil, the truth lies somewhere in between. Although the attempt was made to have the relative density constant all the time, they vary within a range of uncertainty because the preparation does

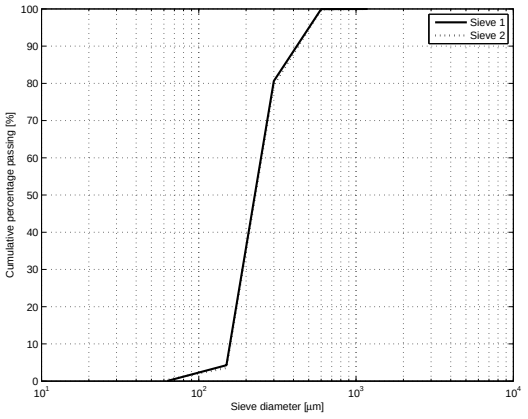

Figure B.1 Grains size distribution

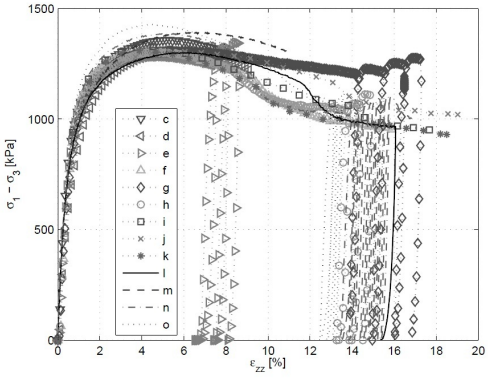

Figure B.2 Stress-strain curve with cell pressure of 500 kPa (Alderlieste [2011]

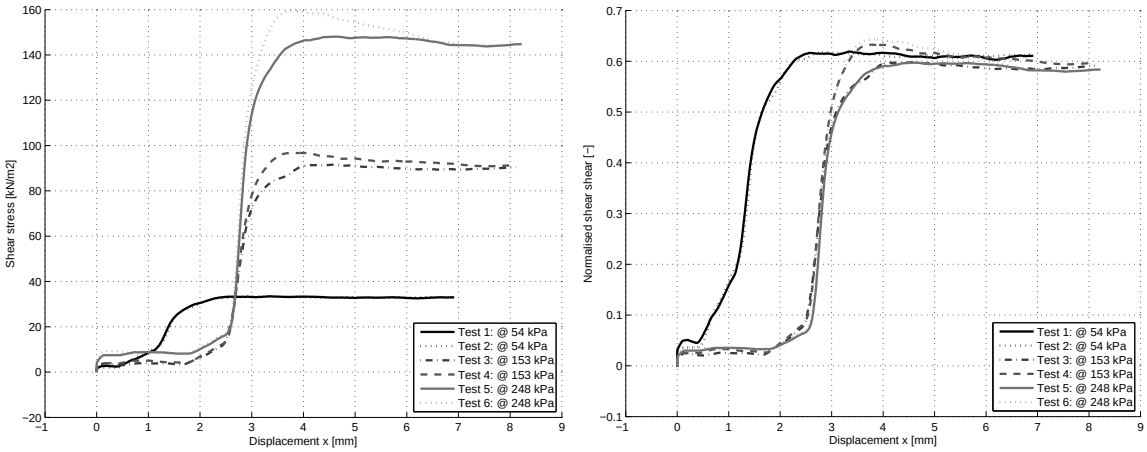

(a) Shear stress versus displacement **(b)** Normalised shear stress versus displacement

Figure B.3 DSS test, ($I_d = 60\% \pm 2\%$)

Table B.3 Soil parameters derived by direct shear test (I_d is 60% ± 2%)

Test	**Normal stress**	**P.F.A.***	**C.V.F.A.****	**Dilation**	**Dilation**
	σ'_v $[kN/m^3]$	ϕ_{max} [°]	ϕ_{cv} [°]	ψ (Eq. B.2) [°]	ψ (measured) [°]
1	54	31.9	31.3	0.7	3.0
2	54	31.8	31.6	0.3	4.5
3	153	31.0	30.5	0.6	4.0
4	153	32.4	30.7	2.1	3.5
5	248	30.9	30.2	0.9	3.5
6	248	32.9	30.3	3.2	3.5

*Peak Friction Angle
**Constant Volume Friction Angle

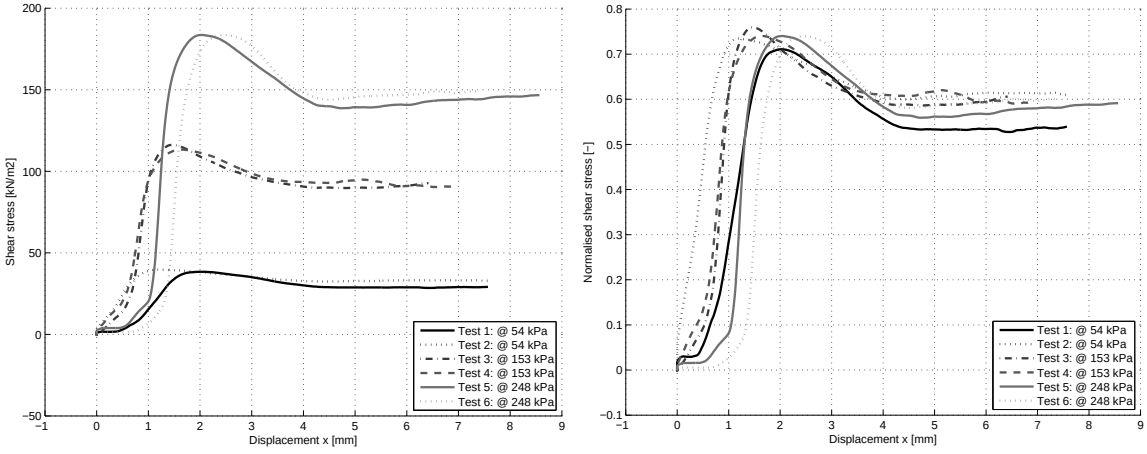

(a) Shear stress versus displacement **(b)** Normalised shear stress versus displacement

Figure B.4 DSS test, ($I_d = 80\% \pm 2\%$)

not assure all grains to be exactly in the mold and the normal stress causes settlement increasing the relative density. Average settlement of 0.3 mm and 0.2 mm, during utilization of the normal stress, are measured for the relative densities of respectively 60% and 80%. Taking into account the two errors the relative densities can be noted as 60% ± 2% and 80% ± 2%.

Table B.4 Soil parameters derived by direct shear test (I_d is 80% ± 2%)

Test	Normal stress	P.F.A.*	C.V.F.A.**	Dilation	Dilation
	σ'_v $[kN/m^3]$	ϕ_{max} [°]	ϕ_{cv} [°]	ψ (Eq. B.2) [°]	ψ (measured) [°]
1	54	35.4	28.2	9.0	12.2
2	54	36.4	31.4	6.2	10.1
3	153	37.3	30.8	8.2	9.0
4	153	36.6	30.5	7.6	10.1
5	248	36.6	30.4	7.6	10.7
6	248	36.5	31.8	7.2	12.8

*Peak Friction Angle
**Constant Volume Friction Angle

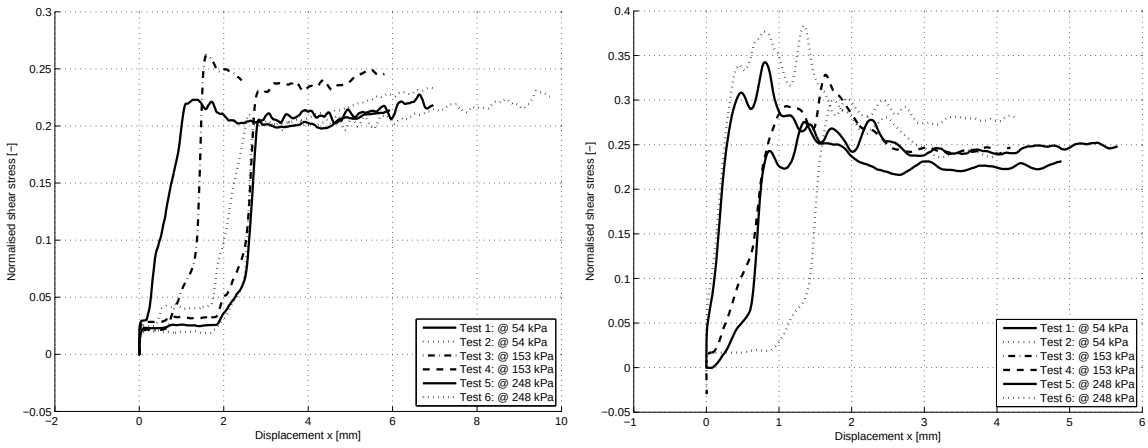

(a) $I_d = 60\% \pm 2\%$ **(b)** $I_d = 80\% \pm 2\%$

Figure B.5 Normalised interface shear stress versus displacement

B.2 Interface friction characteristics

Interface friction characteristics are determined for different relative densities and different normal stresses to give more insight into the pile interface behaviour during installation. This interface friction angle can be determined using a simple shear apparatus. The base of the direct shear box is provided with a messing plate to mimic the surface of the pile. The maximum height of the roughness profile (R_z) of the pile is 1.54 μm and the mean deviation of the roughness profile (R_a) is 0.37 μm. According to Paikowsky et al. [1995] low normalized roughness (calculated by Equation B.5) of 0.007 implies a smooth interface. The interface roughness of the messing plate located in the mold is manually adjusted to equal the roughness of the pile as much as possible. Figure B.5a and Figure B.5b show the normalized shear stresses for various normal stresses and relative densities. Table B.5 and Table B.6 present the interface friction angle for normal various tresses. Again the shear stresses are adjusted for varying surface area over which the shear stress develops (Bardet [1997]).

$$R_n = R_z / D_{50} \tag{B.5}$$

Table B.5 Interface friction characteristics derived by interface direct shear test (I_d is 60% ± 2%)

Test	Normal stress	P.I.F.A*	C.V.I.F.A.**
	σ'_v $[kN/m^3]$	δ_{max} [°]	δ_{cv} [°]
1	54	12.8	12.8
2	54	13.0	12.9
3	153	14.7	14.0
4	153	14.0	14.0
5	248	12.1	11.9
6	248	13.1	13.0

*Peak Interface Friction Angle
**Constant Volume Interface Friction Angle

Table B.6 Interface friction characteristics by interface direct shear test (I_d is 80% ± 2%)

Test	Normal stress	P.I.F.A*	C.V.I.F.A.**
	σ'_v $[kN/m^3]$	δ_{max} [°]	δ_{cv} [°]
1	54	18.9	14.0
2	54	21.0	15.5
3	153	15.3	10.8
4	153	18.2	13.5
5	248	15.4	12.7
6	248	16.7	13.5

*Peak Interface Friction Angle
**Constant Volume Interface Friction Angle

Appendix C

Indicative calculations

This appendix contains calculations to predict both the expected lateral load and axial installation load. It contributes to pre-interpretation of the lateral loading and necessary for designing the novel actuator. §C.1 contains calculations to predict the lateral pile behaviour and it contains the parameters used to calculate the axial installation load and lateral load. This section also describes the model that has been used to calculate the lateral load and the verification of this model using a DPile (Bijnagte & Luger [2010]) calculation. §C.2 contains the expected axial load during installation for plugged, cored or partially plugged installation mode. Some parameters are changed to look at the sensitivity to parameter selection.

C.1 Lateral pile behavior

C.1.1 Modelling the pile behaviour

In order to model the soil-pile behaviour, recommendations made by API [2007] were followed and implemented in the commercial program MATLAB [2011]. One significant assumption is made, namely that the pile is infinitely stiff (non-slender). The range of transition from flexible to rigid (slender tot non-slender) pile behaviour can be evaluated according to Equation C.1 (Poulos & Hull [1989]). The rigidity assumption is also verified by comparing a calculations with a DPile (Bijnagte & Luger [2010]) calculation, see Figure C.1, because the calculations performed by the DPile (Bijnagte & Luger [2010]) does take into account the flexibility (slenderness) of the pile. The two calculations show an almost exact agreement. This MATLAB [2011] model also takes into account changing location of rotation point by checking the horizontal load equilibrium.

$$4.8 < \frac{E_s \cdot L^4}{E \cdot I} < 388.6 \tag{C.1}$$

The pile dimensions used for lateral pile behaviour are presented in Table 3.4 in Chapter 3. Soil parameters necessary for calculating the lateral response and soil-pile characteristics (as elaborated in Chapter B) are presented in Table C.1 and Table C.2, together with parameters derived using API [2007]. Table C.3 presents dimensions of the pile for the two different gravity scale factors at one third of the strongbox height.

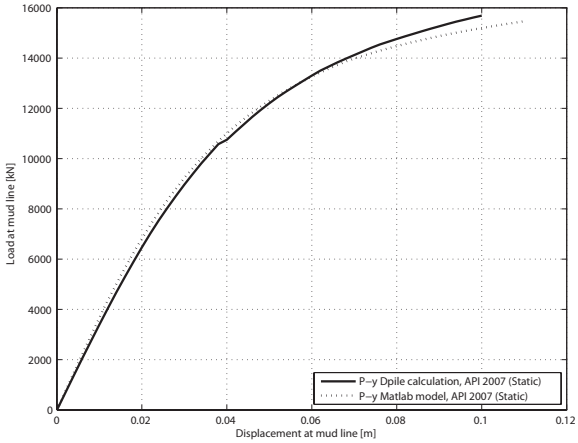

Figure C.1 Deflection versus static lateral load calculated by DPile (Bijnagte & Luger [2010]) by API [2007] method ($I_d = 60\%$)

Table C.3 Pile dimensions per gravity scale factor (N)

parameter			**Unit**
N	76	53	$[-]$
D_o	2.1	1.31	$[m]$
t	0.052	0.032	$[m]$
L_{emb}	10.35	6.45	$[m]$

Table C.1 Parameters for I_d is 60%

Parameter		**Unit**
I_d	60	$[\%]$
ϕ'_{max}	31.8	$[°]$
ϕ'_{cv}	31.1	$[°]$
δ_{max}	13.3	$[°]$
δ_{cv}	13	$[°]$
γ'	16	$[kN/m^3]$
C_1	2.1	$[-]$
C_2	2.8	$[-]$
C_3	30	$[-]$
k	13600	$[kN/m^3]$

Table C.2 Parameters for I_d is 80%

Parameter		**Unit**
I_d	80	$[\%]$
ϕ'_{max}	36.5	$[°]$
ϕ'_{cv}	21.1	$[°]$
δ_{max}	17.4	$[°]$
δ_{cv}	13	$[°]$
γ'	16	$[kN/m^3]$
C_1	3.3	$[-]$
C_2	3.6	$[-]$
C_3	60	$[-]$
k	27000	$[kN/m^3]$

C.1.2 Calculation outcome

The Matlab (MATLAB [2011]) model is used to model load cycle dependency. The big advantage compared to the DPile (Bijnagte & Luger [2010]) calculation is the ability to manually implement cycle dependency. Figure C.2b, Figure C.3b and Figure C.4b shows the behaviour of the pile cap when subjected to purely lateral load at the location at which the lateral load is applied in the centrifuge model (hinge). These calculations agree with the different tests performed as discussed in Chapter 3. Figure C.2a, Figure C.3a and Figure C.4a presents the soil resistance over the depth of the pile. As can be seen, a strange bump occurs in the resistance line for dynamic loading, this is because of the parameter A discussed in §2.2.2.

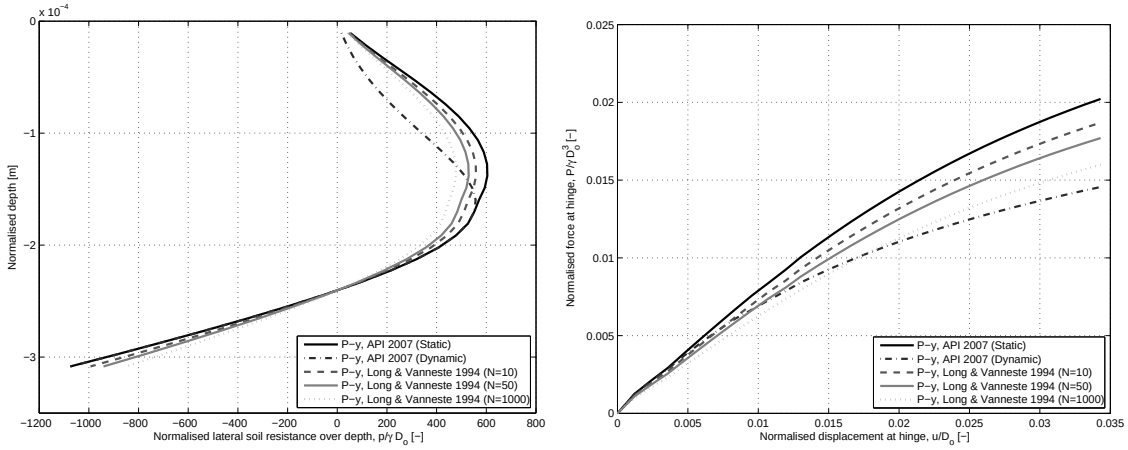

(a) Normalized lateral resistance over depth **(b)** Deflection versus load (normalised) at hinge

Figure C.2 Lateral loading plots in case of Static (API [2007]) and dynamic (API [2007], Long & Vanneste [1994]) loading (§2.2) ($I_d = 60\% \pm 2\%$ and N=76)

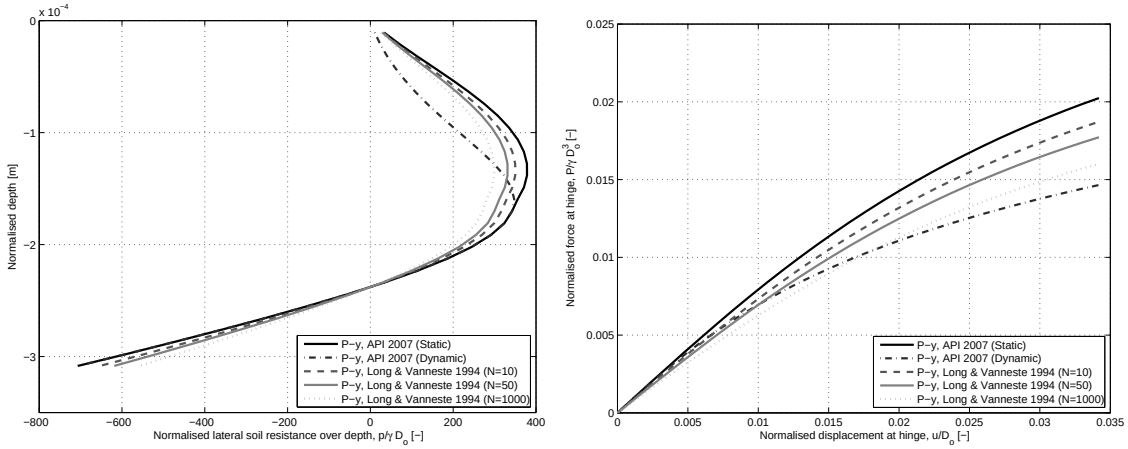

(a) Normalised lateral resistance over depth **(b)** Deflection versus load (normalised) at hinge

Figure C.3 Lateral loading plots in case of Static (API [2007]) and dynamic (API [2007], Long & Vanneste [1994]) loading (§2.2) ($I_d = 60\% \pm 2\%$ and N=48)

C.2 Axial behavior during installation

C.2.1 Cone resistance

Calculating the axial bearing capacity is essential for knowing whether or not the pile can be installed. A direct method (§A.3) is used to calculate both axial bearing capacities in plugged, cored or partially plugged mode. A direct method implies using a relation between relative density and cone resistance. Equations C.2a and C.2b by Jamiolkowski [1985] are used for interpreting the cone resistance. This is one of the most widely used relationships acquired by research on Ticino sand.

$$q_c = C_1 \cdot (\sigma'_m)^{C_2} \cdot e^{D_3 \cdot I_d} \tag{C.2a}$$

$$\sigma'_m = \frac{\sigma'_v(1 + 2 \cdot K_0)}{3} \tag{C.2b}$$

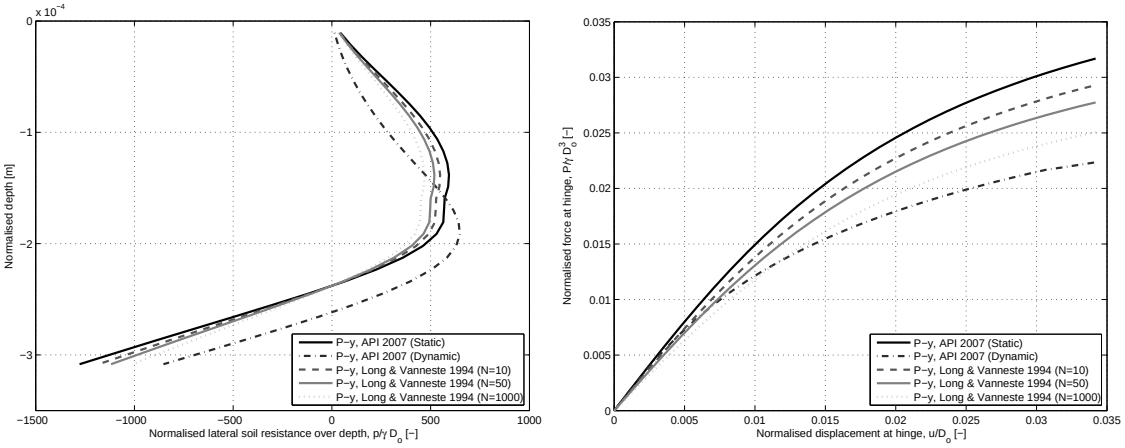

(a) Normalised lateral resistance over depth **(b)** Deflection versus load (normalised) at hinge

Figure C.4 Lateral loading plots in case of Static (API [2007]) and dynamic (API [2007], Long & Vanneste [1994]) loading (§2.2) ($I_d = 80\% \pm 2\%$ and N=53)

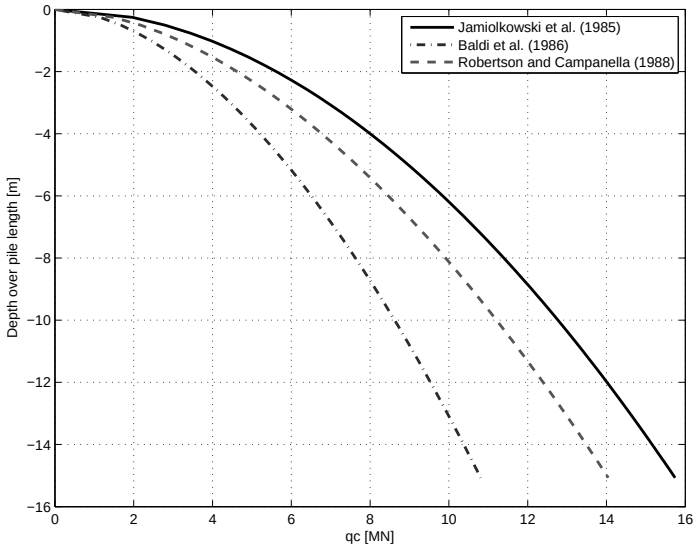

Figure C.5 Cone resistants (q_c) over depth with $I_d = 60\% \pm 2\%$ (Jamiolkowski [1985], Baldi et al. [1986] and Campanella [1988]

Table C.4 Various soil constants

	C_1	C_2	C_3
Jamiolkowski [1985]	205	0.51	2.93
Baldi et al. [1986]	157	0.55	2.41
Campanella [1988]	181	0.55	2.61

Figure C.5 presents various graphs of cone resistance over depth. The soil constants used for calculating these graphs are presented in Table C.4.

C.2.2 Axial capacity

The axial bearing capacity of the pile over depth is calculated for both fully plugged and cored modes (presented in Figure C.6a and Figure C.6b) respectivelu. These Figure also contains the plug bearing capacities calculated in two manners as discussed in §A.3.2. In case of these calculations a δ_{max} was used that equals the measured δ_{max} (Appendix B).

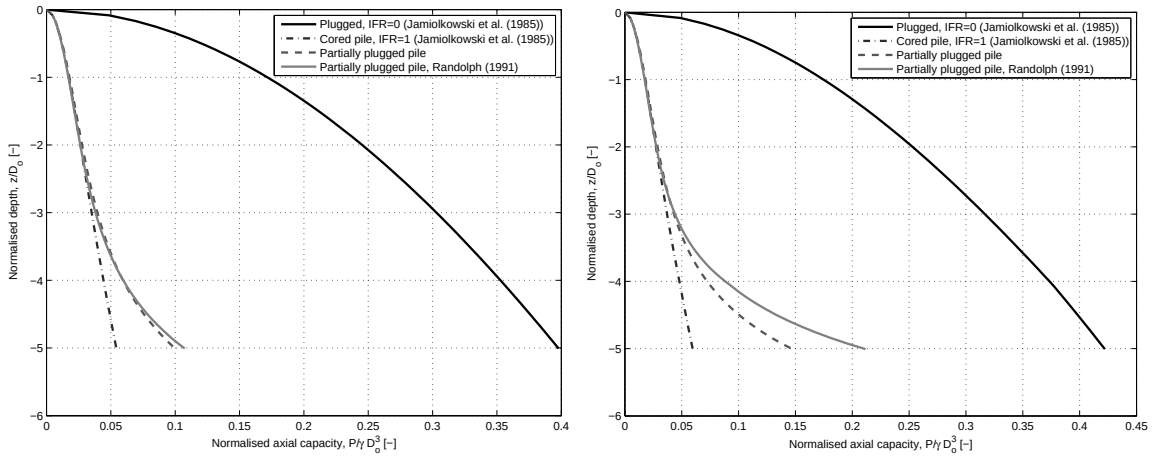

(a) K_0 according to Jaky [1948] **(b)** K_0 according to Paik & Lee [1993]

Figure C.6 Axial bearing capacity cored, plugged or partially plugged pile, δ two-third of ϕ'_{max} for I_d is 80% ± 2%

Table C.5 Buckling loads

	Prototype [MN]	**Model** [N]
Buckling load		
$K = 1.0$	17037.6	1408066
$K = 0.5$	34075.2	2816132

C.3 Pile stability

C.3.1 Enabled installation

As mentioned in previous §C.2.2 the pile will not plug during installation. But because of scaling errors (Chapter 3.1) the possibility of plugging increases and considering the installation of the pile as fully cored could be a wrong assumption. Arching of the soil sample during installation creates a higher internal friction stress. Therefore the actual axial bearing capacity lies between either cored or fully plugged.

C.3.2 Buckling of pile

The critical load for buckling can be approximated by Equation C.3. The value K varies for different conditions of end support of the pile. Two cases can be considered namely where the pile is pinned ($K = 1.0$) and both ends are fixed ($K = 0.5$).

$$F = \frac{\pi^2 \cdot E \cdot I}{(K \cdot L)^2} \tag{C.3}$$

Appendix D

Novel actuator

This chapter contains the design of the newly designed load mechanism (novel actuator) that allows for pile installation and subsequent laterally pile loading. This chapter presents calibrations for the stiffness and hysteresis of the frame. §D.1 contains the design principles and the accuracy of the actuator. §D.2 discusses the correction necessary for taking into account the stiffness of the actuator. Besides, §D.2 commences on the behaviour of the actuator for various displacements, loads and accelerations and discusses how to calibrate for hysteresis. §D.3 evaluates on the sensitivity to various external loads.

D.1 Design principles and accuracy

The main purpose of the new loading mechanism was to allow for both pile installation and subsequent a direct measurement of the load applied to the top of the model pile. A new actuator was designed to allow the pile to be installed after which the load is imposed on a hinged connection between pile and the actuator. The hinged connection consists of a transversal rod that penetrates (perpendicular to the axis of the pile) the pile and fits perfectly in an aluminium frame. The aluminium actuator is designed such that the upper and lower sides are restricted from any form of rotation (clamped). These clamped connections have the big advantage that it creates the largest amount of strain in the frame compared to other connection types, which is ideal for measurements using strain gauges. The frame is designed such that there is enough strain during loading, to ensure optimal measurement. Figure D.1 presents the loading frame, novel actuator in the gondola of the TUD centrifuge. Figure D.2 presents the schematic simplification and a photo of the designed loading mechanism. Figure D.3 depicts the model pile and its dimensions.

The accuracy of the mechanism depends on the magnitude of strain versus undesired noise and the entire load measured. The more strain measured for a certain load the better the signal and more accurate the measurement. Accuracy and measurement resolution are not the same. Unwanted side effects influencing the signal such as temperature, aging and noise in the measurements have a benign effect on the amount of micro-strain measured. These side effects are assumed to be negligible compared to the total amount of micro-strain measured.

As mentioned, aging of the mechanism due to cyclic loading (i.e. yielding of the aluminium) causes a change in strain for similar loadings and thus influences the accuracy. In order to reduce this yielding effect, the mechanism will experience an overload during calibration. Eventually an accuracy of 0.1 % is expected (Van Beek [2012]) due to accurate calibration and limited temperature effects since the geotechnical centrifuge is located in a room with controlled environment. To increase the accuracy various static and cyclic ($1 \cdot g$ and $N \cdot g$) calibration tests are performed to correct for and hysteresis of the frame.

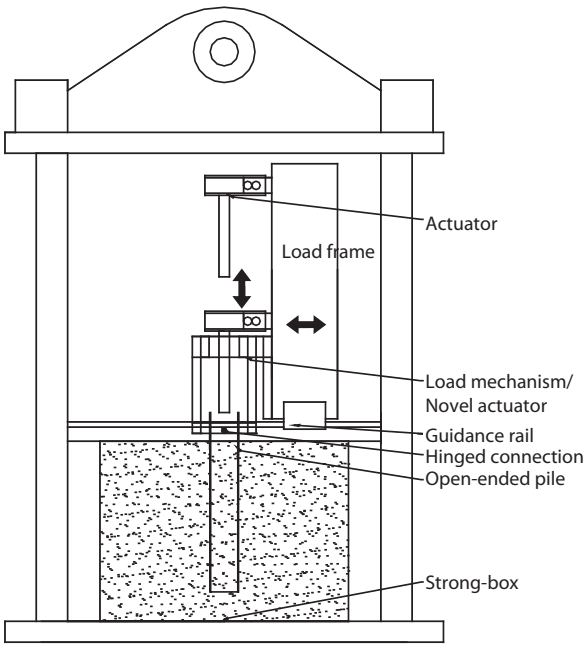

Figure D.1 Schematic presentation of the centrifuge gondola, load frame, load mechanism, strong-box, pile and actuator

D.2 Calibration

D.2.1 Static stiffness calibration

Figure D.4 presents the static calibration set-up. Leverage system was implemented so that the load was quadrupled. Figure D.4 also shows the negative or positive sign designated to the loading direction, displacement and error in displacement which is further used during data acquisition. Figure D.5a presents the load versus strain measured. This included loading in both directions for one entire cycle for two different incremental loading steps. There is hardly any hysteresis according to this static calibration but in one loading direction the relation between load and displacement/strain is multi-linear. Figure D.5b shows the load versus displacement of the frame at which the hinged connection is located. Figure D.5c presents the average calibrated values and a 4^{th} order polynomial fit that is used to correct for the stiffness during data acquisition.

D.2.2 Cyclic hysteresis calibration at $1 \cdot g$ and $N \cdot g$

This calibration is performed using a spring attached to the gondola (as depicted in Figure D.6a). Figure D.6b presents the spring calibration for two different displacements. Both calibrations have the same shape suggesting that the hysteresis of the entire load mechanism is neither load nor displacement dependent. Figure D.6c shows the cyclic calibration at multiple acceleration levels. It indicates that the shape of the hysteresis loop does not significantly depend on elevation of gravitational acceleration.

In order to take into account the hysteresis a specific loop (Figure D.7b) is taken from cyclic spring calibration test at $1 \cdot g$ (Figure D.7a). Figure D.7b shows a 8^{th} order polynomial, for both the forward and backward part of the loop, zoomed in at one end. Besides that, the figure depicts a linear fit through the average values of both displacement directions. Figure D.7d shows the difference, between linear fit through the average values and the simplification of the hysteresis, at the beginning of each loop. Eventually the correction will only be applied at the beginning of the forward or backward loop. A linear adjustment will be applied in the first part from the outer value of the load until 20 N from that outer value. For the first 2.5 N the values will be corrected from 0.006 mm to 0 mm.

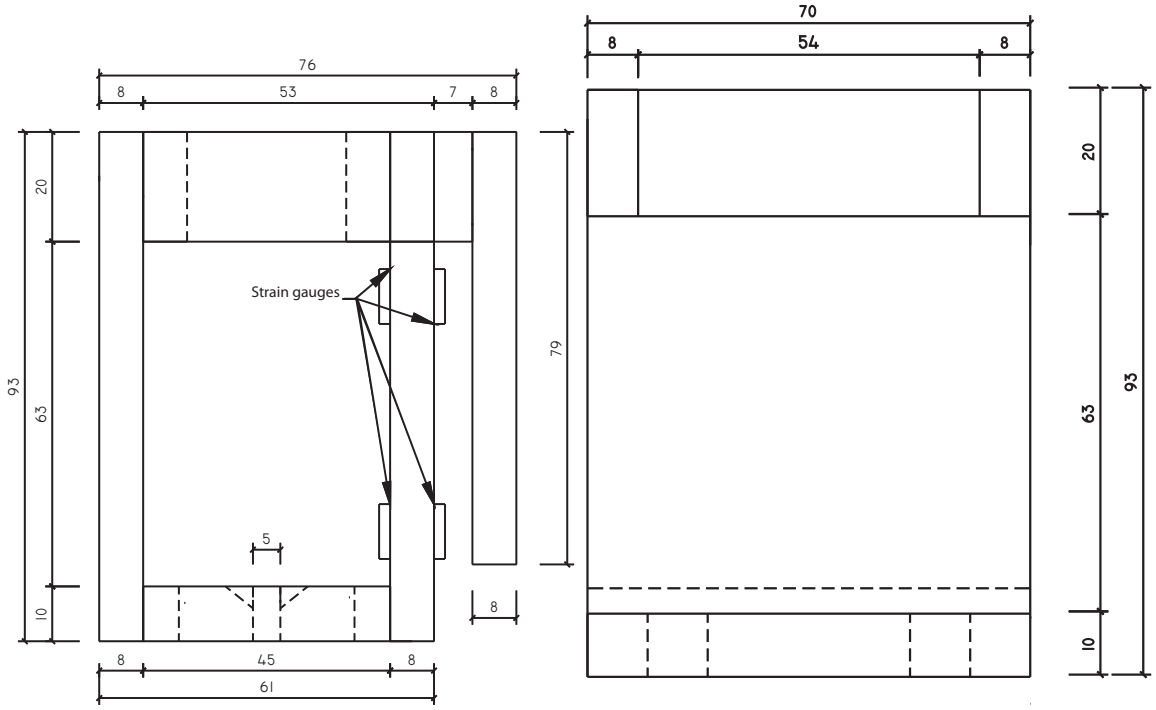

(a) Schematic side view **(b)** Schematic front view

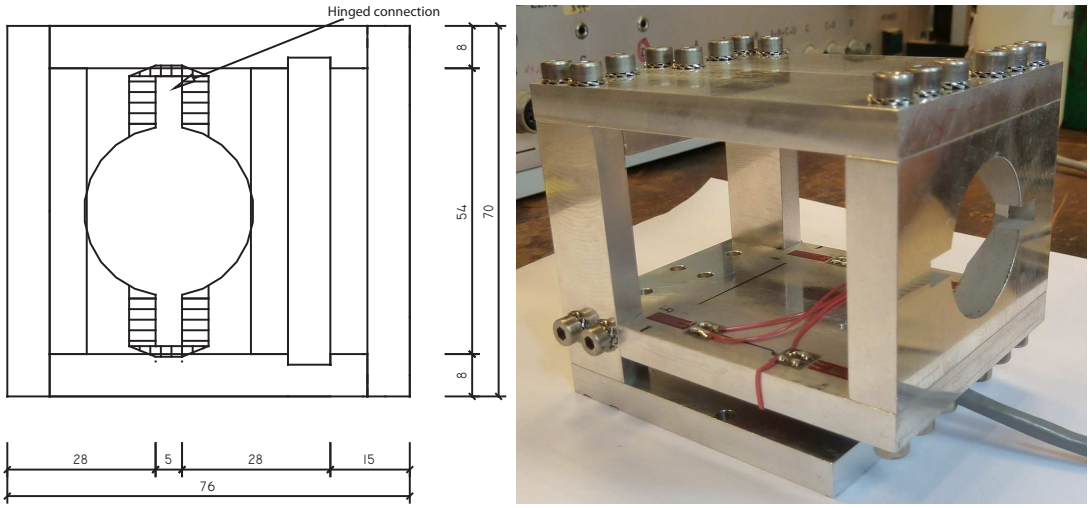

(c) Schematic top view **(d)** Photo of the actuator

Figure D.2 Schematic representation and photo of the actuator

For the following 17.5 N the displacement will be corrected from 0 mm until 0.060 m. From 17 N from the outer value on the correction in displacement is 0.066 mm.

D.3 Sensitivity

This section presents the sensitivity to other external loads in order to explain possible variation in data after acquisition. Figure D.8a and Figure D.8b show spring calibration tests (for all the cycles and a specific cycle) and test in which the signal was affected by other loading conditions. The signal was affected by imposing a moment in the lower part (template) of the frame, torsional moment, a vertical load and the frame was hindered from moving. Only the hindrance of movement showed

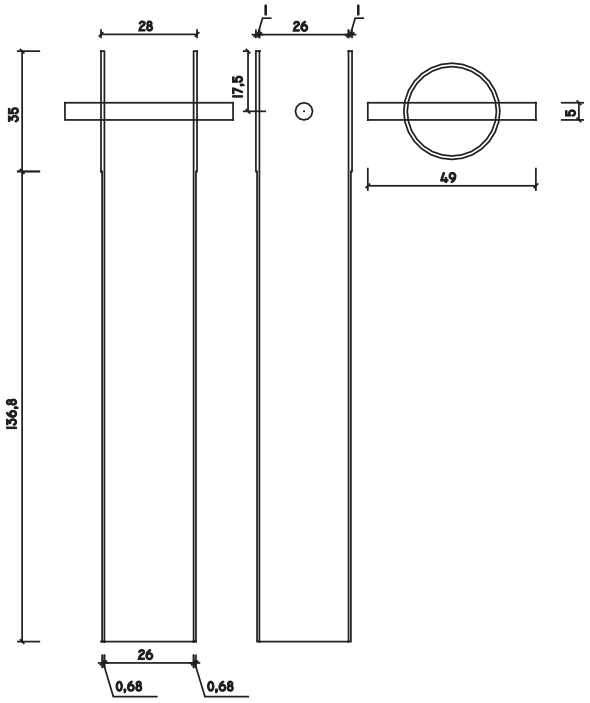

Figure D.3 Model pile dimensions

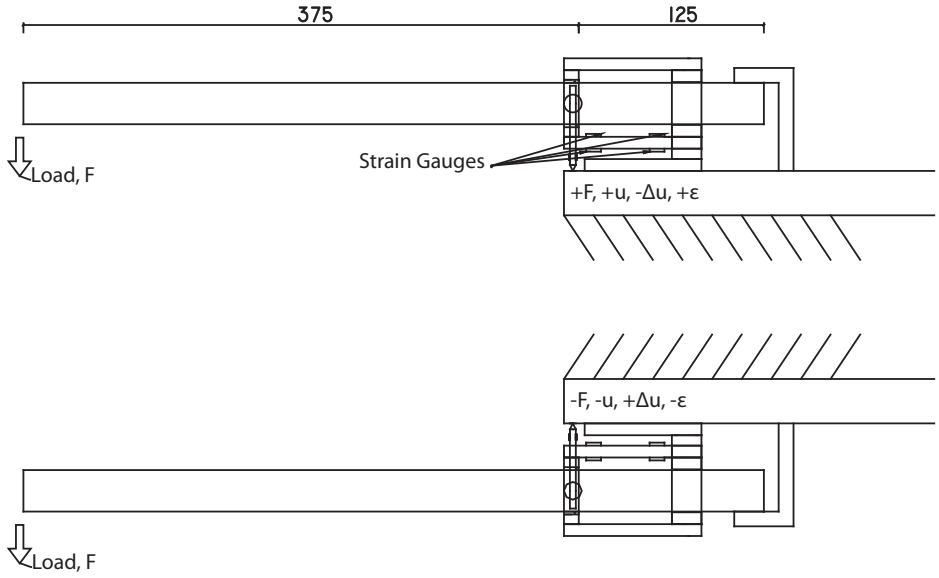

Figure D.4 Set-up for static load testing

significant influence on the signal (logic because of the design principals mentioned in §D.1). Figure D.8c and Figure D.8d show the sensitivity to a factor that is used to filter out high frequencies (Lowpass filter). Initially the factor was set to 10 but reducing it to one significantly influences the outputted data. The decision was made to leave out the Lowpass filter and filter raw data during data acquisition.

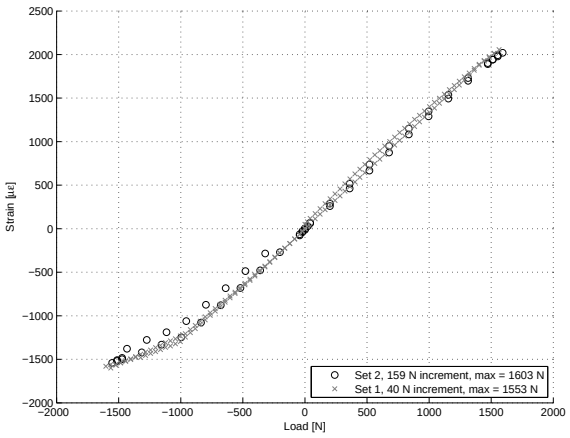

(a) Load versus strain measured in strain gauges

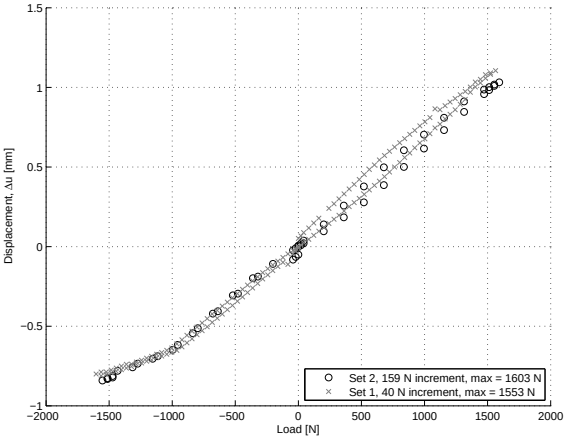

(b) Load versus displacement

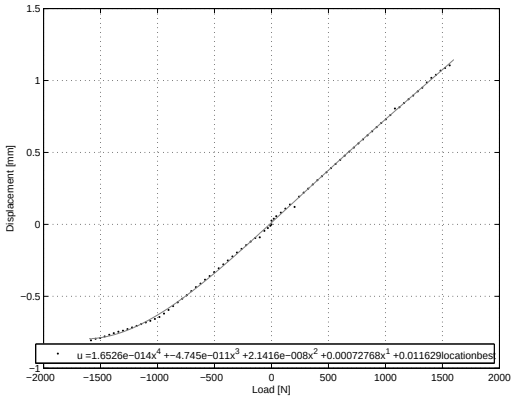

(c) Averaged load versus displacement and 4^{th} order polyfit

Figure D.5 Static calibration of the loading frame stiffness

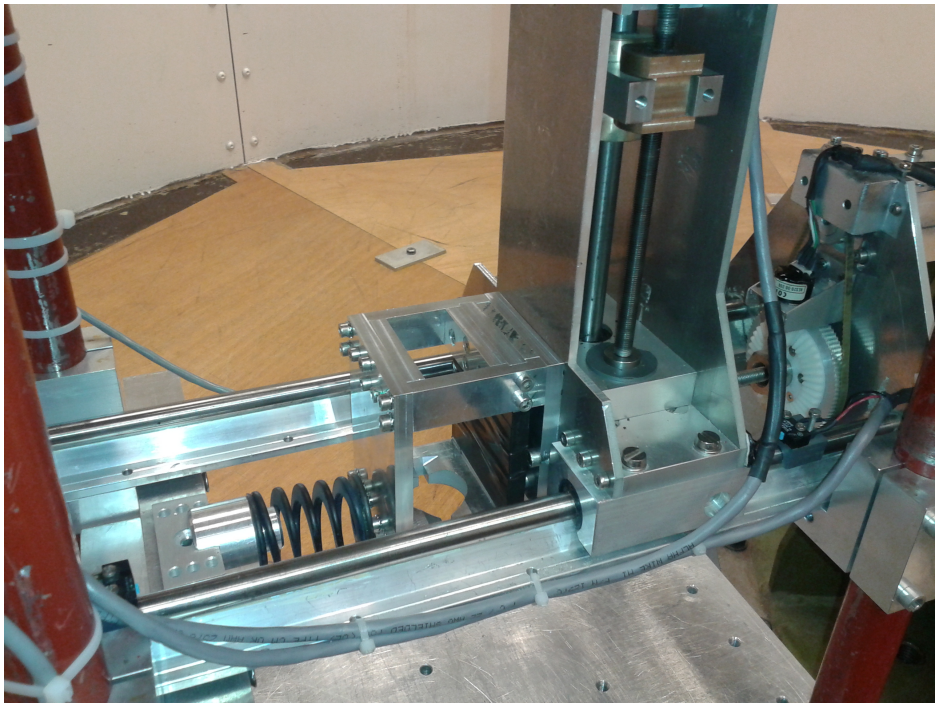

(a) Cyclic calibration set-up

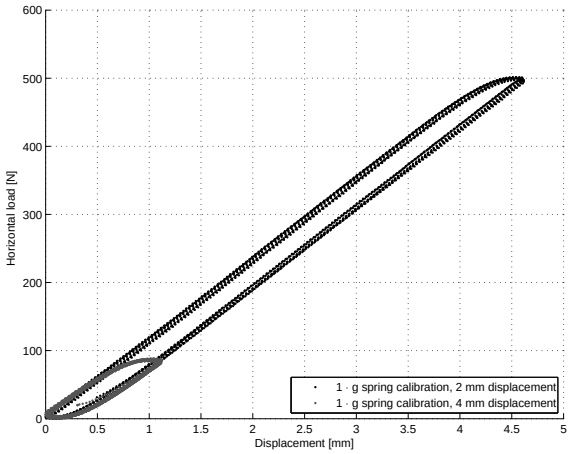

(b) Calibration for various displacements $(1 \cdot g)$

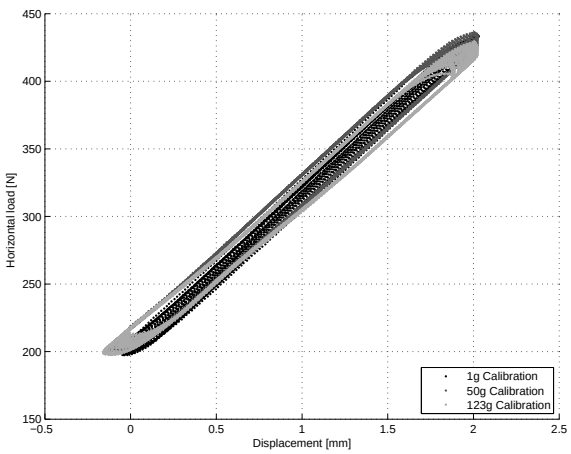

(c) Calibration at multiple g levels

Figure D.6 Cyclic $1 \cdot g$ and $N \cdot g$ calibration

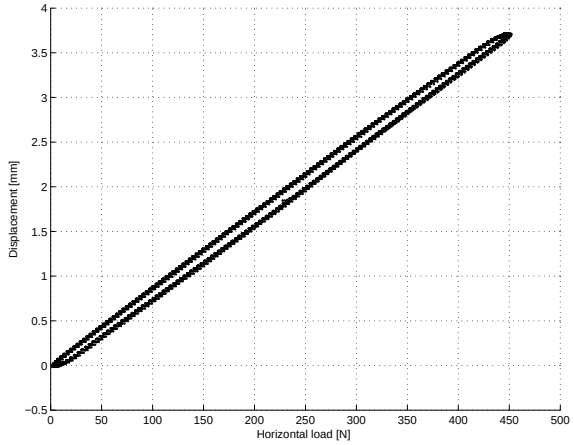

(a) Multiple loops

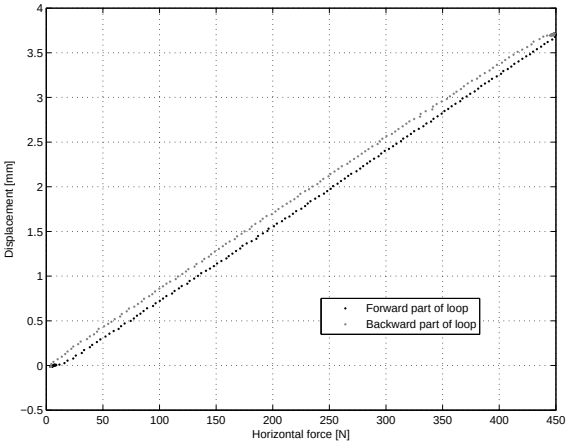

(b) Single loop

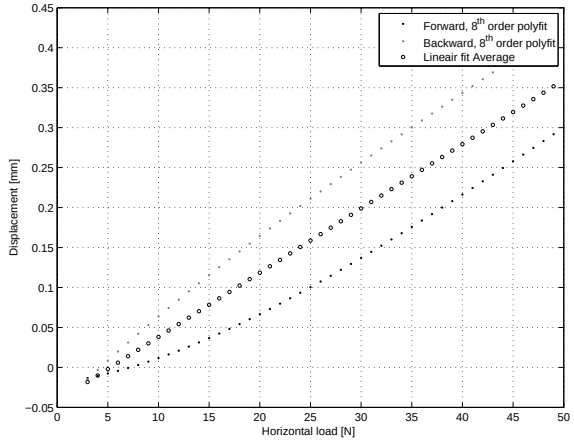

(c) Zoomed in at one end

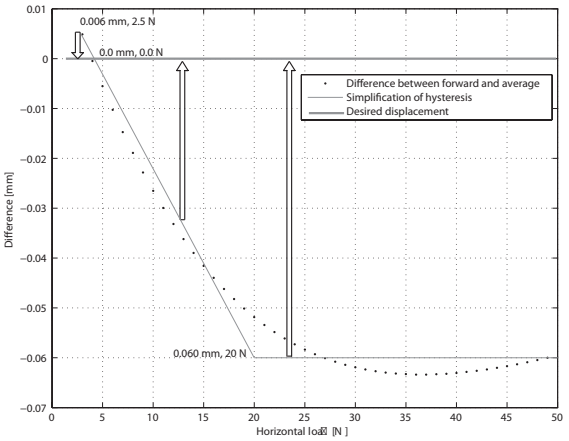

(d) Difference between simplification of hysteresis loop and average value

Figure D.7 Hysteresis loop and quantification of correction

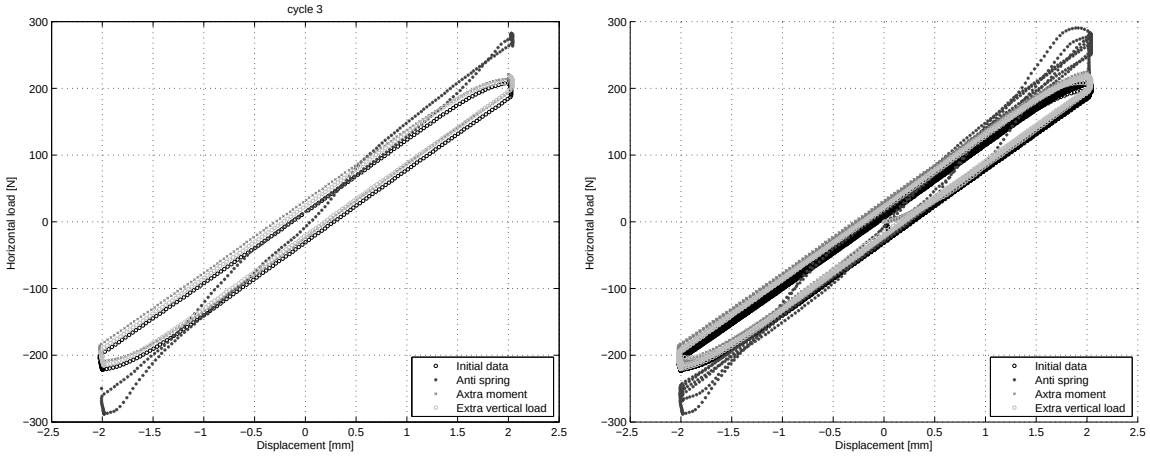

(a) Sensitivity to various external loads during $1 \cdot g$ spring calibration, N^{th} cycle

(b) Sensitivity to various external loads during $1 \cdot g$ spring calibration, all cycles

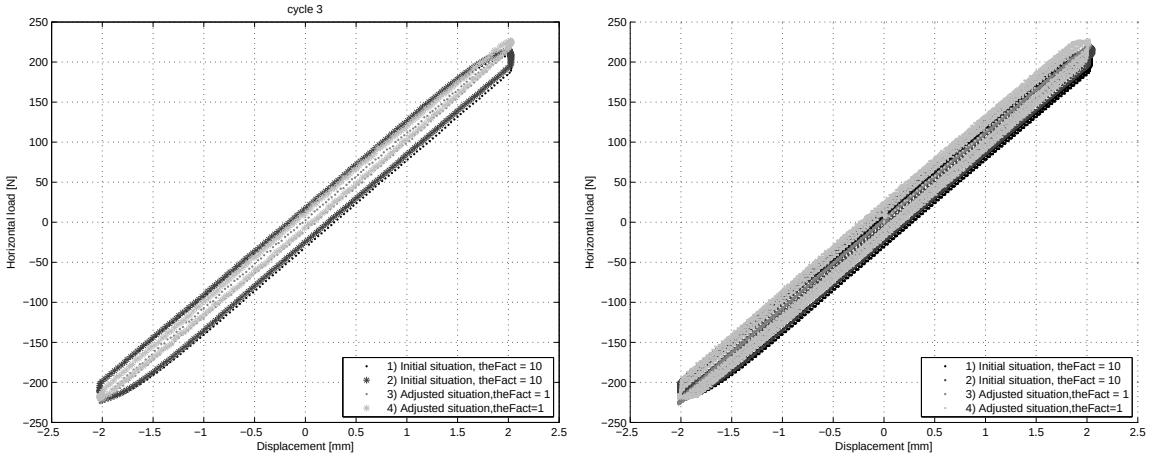

(c) Sensitivity to LowPass filter during $1 \cdot g$ spring calibration, N^{th} cycle

(d) Sensitivity to LowPass filter during $1 \cdot g$ spring calibration, all cycles

Figure D.8 Sensitivity to various variables

Appendix E

Acquisition

This chapter shows the results of the two sets of tests. The first set of tests is treated in §E.1. This data does not present loading loops. The second set of tests, as elaborated in §E.2, does show the loading loops for various cycle numbers. This appendix indicates the influence of calibration corrections, for stiffness and hysteresis, and centralization on the shape and location of the loading loops.

E.1 First test series

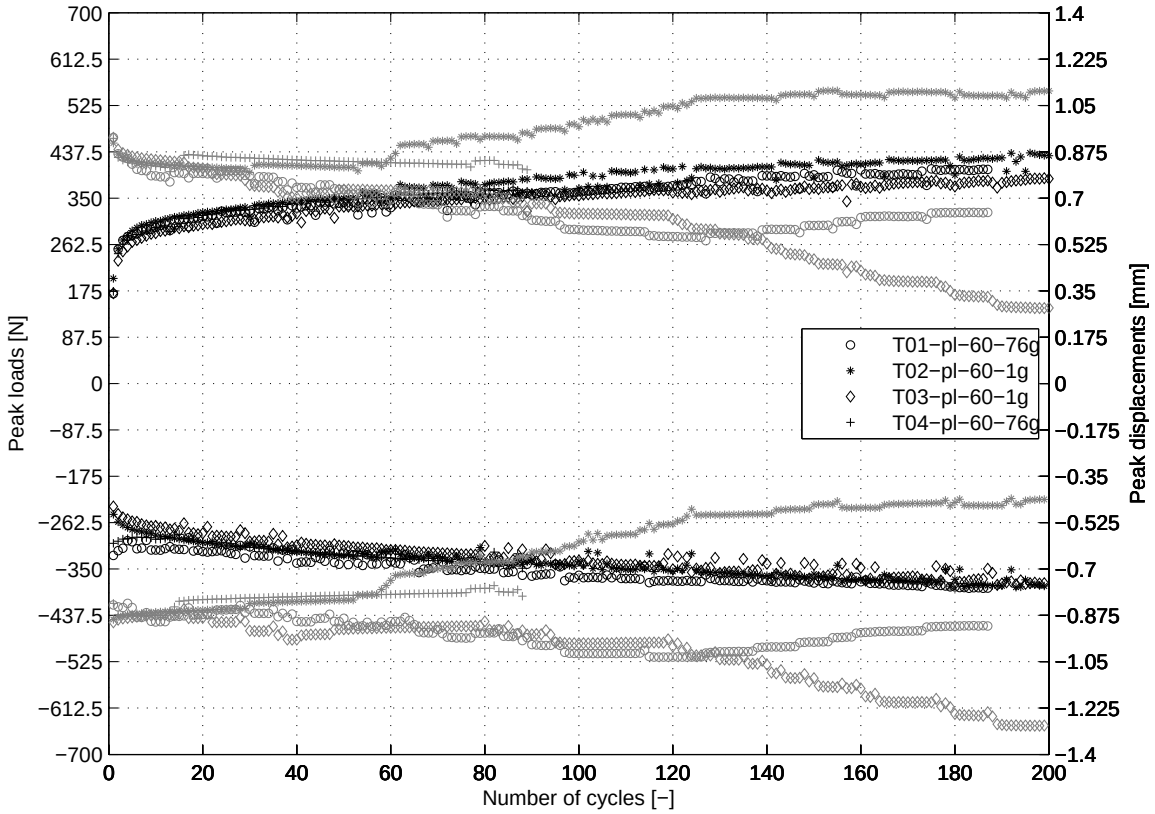

(a) Maximum and minimum horizontal displacement and forces

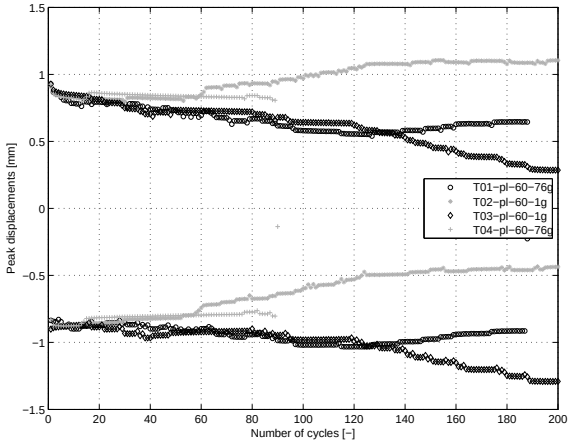

(b) Maximum and minimum horizontal displacement

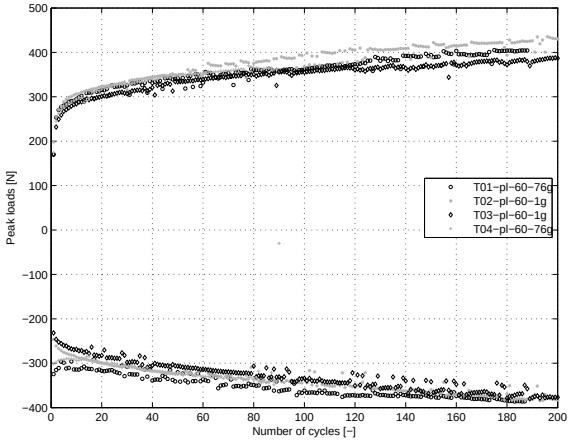

(c) Maximum and minimum horizontal forces

Figure E.1 Comparison between maximum and minimum horizontal forces and displacement for tests; T01-pl-60-76g, T02-pl-60-1g, T03-pl-60-1g and T04-pl-60-76g

E.2 Second test series

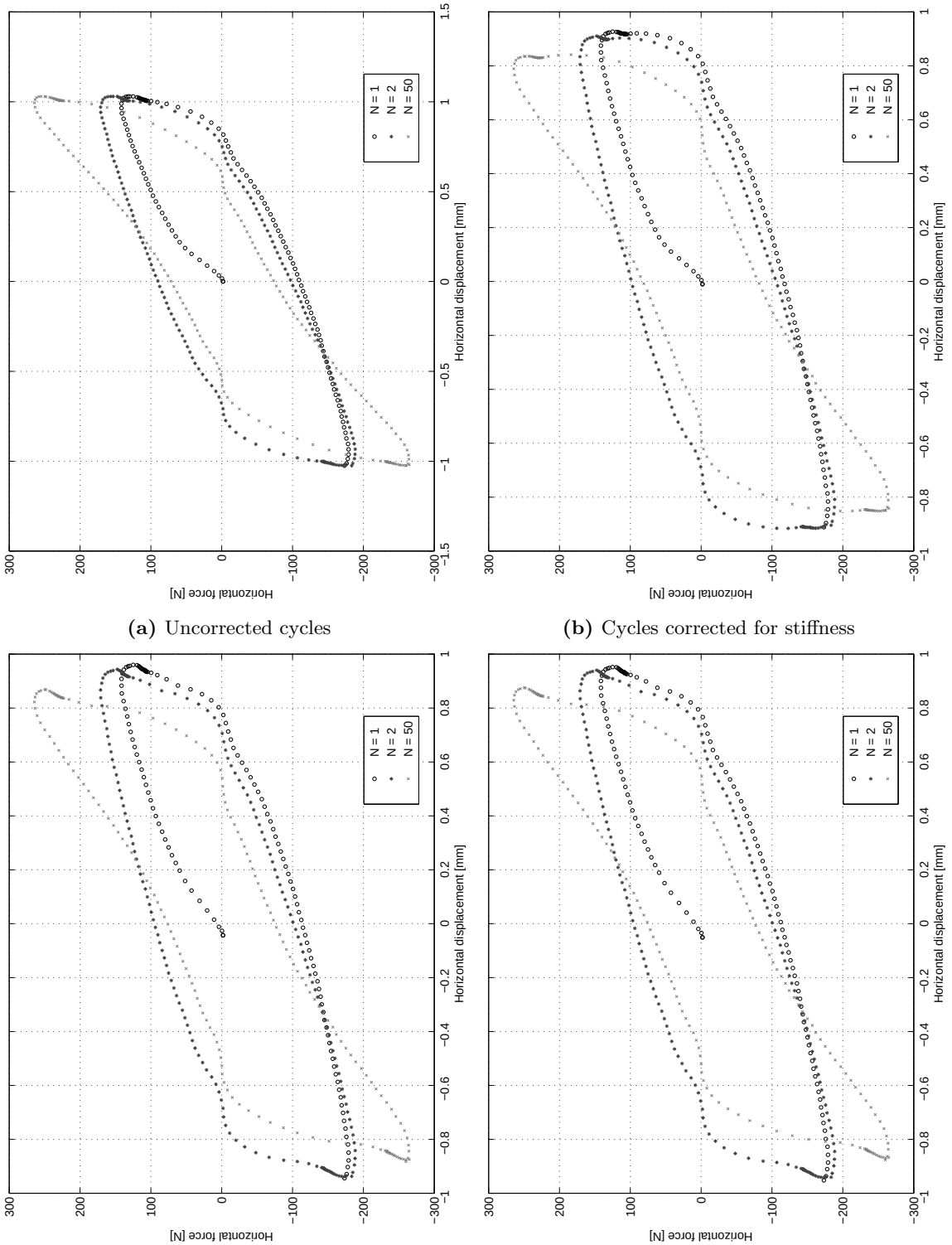

(a) Uncorrected cycles

(b) Cycles corrected for stiffness

(c) Cycles corrected for stiffness and hysteresis

(d) Cycles corrected for stiffness, hysteresis and centralized

Figure E.2 Correction stages for various cycles from test T11-pl-60-1g

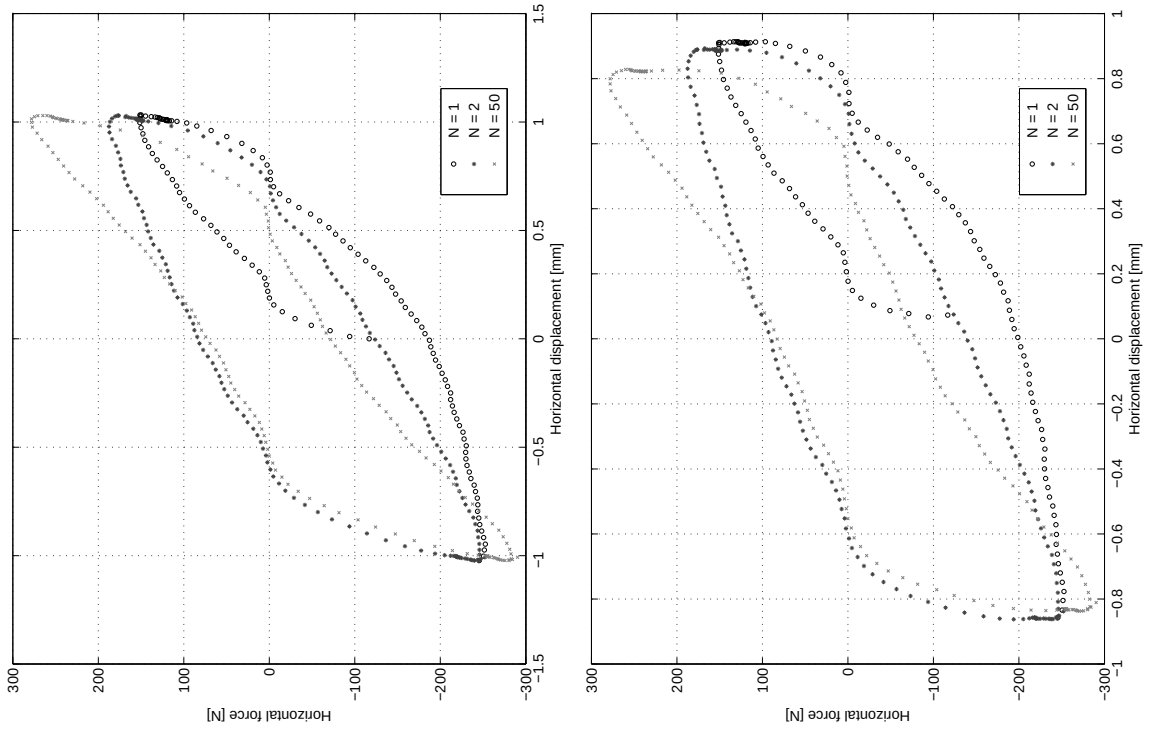

(a) Uncorrected cycles

(b) Cycles corrected for stiffness

(c) Cycles corrected for stiffness and hysteresis

(d) Cycles corrected for stiffness, hysteresis and centralized

Figure E.3 Correction stages for various cycles from test T12-pl-60-48g

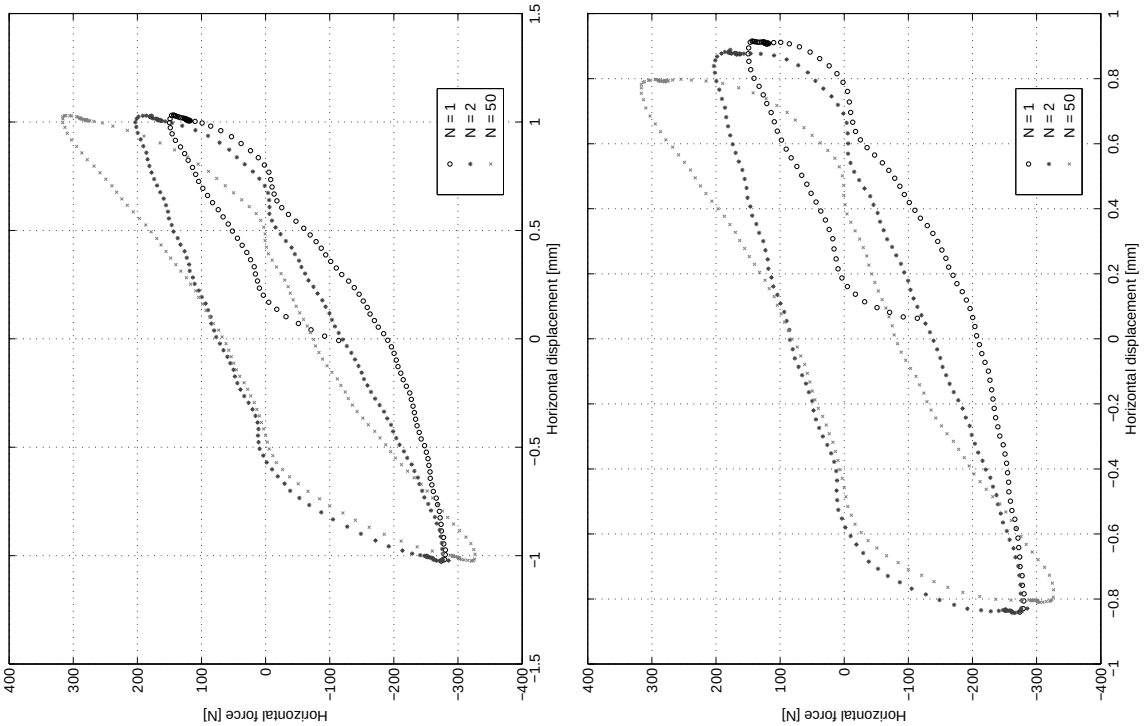

(a) Uncorrected cycles

(b) Cycles corrected for stiffness

(c) Cycles corrected for stiffness and hysteresis

(d) Cycles corrected for stiffness, hysteresis and centralized

Figure E.4 Correction stages for various cycles from test T13-pl-80-48g

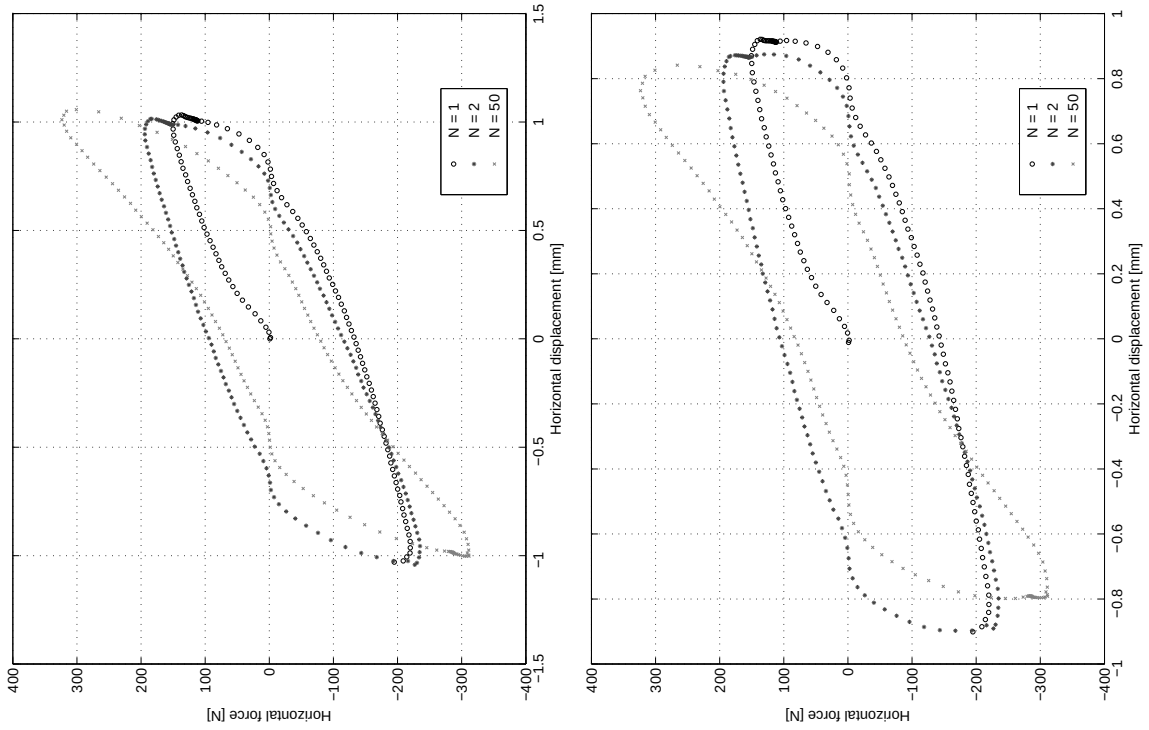

(a) Uncorrected cycles

(b) Cycles corrected for stiffness

(c) Cycles corrected for stiffness and hysteresis

(d) Cycles corrected for stiffness, hysteresis and centralized

Figure E.5 Correction stages for various cycles from test T14-pl-80-1g

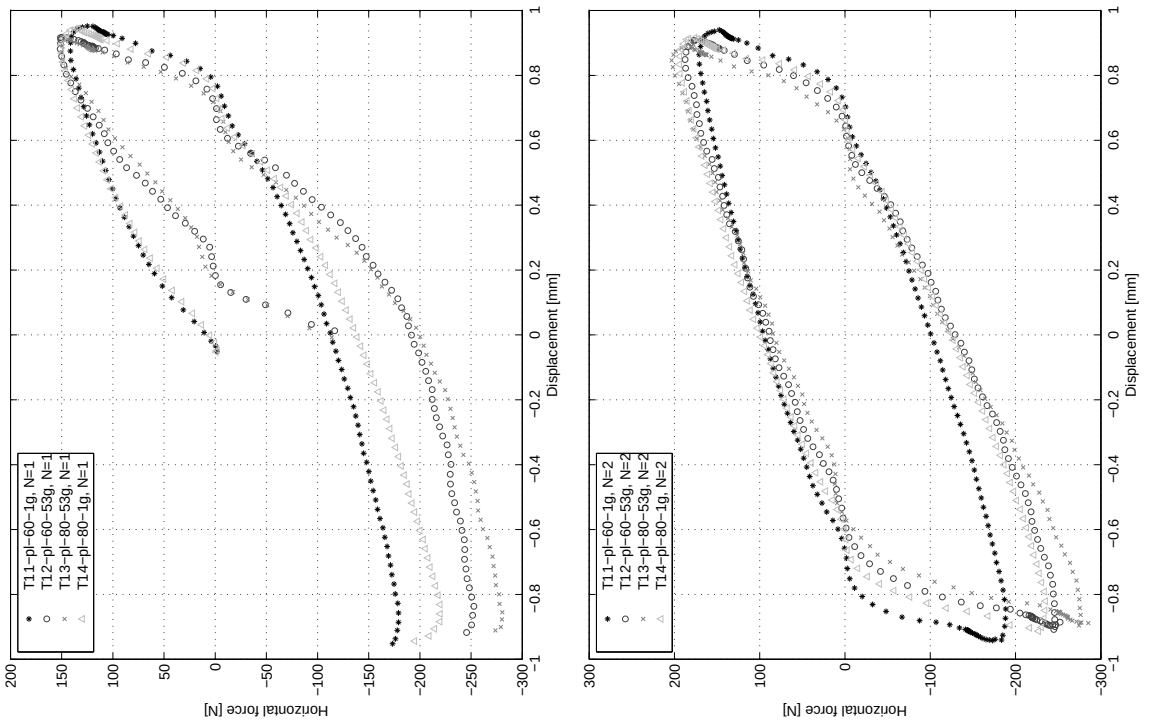

(a) Cycle 1

(b) Cycle 2

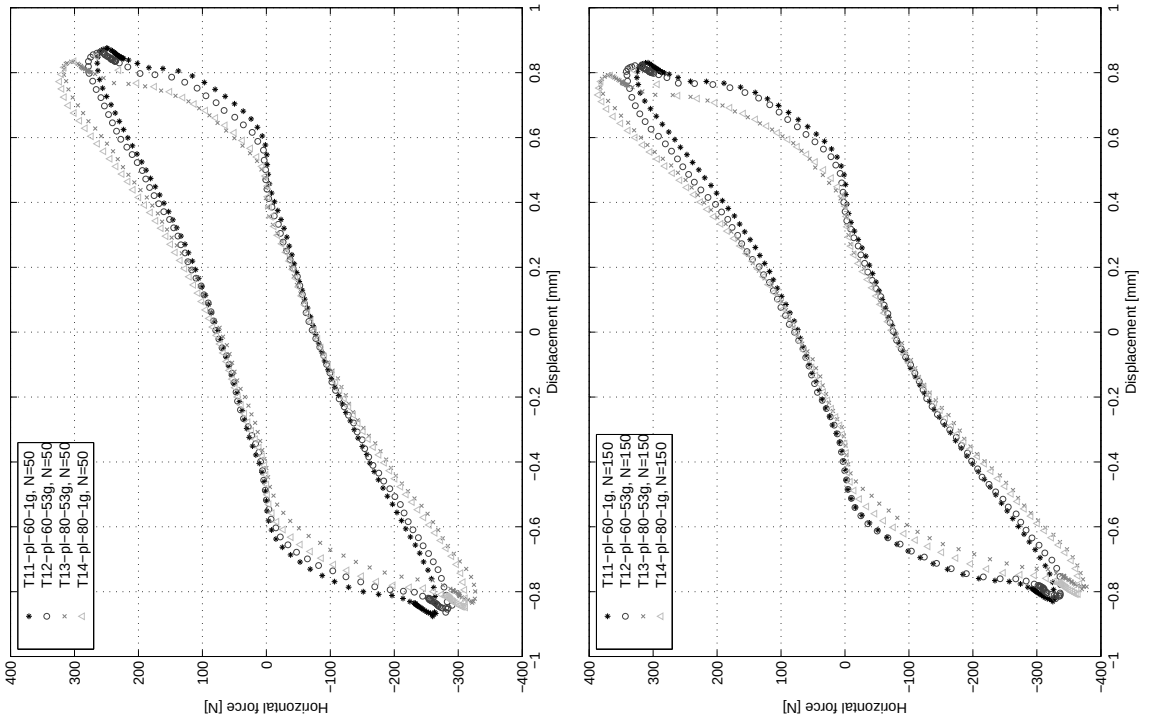

(c) Cycle 50

(d) Cycle 150

Figure E.6 Comparison of various cycles tests;T11-pl-80-1g, T12-pl-60-48g, T13-pl-80-48g, T14-pl-80-1g

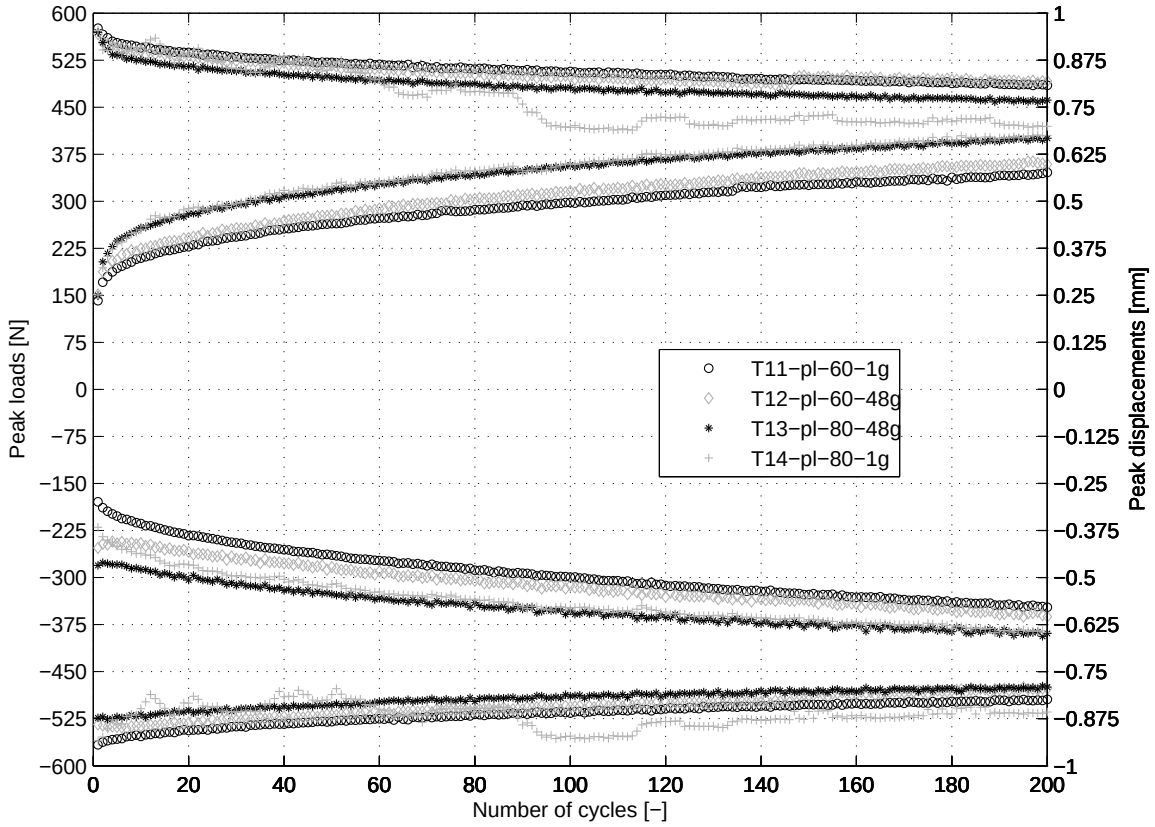

(a) Maximum and minimum horizontal displacement and forces

subcaptionboxMaximum and minimum horizontal displacement

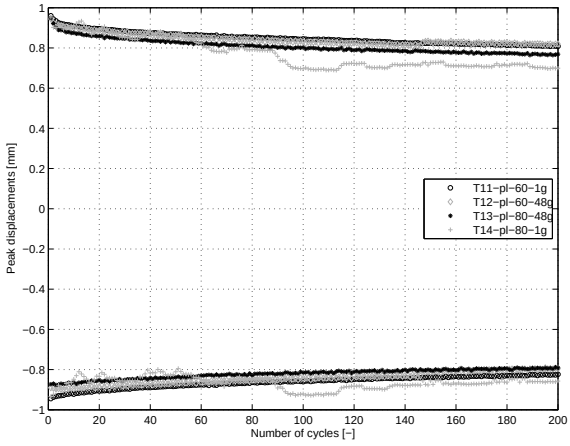

subcaptionboxMaximum and minimum horizontal forces

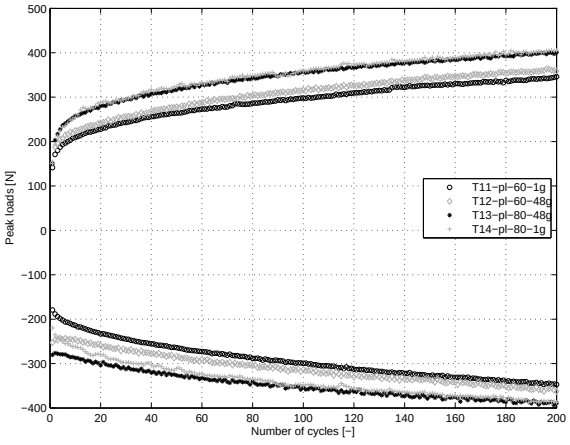

Figure E.7 Comparison between maximum and minimum horizontal forces and displacement for tests; T11-pl-60-1g, T12-pl-60-48g, T13-pl-80-48g and T14-pl-80-1g